Targeted Histone Deacetylase Inhibition

A Dissertation
Presented to
The Academic Faculty

By

William Guerrant

In Partial Fulfillment
Of the Requirements for the Degree
Doctor of Philosophy in Chemistry

Georgia Institute of Technology
August, 2012

Targeted Histone Deacetylase Inhibition

Committee:

Dr. Adegboyega Oyelere, Advisor
School of Chemistry and Biochemistry
Georgia Institute of Technology

Dr. Donald Doyle
School of Chemistry and Biochemistry
Georgia Institute of Technology

Dr. James Powers
School of Chemistry and Biochemistry
Georgia Institute of Technology

Dr. Yuhong Fan
School of Biology
Georgia Institute of Technology

Dr. Loren Williams
School of Chemistry and Biochemistry
Georgia Institute of Technology

Date Approved: May 29, 2012

Acknowledgements

I would like to thank my father for continuously pushing me throughout my childhood and adult life to cultivate a curious mind and pursue an advanced degree. I could never have gotten to where I am today without him. He has always been supportive and there for me when I have needed to talk to him and it has been immensely beneficial for my state of mind to know that he is proud of me. I have been and will continue to be grateful for the love and support, both mental and financial, that he has provided to aid me in my life.

No one has been more inspiring or supportive in my graduate career than my advisor, Dr. Yomi Oyelere. I offer my sincerest gratitude that he has allowed me to work in his lab and share his research goals. Over the course of my time at Georgia Tech, he has been supportive and inspiring and I owe the success that I have had in my graduate career to his patience, understanding, and passion for science.

I would also like to thank my committee members: Dr. James Powers, Dr. Loren Williams, Dr. Donald Doyle, and Dr. Yuhong Fan. Each has played an important role in the maturation of my thesis and my graduate career and I am grateful for the support, helpful comments, and training that they have provided and have been invaluable for the completion of this work.

In my daily work life, I have been fortunate to be surrounded by a group of wonderful graduate students who have been a source of friendship, insight, and good advice. I would like to thank the Oyelere lab, members past and present, for their support in my daily life and

assistance with scientific pursuits. It has been a pleasure to work with them. I would also like to thank the members of the Doyle lab and Fan lab for their assistance with my projects.

Finally, I would like to thank my wonderful friends for their support, patience, and belief in me. Katy and Kyle Rommel, Lisa Pan, Juan Pablo Aragon, and Josh Canzoneri have been excellent, supportive friends for as long as I have known them and have been integral for my state of mind and week-to-week life. I wish them all the greatest of success in their lives and pursuits.

Table of Contents

List of Tables

List of Figures

List of Abbreviations

ADP	Adenosine Diphosphate
BSA	Bovine Serum Albumin
CTCL	Cutaneous T-cell Lymphoma
DAU	Daunorubicin
DMSO	Dimethyl Sulfoxide
DOX	Doxorubicin
EGFR	Epidermal Growth Factor Receptor
HAT	Histone Acetyltransferase
HDAC	Histone Deacetylase
HDACi	Histone Deacetylase Inhibitor(s)
HDLP	Histone Deacetylase-like Protein
IC_{50}	Half Maximal Inhibition Concentration
KDNA	Kinetoplast DNA
LHRH	Luteinizing Hormone Releasing Hormone
LLC	Lewis Lung Carcinoma
MRP	Multidrug Resistance Protein

N.D.	Nondeterminable
NMR	Nuclear Magnetic Resonance
NSCLC	Non-Small Cell Lung Cancer
N.T.	Not Tested
PBS	Phosphate-buffered Saline
RIPA	Radioimmunoprecipitation Assay
SAHA	Suberoylanilide hydroxamic acid
SAR	Structure-activity Relationship
SCLC	Small Cell Lung Cancer
Topo	Topoisomerase
Topo II	Topoisomerase II
TSA	Trichostatin A
ZBG	Zinc-binding Group

Summary

Histone deacetylase inhibitors (HDACi) have shown great promise as cancer therapeutics through their ability to arrest proliferation in many transformed cell lines through cell cycle arrest, apoptosis, cellular differentiation, and inhibition of angiogenesis and cell migration. Moreover, as HDACs regulate many essential cellular processes, not only through epigenetic control, but also through non-epigenetic protein deacetylation, design of novel HDACi has become a popular research avenue in recent years. Upregulation of HDAC isoforms has been observed in many cancer types and it is known that HDACs contribute to cancer survival through epigenetic silencing of tumor suppressor genes and deacetylation of tumor suppressor proteins. The FDA approval of SAHA and FK-228, two HDACi indicated for use in cutaneous T cell lymphoma (CTCL), has further stimulated the pursuit of effective HDACi-based therapies. However, several drawbacks have limited HDACi efficacy and broader use in cancer therapy. First, most small molecule HDACi suffer from low oral bioavailability and few are targeted to particular cell or tissue types. More importantly, most HDACi are non-selective "pan-inhibitors" of several HDAC isoforms, leading to a reduction in overall *in vivo* potency and debilitating side effects. The greatest overall impediment to broad HDACi validation is the lack of demonstrated clinical efficacy in treating solid tumors. In this thesis, I document the discovery and biological activities of three novel classes of HDACi with enhanced potency and pharmacokinetic advantages that could address many of the shortcomings of current HDACi agents.

Nearly all HDACi derive their inhibition activities from concurrent zinc chelation in the HDAC active site and interaction with residues on the exterior of the enzyme. Moreover, the surface recognition cap groups of most HDACi are linked without preference to hydrogen bond

accepting or donating groups, such as keto and amide groups. We reasoned that substituting these groups with an appropriate, more pharmacokinetically-desirable moiety could improve activity if the replacement were a functional isostere. Replacement of these groups with a triazole ring yielded novel aryltriazolylhydroxamate HDACi that have enhanced potency against nuclear HDACs and low micromolar anticancer activities.

Two of the challenges facing current HDACi agents, as mentioned above, are a lack of specific targeting and compromised efficacy against solid tumors. One mode of addressing these drawbacks is through a designed multiple ligand capable of inhibiting multiple proliferative pathways that also improves the delivery of HDACi to a specific target. To this end, dual-acting inhibitors of Topoisomerase II (Topo II) and HDACi have been designed using the standard HDAC and Topo II inhibitors SAHA and Daunorubicin, respectively. These compounds inhibit both HDAC and Topo II, some more potently than the standards. Significantly, one dual-acting compound has sub-micromolar anticancer activity and is delivered in high concentrations intracellularly to the perinuclear region.

Continuing with the theme of targeted HDACi delivery, the need for lung-targeted cancer therapies is underscored by the high incidence and mortality associated with cancers of the lung. The macrolide antibiotics are antibacterial agents that possess exceptional pharmacokinetics, specifically lung delivery and significant lung residence. In an attempt to harness the outstanding properties of macrolides for a lung cancer therapy, macrocyclic HDACi have been generated, incorporating macrolide skeletons of azithromycin and clarithromycin macrolides as surface recognition cap groups. A subset of these compounds potently inhibits HDAC and also inhibits lung cancer cell viability in low micromolar concencentrations. Most importantly,

azithromycin-based macrocyclic HDACi display a lung-targeted tissue distribution *in vivo* that indicates the significant potential of these compounds against solid lung tumors.

Chapter 1

Histone Deacetylase, HDAC Inhibitors, and Cancer Treatment

1.1 Histone Deacetylase

Control of the integrity and expression of double-stranded DNA is essential for the health and survival of all living cells.[1] Epigenetic control, regulation of gene expression independent of changes to the DNA sequence, is a powerful means of regulating cellular function.[2] This process is essential in normal development as transcription of certain genes are necessary only in certain cell types.[3] The main eukaryotic epigenetic mechanisms are DNA methylation and post-translational modifications of histone proteins, including acetylation, methylation, phosphorylation, ubiquitination, ADP-ribosylation, and sumoylation.[4-8]

Modification of histones via acetylation is controlled by two opposing enzymes: histone acetyltransferase (HAT) and histone deacetylase (HDAC).[9-11] HAT transfers acetyl groups onto the ε-NH_3 groups of histone lysine residues in a reversible process involving acetyl coenzyme A.[12] Acetylation neutralizes the charge interaction between the negatively-charged DNA backbone and positively-charged histone lysines, resulting in a more relaxed nucleosomal structure with accessibility of DNA to transcription factors.[13-15] Conversely, HDAC removes acetyl groups from histone lysines, resulting in decreased transcription through inaccessibility of nucleosome-associated DNA.[10]

Histones were first revealed as substrates for HDAC activity four decades ago in 1969.[16,17] Discovery of non-specific inhibition of HDAC activity by butyrate followed in 1978, while Trichostatin A, a fungal antibiotic, was shown to be the first specific inhibitor of HDAC in

1990.[17-19] Using the cyclic-tetrapeptide Trapoxin, an irreversible HDAC inhibitor (HDACi), the first HDAC was purified from cow thymus in 1996.[20] This HDAC, termed HDAC1, was discovered to be an orthologue of yeast protein Rpd3, which had already been profiled as an extensive regulator of transcription.[21] This link further encouraged the connection between histone acetylation and gene regulation, and led to the theory that HDACs serve as epigenetic transcriptional repressors.[22]

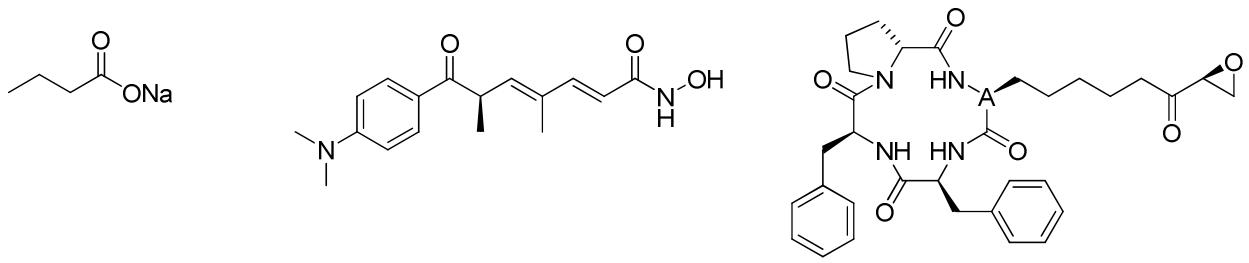

Sodium butyrate (NaB) | Trichostatin A | Trapoxin B

Figure 1-1: Early HDACi used to profile the link between HDAC, histone acetylation, and transcriptional repression.

1.2 HDAC Biology

To date, the HDAC family of enzymes contains 18 known isoforms organized into 4 classes: class I (HDACs 1, 2, 3, and 8), class II (HDACs 4, 5, 6, 7, 9, and 10), and class IV (HDAC11) are zinc metalloenzymes, while class III, referred to as sirtuins, have a different mechanism of action, requiring NAD^+ for activity. The group organization is based largely on sequence homology to yeast analogues and cellular localization. Class I is primarily nuclear-localized, while class II is further divided into class IIa (HDACs 4,5,7, and 8) which is found in

both the nucleus and cytoplasm, and class IIb (HDACs 6 and 10) which is primarily cytoplasmic and has two active sites.[23] HDAC11, the sole member of class IV, is structurally related to both class I and II HDACs and is found in both nuclear and cytoplasmic cell fractions.[23]

Class I HDACs 1, 2, and 3 have been identified as subunits of nuclear protein complexes that function in global transcriptional repression. Complexes including CoRest,[24,25] NuRD,[26,27] and Sin3[28] contain HDAC1 and HDAC2, which confer deacetylase activity to these corepressors. HDAC3 has been identified as part of N-Cor /SMRT repressor complex, which regulate the repression of nuclear hormone receptors and other transcriptional repressors.[29,30] Conversely, HDAC8 has not been identified as a part of a transcriptional repression complex and its repression functions are still under investigation.

By contrast, Class IIa HDACs 4, 5, 7, and 9 localize to the nucleus and cytoplasm and their shuttling between the two is regulated by the 14-3-3 proteins which bind to these HDACs at conserved N-terminal sites and mediate their localization based on the phosphorylation of key residues within the 14-3-3 binding sites on HDACs.[31,32] Key signaling pathways regulate the phosphorylation of these sites, thereby regulating HDAC activities through nuclear translocation.[33-35] Importantly, class IIb HDAC6 was identified as a microtubule-associated deacetylase, and highlighted a key revelation: HDACs deacetylate a range of non-histone proteins in addition to their classical targets, and perhaps a more appropriate title for these enzymes would be “lysine deacetylases”.[36,37] HDAC10 was shown to repress transcription and interact with HDAC3, but its function is still largely unknown.[38] HDAC11, the sole member of class IV, is structurally related to both class I and class II, but very little is known about its function.[39,40]

Structural information of all HDAC enzymes is still elusive. To date, only HDAC8[41] and HDAC3[42] have been crystallized in full, but several catalytic domains of other HDACs have been elucidated and are available in the literature.[43-45] In the absence of these structures, the crystal structure of histone deacetylase-like protein (HDLP), an *Aquifex aolicus* HDAC homologue with 35.2% overall sequence homology to human HDAC1, has been used to profile many HDAC ligands and conceptualize the catalytic core, which has high sequence homology.[46] The structural architectures of the HDLP and HDAC8 active sites are conserved in other class I and II HDACs. In HDLP, the Zn^{2+} ion is buried in the active site, reached by a 14 Å hydrophobic tunnel (Figure 1-2).[46] Amino acid residues Pro22, Gly140, Phe141, His 180, Phe198, Leu265, and Tyr297 form the tunnel wall, while Asp168, His170, and Asp258, and water molecules coordinate the Zn^{2+} ion for deacetylation activity.[46] HDAC8 is structured similarly but with a shallower tunnel of 12 Å (Figure 1-3).[47]

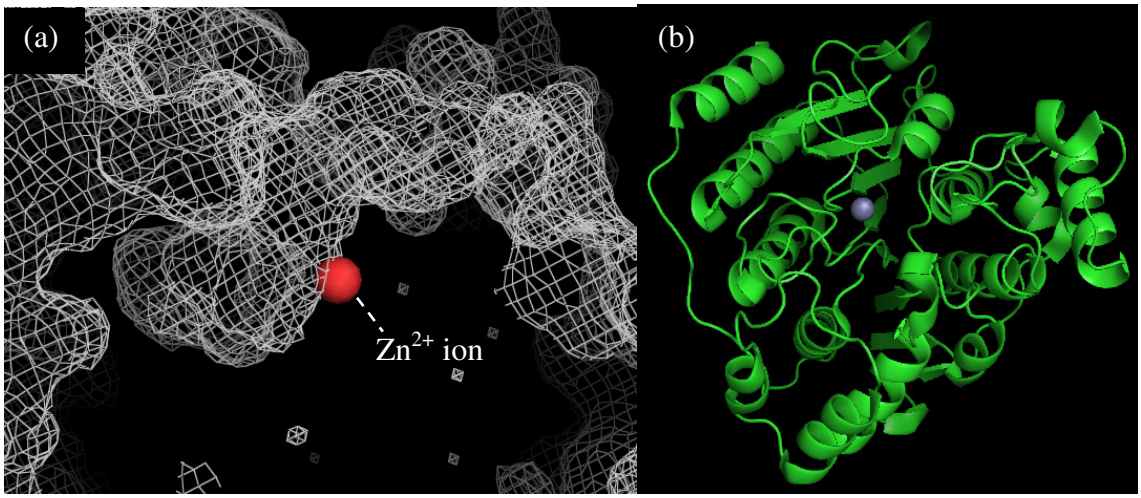

Figure 1-2: Active site (a) and secondary structure (b) of HDLP, a homologue of human HDAC1. The zinc ion is presented as spheres. Viewed in Pymol. PDB = 13CS.

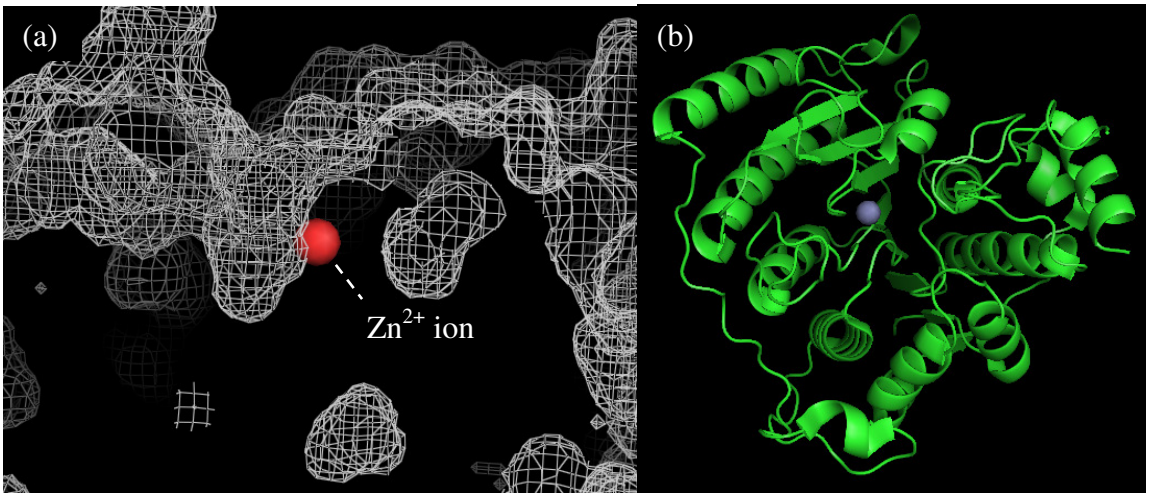

Figure 1-3: Active site and secondary structure of human HDAC8. The zinc ion is presented as spheres. Viewed with Pymol. PDB = 1T69.

The accepted mechanism of deacetylase action on acetylated lysines by HDAC enzymes was proposed based on the binding contacts made by the HDAC inhibitors TSA and SAHA on HDLP.[46] It is thought that the zinc ion binds the carbonyl oxygen of the N-acetyl amide, activating the acetylated lysine and orienting the carbonyl carbon close to an activated water molecule (Figure 1-4). The water molecule then attacks, resulting in formation of a tetrahedral intermediate with the carbonyl carbon. Finally, the carbon-nitrogen bond breaks and nitrogen accepts a proton from a histidine residue, producing lysine and acetate. This mechanism is supported by studies reporting a complete loss of both deacetylase activity and subsequent transcriptional repression caused by mutations of HDAC analogue active site histidines in yeast.[48]

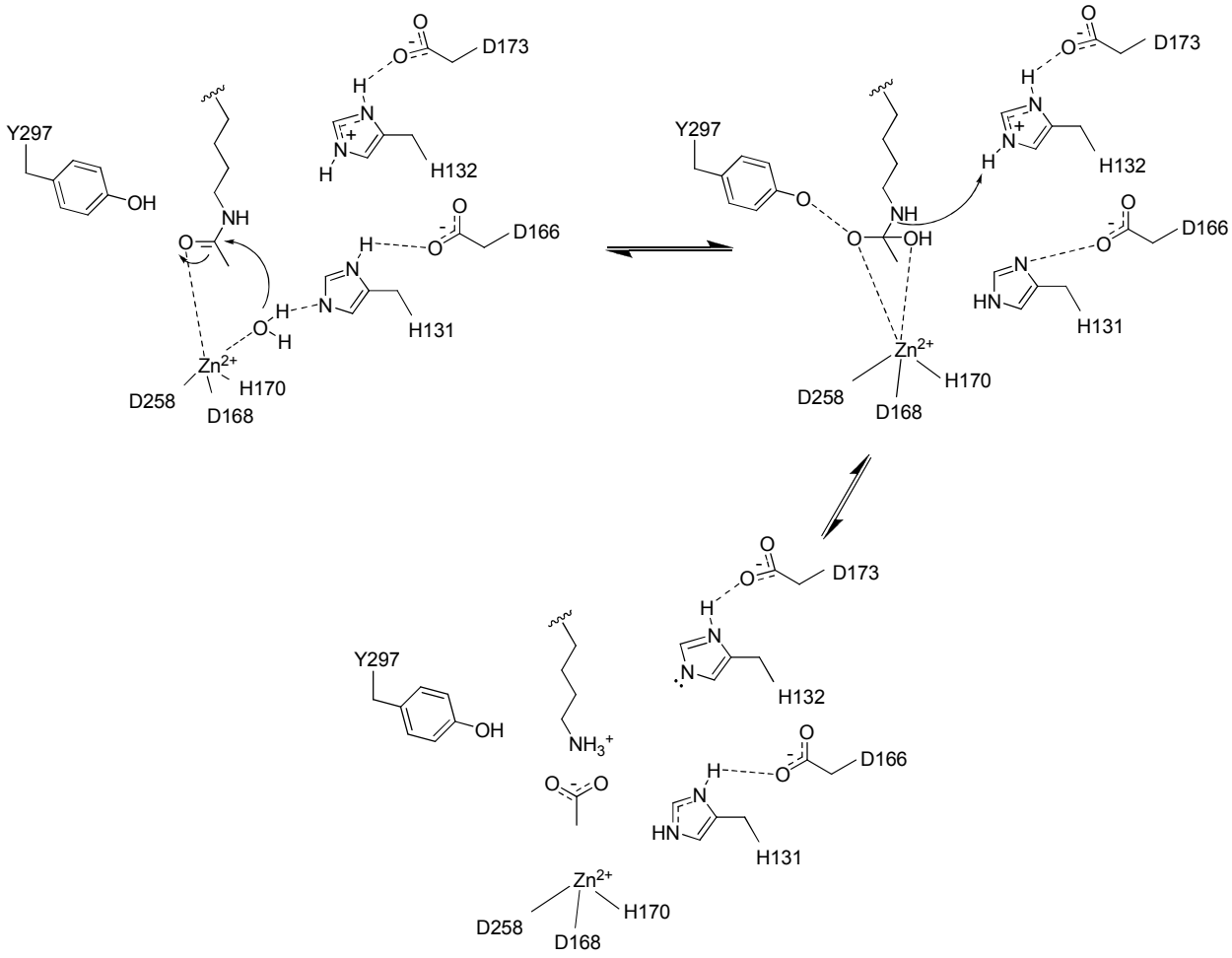

Figure 1-4: Proposed mechanism of deacetylation of lysines by HDAC, based on HDLP residue contacts.[46]

1.3 Histone Deacetylases and Cancer

It is now known that HDACs contribute to cancer progression in a variety of ways. Dysregulation of the acetylation status of histones has been linked with transcriptional silencing of key suppressors of tumorigenesis. Specifically, HDACs have been shown to be recruited by oncoproteins in several cancers in order to aberrantly repress transcription.[49-52] Moreover, several knockdown experiments have demonstrated the necessity of HDAC expression in cancers. HDACs 1 and 2 have redundant function in cancer, and deletion of both is required to halt tumor growth completely.[53] Similarly, knockdown of HDAC 1 and 3 is sufficient to inhibit proliferation in HeLa cells,[54] and siRNA knockdown of HDAC1 causes cell cycle arrest, inhibit cell growth, and lead to increased numbers of apoptotic cells, while overexpression of HDAC1 led to a proliferative phenotype in cultured prostate cells.[55,56] HDAC2 knockdown has also demonstrated an antiproliferative effect with increased $p21^{waf1}$-associated apoptosis in cervical cancer cells, as well as increases in p53-induced antiproliferative and cell senescence effects in breast cancer.[57,58] Similarly, separate knockdowns of class I HDACs 3 and 8 caused apoptosis and a restoration of gene expression.[59,60] By contrast, the cancer-specific contributions of class II and IV HDACs are less clear, although HDAC6 is a notable exception with pro-angiogenic and prometastatic activities through binding to hypoxia inducible factors (HIFs) and vascular endothelial growth factors, respectively. Overall, the overexpression of many HDAC isoforms are associated with specific cancers, and the potent proliferative effects seen by dysregulation of HDACs make them prime targets for cancer therapeutics.

1.4 HDAC Inhibition

1.4.1 HDAC Inhibitors

To date, a diverse range of natural product and synthetic HDACi have been discovered and profiled. In spite of the significant structural diversity among HDACi, they generally conform to a three-motif pharmacophoric model containing a surface recognition cap group, a linker chain, and a zinc binding group (ZBG) (Figure 1-5). The accepted mode of inhibition involves the ZBG interacting with the catalytic zinc ion in the active channel, while the linker efficiently positions the cap group to make interactions with amino acid residues on the surface of the enzyme (Figure 1-6).[46]

Selected identified classes of HDACi include short chain fatty acids(butyrate and valproic acid), linear hydroxamic acids (SAHA and TSA), benzamides (MS-275), and cyclic peptides (FK-228 and CHAPs). Potencies against HDAC vary by class with activities in the millimolar range (fatty acids, micromolar range (benzamides), nanomolar range (linear hydroxamates and FK-228), and picomolar (CHAPs).[61] Most currently reported HDACi inhibit HDAC by liganding the zinc ion and preventing substrate entry into the active site. Specific interactions with the enzyme surface residues correlate well with potency and are thought to be essential for activity towards individual isoforms. This is an attractive pursuit due to the fact that certain cancers only upregulate distinct HDAC isoforms,[23] and since most HDACi so far discovered are non-selective "pan inhibitors" of many isoforms, better efficacy might be achieved with a more selective inhibitor. In addition, more selective inhibitors could be used to further probe the activities and functions of specific HDAC isoforms, as well as assist in structure-activity relationship studies.

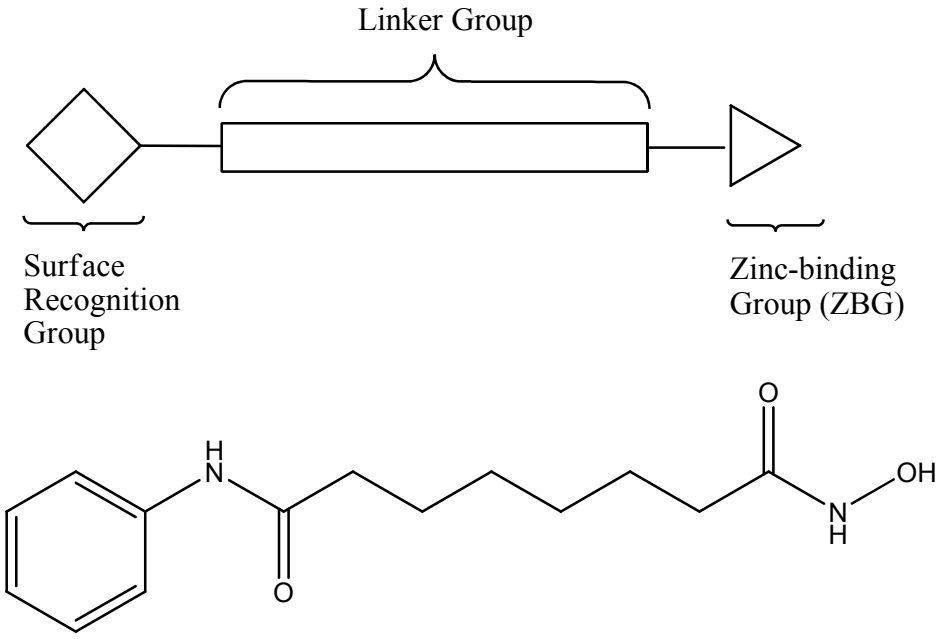

Suberoylanilide Hydroxamic Acid (SAHA)

Figure 1-5: General HDACi pharmacophore with SAHA for reference.

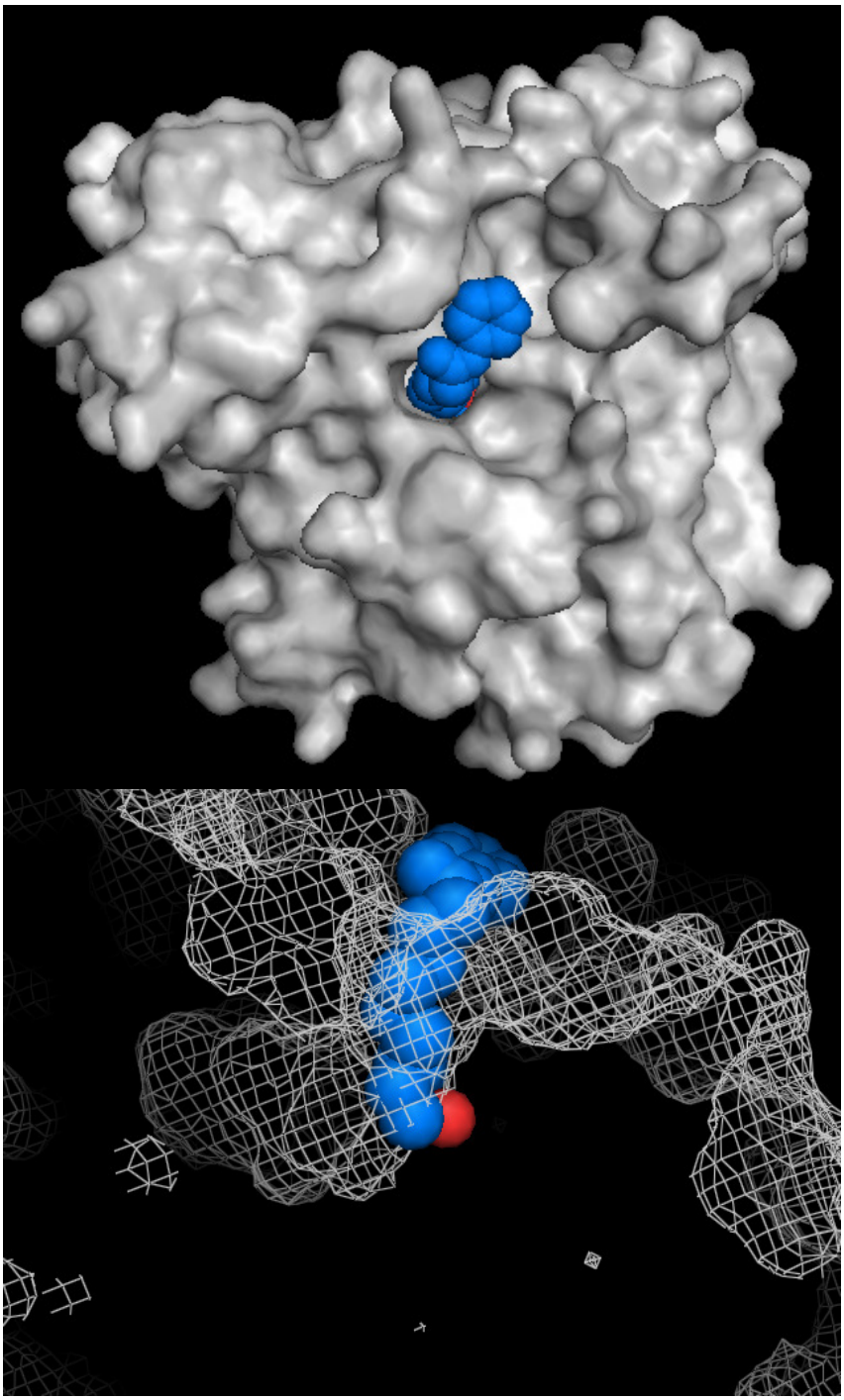

Figure 1-6: Crystal structure of SAHA (blue) bound to HDLP (gray). Consistent with the accepted mode of inhibition, the hydroxamic acid binds the zinc ion (red), the linker fills the active site channel, and the surface recognition group interacts with surface residues on the exterior of the enzyme.

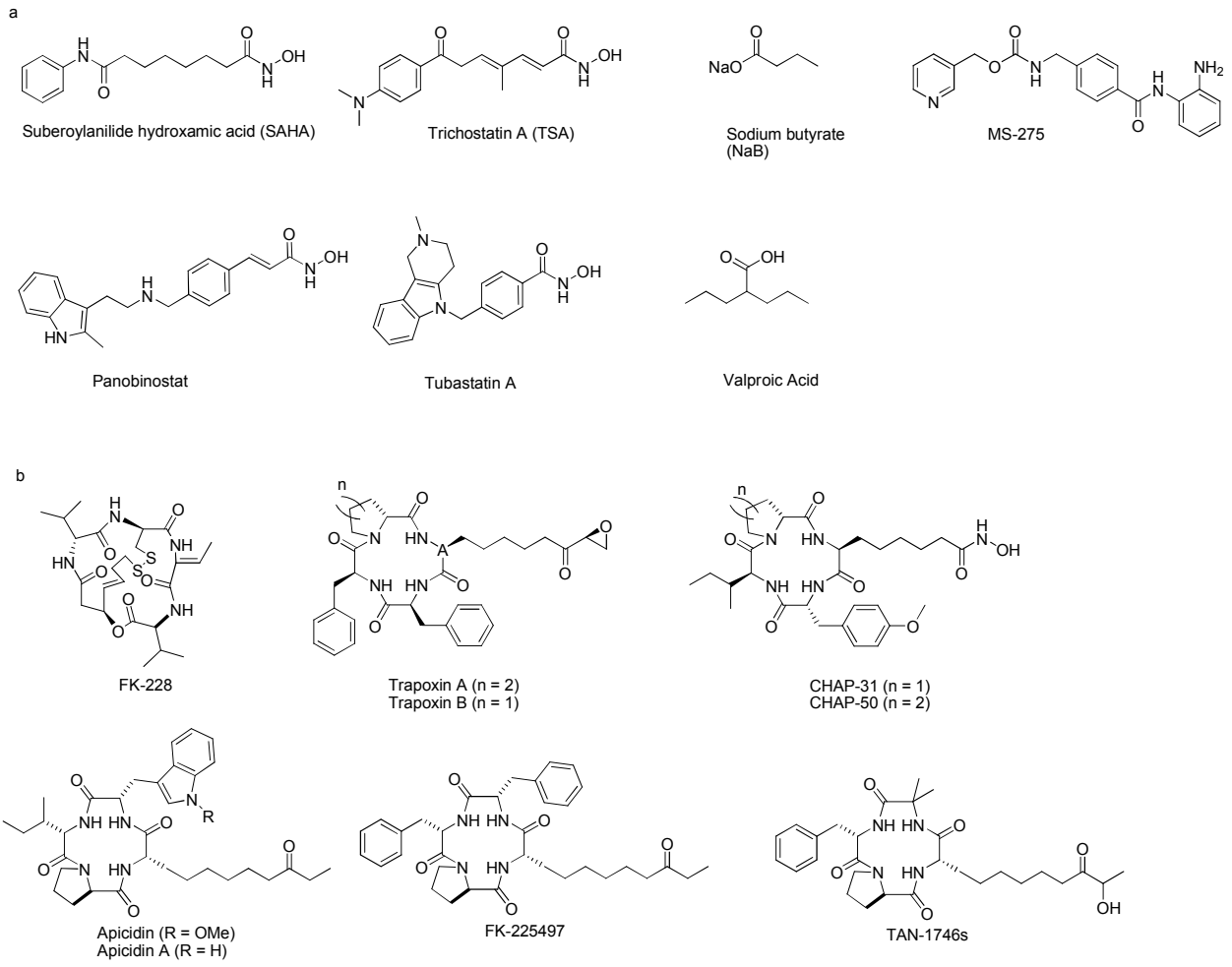

Figure 1-7: Representative HDACi. (a) linear HDACi, (b) macrocyclic HDACi.

1.4.2 In Vitro HDAC Inhibition

For the past 15 years, HDAC inhibition has been a prominent and rapidly expanding research avenue. HDAC inhibitors (HDACi) have demonstrated great potential as *in vitro* anticancer agents through their ability to arrest the growth of nearly all transformed cell types, initiate differentiation, promote apoptosis, and inhibit angiogenesis.[62-64] Treatment of cultured cancer cells with HDACi results in cell cycle arrest at G1 and, occasionally, G2 checkpoints at concentrations of drug that also cause accumulation of acetylated histones.[62] Histones become acetylated in response to HDACi in both normal and cancerous cells, with acetylation of H2A, H2B, H3, and H4 commonly observed.[65] Importantly, HDACi-induced toxicity is cancer-specific, as doses that are toxic to transformed cells cause no apoptosis in normal cell lines.[66]

One of the main intracellular effects observed with HDACi treatment, is increase in the expression of $p21^{waf1}$, a cyclin dependent kinase inhibitor.[67,68] p21 is a regulator of the cell cycle through its inhibition activity and causes cell cycle arrest at G1. SAHA treatment specifically causes increases in acetylated histones associated with the p21 gene promoter.[67] Likewise, many of the gene targets that are upregulated with HDACi treatment have been identified as antiproliferative proteins.[69a] This has led to the theory that recruitment of HDACs and subsequent transcriptional dysregulation, specifically of tumor suppressor genes, could be a common modality for initiation of proliferation. Of great significance is the discovery that HDACs have a diverse range of non-histone substrates, many of which are attractive cancer targets themselves, such as $p53$[69b], $E2F$[69c/d], tubulin[37], and $Hsp90$[69e]. This revelation greatly broadened the scope by which these inhibitors were thought to exert their activities and further

underscores the promising anticancer activities that could be possible through the appropriate modification of HDACi molecules.

1.4.3 HDAC Inhibition in Animal Models

Several HDACi inhibit *in vivo* tumor growth when adiministered intravenously or intraperitoneally in a variety of animal cancer models, including lung, breast, prostate, and leukemia models, with little toxicity.[22,62,70] Treatment with HDAC inhibitors results in acetylated histones in tumor tissues and normal tissues, such as the spleen and liver,[71] but it should be noted that increased amounts of acetylated histones in normal cells are not correlated with growth inhibition.[62]

One animal model for human prostate cancer showed remarkable susceptibility to SAHA-induced cytotoxicity.[62] CWR22 human prostate xenografts that were dosed with 25, 50, and 100 mg/kg/day with SAHA were reduced by 78%, 97%, and 97% tumor volume, respectively, compared to vehicle-treated control animals. The most effective dosing concentration was determined to be 50 mg/kg, as the lower dose showed less tumor regression and the higher dose had equivalent activity, but with evidence of toxicity.[62] Moreover, both the 25 mg/kg/day and 50 mg/kg/day treatment groups were tested for HDAC activity in the CWR22 tumors. Both groups showed significant increases in acetylated histones H3 and H4 at 6 hours post-treatment. These levels fell, however, with only the 50 mg/kg/day dose causing noticeable histone acetylation after 12 hours. The encouraging *in vivo* anticancer data shown against this

mouse tumor model provided the basis for human testing in clinical trials that followed shortly after.

1.5 Clinical Successes with HDAC Inhibitors

1.5.1 SAHA

SAHA was initially investigated in a Phase I intravenous dosing study.[73] Two treatment cohorts were tested. The first started patients on doses ranging from 75 to 900 mg/m^2/day for 3 consecutive days, 21 days apart. The second cohort started patients on infusions of 300 mg/m^2/day for 5 consecutive days on 3 consecutive weeks and then the dose was increased to either 600 or 900 mg/m^2/day. 37 patients were treated with 25 having solid tumors and 12 with hematological malignancies. Patients with solid tumors were placed on higher dosage cohorts and were safely administered doses of SAHA 3 times higher than patients with hematological malignancies.

From this study, 2 patients with refractory bladder cancer had reductions in pelvic tumor masses and improvements in tumor-related pain. However, once these patients were taken off of the treatment regimen, their disease progressed within 2 months. Two patients with refractory Hodgkin's lymphoma also responded to treatment with SAHA. The first patient was dosed with the 600 mg/m^2 concentration and showed 30% reduction in her lung lesions, before she had to discontinue treatment due to a secondary infection, after which her disease again progressed. The second patient on the 300 mg/m^2 dose demonstrated a stable disease phenotype through CT and PET scans and was maintained on the treatment regimen for 8 months, during which time

she was able to return to work. She later converted to an oral SAHA treatment for ease of administration, as it became available after the Phase I trial was concluded.

Significantly, 1 patient had an acute myocardial infarction and died while on the treatment regimen. He was a life-long cigarette smoker and an autopsy could not determine a reasonable link between his cardiac event and SAHA treatment. However, this event, coupled with irregularities in cardiac nerve repolarization (QTc elongation) that have been observed in all HDACi clinical trials, created initial concern for heart-related cytotoxicity. Electrocardiogram monitoring of patients was subsequently performed before, during, and after treatment with SAHA.

Histone acetylation was investigated via blood samples in patients with hematological malignancies. Lower doses of SAHA did not cause observable histone acetylation when blood was assayed 2 hours post-treatment. Higher doses of SAHA caused accumulation of acetylated histones for at least 4 hours post-treatment. This result was underscored by the short half-life of SAHA (0.35-1.3 hours) when administered intravenously. Solid tumors that were biopsied and tested for acetylated histones were positive for acetylated histones in 60% of the patients tested.

Subsequently, an oral formulation of SAHA became available and was assayed by a Phase I trial in patients with advanced-stage cancers.[74] 73 patients were tested and dose-limiting toxicities were effects also common to the previous study: anorexia, dehydration, diarrhea, and fatigue. Maximum tolerated doses of 400 mg/day, or alternatively, 200 mg taken twice daily for continuous dosing. 300 mg taken twice daily could be tolerated on a 3 day/week regimen. Oral SAHA was shown to have 43% bioavailability with peak plasma concentrations between 2 and 3 hours. Half-lives were dose-dependent and were improved by fasting the patient. The resulting

half lives were between 1.5 and 2 hours, depending on the dose. This study resulted in 1 complete response, 3 partial responses, and 2 unconfirmed partial responses. Moreover, SAHA was well tolerated and 22 patients remained on the treatment for between 4 and 37 months. Common side effects included nausea, vomiting, diarrhea, and dehydration. More serious side effects, specifically neutropenia (decrease in blood neutrophils) and thrombocytopenia (decreased platelets) were observed uncommonly. Oral SAHA also caused accumulation of acetylated histone, more commonly observed at higher doses of drug.

A phase II trial of oral SAHA centered on treating patients with refractory cutaneous T-cell lymphoma.[75] This study tested doses of 400 mg/day, 300 mg twice daily for 3 consecutive days, or 300 mg/day for 14 consecutive days followed by 7 days rest. The primary objective focused on determining the clinical response to oral SAHA. 33 patients were enrolled and all had received previous therapies for CTCL. The 400 mg/day regimen demonstrated the highest safety profile. Adverse effects included nausea and fatigue with more serious thrombocytopenia rarely observed. There were no complete responses, but 8 patients showed partial responses to treatment, of which 1 had early-stage disease and 7 had more progressive CTCL. The cancer response rate to oral SAHA was determined to be 24%, while 58% received some sort of clinical benefit, such as decreased inflammation or pain relief. Significantly, tested CTCL lesions demonstrated apoptosis of malignant T-cells, a cell cycle arrest at the G2 checkpoint, and higher levels of $p21^{waf1}$ expression.

Overall, these clinical trials demonstrated the anticancer action of SAHA in vivo. Consistent with the accepted mechanism of HDAC inhibition, SAHA caused acetylation of histones in many patients and achieved moderate efficacy against CTCL. However, acetylated

histones were only seen with higher doses of SAHA and even then, acetylated histones were not observed in all tumors. Based on the clinical successes, SAHA was approved for the treatment of CTCL in 2006, however, the low half-life and limited efficacy against solid tumors are both serious obstacles to broad use.

1.5.2 FK-228

To date, FK-228 (Romidepsin) is the only macrocyclic HDACi to progress through clinical trials. FK-228 was initially assessed for responses against a range of solid tumors, and results from these studies showed promising responses among tested patients.[76] Initially two Phase I dosing trials were carried out. The first trial incorporated two doses at days 1 and 5, repeating every three weeks, while the second trial administered three doses on days 1, 8, and 15, repeating every four weeks. The maximum tolerated dose for each study was determined to be 17.8 mg/m^2 and 14 mg/m^2, respectively. Most patients showed limited activity, although promising responses against cutaneous T-cell lymphoma (CTCL) were observed.[76] It should be noted that in an additional cohort, included after completion of the first trial, a patient with peripheral T-cell lymphoma experienced complete remission in response to FK-228. Following this success and similar results obtained in patients with cutaneous T-cell lymphomas, a Phase II trial was launched with a recommended dose of 17.8 mg/m^2, administered on days 1 and 5 of a 21 day rotation.[77]

While responses against CTCL were promising, none of the patients experienced a complete remission.[77] Because of this, other Phase II trials were initiated with the focus on combination therapies of FK-228 and cytotoxic anticancer agents such as the proteasome inhibitor bortezomib and the nucleoside analogue gemcitabine.[78,79] Additionally, a Phase II trial

involving FK-228 as a single agent against previously-treated colorectal cancer was completed, but no objective responses were observed.[80]

Since the publication of the initial clinical results, FK-228 has entered numerous clinical trials against other forms of cancer, including lung cancer and various types of leukemia.[81,82] In trials against acute myeloid leukemia (AML), apoptosis has been observed at concentrations that suggest HDAC inhibition as a mechanism.[81] After completion of that study, several patients showed measurable antitumor responses, but no complete responses were observed.[80] Contrasting with this result, another clinical trial using FK-228 against AML showed no significant change in chromatin acetylation, specifically on histone H3 and H4, but did result in one complete remission and six stable disease conditions.[83] In a trial against lung cancer, FK-228 produced no objective responses, but did confirm in vitro findings, namely resulting in histone H4 acetylation, p21 expression, and a general shift in gene expression towards normal lung epithelia.[82]

There has been some concern over preclinical data that suggests that FK-228 could result in cardiac toxicity. One trial reported serious cardiac complications in tested participants and had to be terminated due to the death of one patient.[84] The cause of death could not be determined, but was assumed to be due to a ventricular arrhythmia that may have been related to several other factor, FK-228 treatment being one. On the basis of this, the trial was terminated. Also two patients were observed with asymptomatic ventricular tachycardia and three experience QTc prolongations, but these resolved between doses. It should be noted that the results of this trial contrast greatly with subsequent clinical results. To date, no other clinical observations of significant cardiac toxicity have been reported in studies using FK-228 however it is important to

underscore that the serious adverse cardiac effects seen with FK-228 treatment could be cause for concern. [80,82,83,85,86] With the exception to this mar, Fk-228 has shown great promise in the clinic, specifically against T-cell lymphoma. Of particular note is the remarkable length of response to FK-228, even after treatment has ceased, extending over 3 years in some cases.[87] Due to the successes of these clinical trials, FK-228 (Istodax) was approved by the FDA for treatment of CTCL.[88] However, the cardiac-related death, in conjunction with a similar event in the SAHA clinical trials and cardiac effects common to HDACi, have created concerns over the safety and cardiotoxicity of HDACi. Moreover, in spite of promising clinical results by SAHA and FK-228, clinical efficacy against solid tumors has remained a significant challenge. In order to further HDACi-based therapies, these issue will need to be addressed.

1.6 Current Strategies to Increase the Efficacy of HDACi

In spite of the successes of SAHA (Vorinostat) and FK-228 (Istodax) against CTCL, several challenges remain to HDACi-based cancer chemotherapeutics. First, concerns over dose-limiting cardiotoxicity have created the perception that HDACi use is plagued by serious side effects. This has only been exacerbated by the lack of clinical efficacy shown against solid tumors.[89,90] No patient to date has experienced a complete or even a partial response of a solid tumor with HDACi therapy. The prevalence of dose-limiting side effects such as fatigue, anorexia, diarrhea, or more serious hematological and cardiac adverse effects like thrombocytopenia and QTc prolongation, respectively, further limit the broad applicability of these compounds. Overcoming these challenges will require innovation, both in terms of the design of new agents, as well as strategies to increase their efficacy and limit off-target toxicity.

1.6.1 Localized Administration

One strategy that is currently being pursued to limit toxicity and more specifically deliver HDACi is local administration to cancerous tissue. Localizing HDACi has been achieved through surgically-placed biodegradable polymers, intratumoral injection, and topical application.[91-93] Specifically, topical FK-228 administration to skin lesions on patients with CTCL achieved selective delivery with low systemic side effects.[94] Topical administration of other HDACi have shown promising results in phase II trials against non-melanoma skin cancer with complete or near complete remission in 75% of patients treated and partial responses in the remaining, with only mild inflammatory side effects.[92] Local administration of HDACi, while promising in these studies, is not a viable strategy for most tumors, but it does demonstrate the potential that localized delivery of HDACi could have for improving efficacy and reducing the side effects common to clinical HDACi trials.

1.6.2 Targeted HDAC Inhibitors

Selective biological targeting of HDACi could address many of the shortcomings of current inhibitors. Targeted delivery of anticancer agents is a proven strategy for increasing efficacy by selectively accumulating chemotherapeutics to the target of interest, while limiting side effects brought about by off-target interactions.[95-98] Specific targeting of HDACi through moieties that also function to selectively deliver or target the HDACi to distinct tissues or cell types could confer interesting and beneficial effects on current agents. Because the HDAC enzyme surface is relatively tolerant of a diverse range of HDACi cap groups[99], modification of this moiety could be a viable strategy for introducing targeting groups to confer better specificity to HDACi. Targeting this new generation of HDACi to specific tissues or cell types has the

potential for vastly decreasing the side effects currently associated with HDACi, while also conferring greater efficacy by concentrating more drug in target sites. This could allow for a lower therapeutic dose, further minimizing side effects. The HDACi surface recognition cap group, which is the most substitution-tolerant moiety of the HDACi pharmacophore, could be modified to incorporate appropriate groups that would not only interact favorably with HDAC residues, but also target the inhibitor specifically to certain cell types in the body. By combining targeting and inhibition capabilities within a single agent, it is possible that this type of integrated HDACi could improve the therapeutic profile by reducing off-target side effects and accumulating in solid tumors.

On the other hand, targeting HDAC as part of a designed multiple ligand could confer the broad anticancer effects concomitant with HDACi along with potent chemotoxic effects inherent to other anticancer agents. A dual targeted agent of this type could broadly arrest cancer proliferation through multiple pathways, achieving greater efficacy than a highly selective inhibitor. Moreover, nucleosomal relaxation conferred by inhibition of nuclear HDACs could be used to potentiate DNA-binding anticancer agents.[100] The association of nuclear HDACs with Topoisomerase II (Topo II) *in vivo*[101] offers a unique opportunity to harness the potent activity of anthracyclines and the broad effects of HDACi in a single, multi-targeted drug.

Both of these approaches represent novel targeted HDACi-based strategies aimed at overcoming the clinical inefficacy of HDACi and creating more potent, multifunctional drugs. To this end, I will document in this thesis the profiling and biological activities of four new classes of HDACi. (1) aryltriazolylhydroxamate HDACi that potently inhibit HDAC activity and prostate cancer cell growth, (2) dual-targeted inhibitors of Topoisomerase II and HDAC and

(3) dual-targeted inhibitors of Topoisomerase I and HDAC, both of which have potent inhibition against both target enzymes as well as cancer cell lines, and finally (4) macrocyclic HDACi that potently inhibit the growth of lung cancer cell lines and preferentially target lung tissue *in vivo*.

1.7 References

1.) Hartwell, L.H.; Kastan, M.B. Cell cycle control and cancer. *Science*, **1994**, 266, 1821-1828.

2.) Carey, N.; La Thangue, N. B. Histone deacetyalse inhibitors: Gathering pace. *Curr. Opin. Pharmacol.,* **2006**, *6,* 369-375.

3.) Wolffe, A.P.; Matzke, M.A. Epigenetics: regulation through repression. *Science* **1999**, 286, 481-486.

4.) Ropero, S.; Esteller, M. The role of histone deacetylases (HDACs) in human cancer. *Mol. Oncol*., **2007**, 1, 19-25.

5.) Jenuwein, T.; Allis, C.D. Translating the histone code. *Science*, **2001**, 293, 1074-1080.

6.) Strahl, B.D.; Allis, C.D. The language of covalent histone modifications. *Nature*, **2000**, 403, 41-45.

7.) Althaus, F.R.; Höfferer, L; Kleczkowska, H.E.; Malanga, M.; Naegeli, H.; Panzeter, P.L.; Realini, C.A. Histone shuttling by poly ADP-ribosylation. *Mol. Cell. Biochem.*, **1994**, 138, 53-59.

8.) Shiio, Y.; Eisenman, R. N. Histone Sumoylation is Associated with Transcriptional Repression. *Proc. Natl. Acad. Sci. USA,* **2003**, *100*, 13225-13230.

9.) Kuo, M. H.; Allis, C. D. Roles of histone acetyltransferases and deacetylases in gene regulation. *BioEssays,* **1998**, *20*, 615-626.

10.) Grunstein, M. Histone acetylation in chromatin structure and transcription. *Nature*, **1997**, 389, 349-352.

11.) Davie, J.R.; Adcock, I.M.; Ito, K. Multiple functions of dynamic histone deacetylation. *J. Cell. Biochem.*, **1994**, 55, 98-105.

12.) Kuo, M.H.; Allis, C.D. Roles of histone acetyltransferases and deacetylases in gene regulation. *Bioessays*. **1998**, 20, 615-626.

13.) Hong, L.; Schroth, G.P.; Matthews, H.R.; Yau, P.; Bradbury, E.M. Studies of the DNA binding properties of histone H4 amino terminus. Thermal denaturation studies reveal that acetylation markedly reduces the binding constant of the H4 "tail" to DNA. *J. Biol. Chem*. **1993**, 268, 305-324.

14.) Lee, D.Y.; Hayes, J.J.; Pruss, D.; Wolffe, A.P. A positive role for histone acetylation in transcription factor access to nucleosomal DNA. *Cell*. **1993**, 72, 73-84.

15.) Vettese-Dadey, M.; Grant, P.A.; Hebbes, T.R.; Crane-Robinson, C.; Allis, C.D.; Workman, J.L. Acetylation of histone H4 plays a primary role in enhancing transcription factor binding to nucleosomal DNA in vitro. *Embo J.* **1996**, 15, 2508-2518.

16.) Inoue, A.; Fujimoto, D. Enzymatic deacetylation of histone. *Biochem. Biophys. Res. Commun*. **1969**, 36, 146-150.

17.) Yang, X.-J.; Seto, E. The Rpd3/Hda1 family of lysine deacetylases: from bacteria and yeast to mice and men. *Nat. Rev. Mol. Cell Biol*. **2008**, 9, 206-218.

18.) Cadido, E.P.; Reeves, R.; Davie, J.R. Sodium butyrate inhibits histone deacetylation in cultured cells. *Cell*. **1978**, 14, 105-113.

19.) Yoshida, M.; Kijima, M.; Akita, M.; Beppu, T. Potent and specific inhibition of mammalian histone deacetylase both in vivo and in vitro by trichostatin A. J. *Biol. Chem*. **1990**, 265, 17174-17179.

20.) Taunton, J.; Hassig, C.A.; Schreiber, S.L. A mammalian histone deacetylase related to the yeast transcriptional regulator Rpd3p. *Science* **1996**, 272, 408-411.

21.) Vidal, M.; Gaber, R.F. RPD3 encodes a second factor required to achieve maximum positive and negative transcriptional states in Saccharomyces cerevisiae. Mol. Cell *Biol*. **1991**, 11, 6317-6327.

22.) Rundlett, S.E.; Carmen, A.A.; Kobayashi, R.; Bavykin, S.; Turner, B.M.; Grunstein, M. HDA1 and RPD3 are members of distinct yeast histone deacetylase complexes that

regulate silencing and transcription. *Proc. Natl. Acad. Sci. U.S.A.* **1996**, 93, 14503-14508.

23.) Witt, O.; Deubzer, H.E.; Milde, T.; Oehme, I. HDAC family: what are the cancer relevant targets? *Cancer Lett.* **2009**, 277, 8-21.

24.) Humphrey, G.W.; Wang, Y.; Russanova, V.R.; Hirai, T.; Qin, J.; Nakatani, Y.; Howard, B.H. Stable histone deacetylase complexes distinguished by the presence of SANT domain proteins CoRest/kiaa0071 and Mta-L1. *J. Biol. Chem.* **2001**, 276, 6817-6824.

25.) You, A.; Tong, J.K.; Grozinger, C.M.; Schreiber, S.L. CoRest in an integral component of the CoRest-human histone deacetylase complex. *Proc. Natl. Acad. Sci. U.S.A.* **2001**, 98, 1454-1458.

26.) Xue, Y.; Wong, J.; Moreno, G.T.; Young, M.K.; Côté, J.; Wang, W. NURD, a novel complex with both ATP-dependent chromatin-remodeling and histone deacetylase activities. *Mol. Cell.* **1998**, 2, 851-861.

27.) Heinzel, T.; Lavinsky, R.M.; Mullen, T.M.; Soderstrom, M.; Laherty, C.D.; Torchia, J.; Yang, W.M.; Brard, G.; Ngo, S.D.; Davie, J.R.; Seto, E.; Eisenman, R.N.; Rose, D.W.; Glass, C.K.; Rosenfield, M.G. A complex containing N-CoR, mSin3 and histone deacetylase mediates transcriptional repression. *Nature.* **1997**, 387, 43-48.

28.) Alland, L.; David, G.; Shen-Li, H.; Potes, J.; Muhle, R.; Lee, H.-C.; Hou, Jr., H.; Chen, K.; DePinho, R.A. Identification of mammalian Sds3 as an integral component of the Sin3/histone deacetylase corepressor complex. *Mol. Cell Biol.* **2002**, 22, 2743-2750.

29.) Guenther, M.G.; Lane, W.S.; Fischle, W.; Verdin, E.; Lazar, M.A.; Shiekhattar, R. A core SMRT corepressor complex containing HDAC3 and TBL1, a WD40-repeat protein linked to deafness. *Genes Dev*. **2000**, 14, 1048-1057.

30.) Wen, Y.-D.; Perissi, V.; Staszewski, L.M.; Yang, W.-M.; Krones, A.; Glass, C.K.; Rosenfeld, M.G.; Seto, E. The histone deacetylase-3 complex contains nuclear receptor corepressors. *Proc. Natl. Acad. Sci. U.S.A*. **2000**, 97, 7202-7207.

31.) Grozinger, C.M.; Schreiber, S.L. Regulation of histone deacetylase 4 and 5 and transcriptional activity by 14-3-3-dependent cellular localization. *Proc. Natl. Acad. Sci. U.S.A*. **2000**, 97, 7835-7840.

32.) Kao, H.Y.; Verdel, A.; Tsai, C.C.; Simon, C.; Juguilon, H.; Khochbin, S. Mechanism for nucleocytoplasmic shuttling of histone deacetylase 7. *J. Biol. Chem*. **2001**, 276, 47496-47507.

33.) McKinsey, T.A.; Zhang, C.L.; Lu, J.; Olsen, E.N. Signal-dependent nuclear export of a histone deacetylase regulates muscle differentiation. *Nature*. **2000**, 408, 106-111.

34.) Vega, R.B.; Harrison, B.C.; Meadows, E.; Roberts, C.R.; Papst, P.J.; Olsen, E.N.; McKinsey, T.A. Protein kinases C and D mediate agonist-dependent cardiac hypertrophy through nuclear export of histone deacetylase 5. *Mol. Cell Biol*. **2004**, 24, 8374-8385.

35.) Kim, M.A.; Kim, H.J.; Brown, A.L.; Lee, M.Y.; Bae, Y.S.; Park, J.I.; Kwak, J. Y.; Chung, J.H.; Yun, J. Identification of novel substrates for human checkpoint kinase Chk1 and Chk2 through genome-wide screening using a consensus Chk phosphorylation motif. *Exp. Mol. Med*. **2007**, 39, 205-212.

36.) Zhang, Y.; Li, N.; Caron, C.; Matthias, G.; Hess, D.; Khochbin, S.; Matthias, P. HDAC-6 interacts with and deacetylates tubulin and microtubules in vivo. *Embo J.* **2003**, 22, 1168-1179.

37.) Hubbert, C.; Guardiola, A.; Shao, R.; Kawaguchi, Y.; Ito, A.; Nixon, A. HDAC6 is a microtubule-associated deacetylase. *Nature*. **2002**, 417, 455-458.

38.) Tong, J.J.; Liu, J.; Bertos, N.R.; Yang, X.J. Identification of HDAC10, a novel class II human histone deacetylase containing leucine-rich domain. *Nucleic Acids Res*. **2002**, 30, 1114-1123.

39.) Villagra, A.; Cheng, F.; Wang, H.W.; Suarez, I.; Glozak, M.; Maurin, M.; Nguyen, D.; Wright, K.L.; Atadja, P.W.; Bhalla, K.; Pinilla-Ibarz, J.; Seto, E.; Sotomayor, E.M. The histone deacetylase HDAC11 regulates the expression of interleukin 10 and immune tolerance. *Nat. Immunol*. **2009**, 10, 92-100.

40.) Gao, L.; Cueto, M.A.; Asselbergs, F.; Atadja, P. Cloning and functional characterization of HDAC11, a novel member of the human histone deacetylase family. *J. Biol. Chem.* **2002**, 277, 25748-25755.

41.) Vannini, A.; Volpari, C.; Filocamo, G.; Casavola, E.C.; Brunetti, M.; Renzoni, D.; Chakravarty, P.; Paolini, C.; De Francesco, R.; Gallinari, P.; Steinkühler, C.; Di Marco, S. Crystal structure of a eukaryotic zinc-dependent histone deacetylase, human HDAC8, complexed with a hydroxamic acid inhibitor. *Proc. Natl. Acad. Sci. U.S.A.* **2004**, 101, 15064-15069.

42.) Watson, P.J.; Fairall, L.; Santos, G.M.; Schwabe, J.W. Structure of HDAC3 bound to co-repressor and inositol tetraphosphate. *Nature*. **2012**, 481, 335-340.

43.) Bressi, J.C.; Jennings, A.J.; Skene, R.; Wu, Y.; Melkus, R.; De Jong, R.; O'Connell, S.; Grimshaw, C.E.; Navre, M.; Gangloff, A.R. Exploration of the HDAC2 foot pocket: Synthesis and SAR of substituted N-(2-aminophenyl)benzamides. *Bioorg Med. Chem. Lett*. **2010**, 20, 3142-3145.

44.) Bottomley, M.J.; Lo Surdo, P.; Di Giovine, P.; Cirillo, A.; Scarpelli, R.; Ferrigno, F.; Jones, P.; Neddermann, P.; De Francesco, R.; Steinkuhler, C.; Gallinari, P.; Carfi, A. Structural and functional analysis of the human HDAC4 catalytic domain reveals a regulatory structural zinc-binding domain. *J. Biol. Chem*. **2008**, 283, 26694-26704.

45.) Schuetz, A.; Min, J.; Allali-Hassani, A.; Schapira, M.; Shuen, M.; Loppnau, P.; Mazitschek, R.; Kwiatkowski, N.P.; Lewis, T.A.; Maglathin, R.L.; McLean, T.H.; Bochkarev, A.; Plotnikov, A.N.; Vedadi, M.; Arrowsmith, C.H. Human HDAC7 harbors a class IIa histone deacetylase-specific zinc binding motif and cryptic deacetylase activity. *J. Biol. Chem*. **2008**, 283, 11355-11363.

46.) Finnin, M.S.; Donigian, J.R.; Cohen, A.; Richon, V.M.; Rifkind, R.A.; Marks, P.A; Breslow, R.; Pavletich, N.P. Structures of a histone deacetylase homologue bound to the TSA and SAHA inhibitors. *Nature* **1999**, 401, 188-193.

47.) Krennhrubec, K.; Marshall, B.L.; Hedglin, M.; Verdin, E.; Ulrich, S.M. Design and evaluation of "Linkerless" hydroxamic acids as selective HDAC8 inhibitors. *Bioorg. Med. Chem. Lett.* **2007**, 17, 2876-2878.

48.) Kadosh, D.; Struhl, K. Histone deacetylase activity of Rpd3 is important for transcriptional repression in vivo. *Genes Dev*. **1998**, 12, 797-805.

49.) Fenrick, R.; Hiebert, S.W. Role of histone deacetylases in actue leukemia. *J. Cell Biochem. Suppl*. **1998**, 30-31, 194-202.

50.) Pandolfi, P.P. Transcriptional therapy for cancer. *Oncogene*. **2001**, 20, 3116-3127.

51.) Brehm, A.; Miska, E.A.; McCance D.J.; Reid, J.L.; Bannister, A.J.; Kouzarides, T. Retinoblastoma protein recruits histone deacetylase to repress transcription. *Nature*. **1998**, 391, 597-601.

52.) Dhordain, P.; Quief, S.; Lantoine, D.; Kerckaert, J.-P.; Albagli, O. The LAZ3(BCL-6) oncoprotein recruits SMRT/mSIN3A/histone deacetylase containing complex to mediate transcriptional repression. *Nucleic Acids Res*. **1998**, 26, 4645-4651.

53.) Haberland, M.; Johnson, A.; Mokalled, M.H.; Montgomery, R.L.; Olsen, E.N. Genetic dissection of histone deacetylase requirement in tumor cells. *Proc. Natl. Acad. Sci. U.S.A*. **2009**, 106, 7751-7755.

54.) Glaser, K.B.; Li, J.; Staver, M.J.; Wei, R.Q.; Albert, D.H.; Davidsen, S.K. Role of class I and class II histone deacetylases in carcinoma cells using siRNA. *Biochem. Biophys. Res. Commun*. **2003**, 310, 529-536.

55.) Senese, S.; Zaragoza, K.; Minardi, S.; Muradore, I.; Ronzoni, S.; Passafaro, A.; Bernard, L.; Draetta, G.F.; Alcalay, M.; Seiser, C.; Chiocca, S. Role for histone deacetylase 1 in human tumor cell proliferation. *Mol. Cell Biol*. **2007**, 27, 4784-4795.

56.) Halkidou, K.; Gaughan, L.; Cook, S.; Leung, H.Y.; Neal, D.E.; Robson, C.N. Upregulation and nuclear recruitment of HDAC1 in hormone refractory prostate cancer. *Prostate*. **2004**, 59, 177-189.

57.) Huang, B.H.; Laban, M.; Leung, C.H.; Lee, L.; Lee, C.K.; Salto-Tellez, M.; Raju, G.C.; Hooi, S.C. Inhibition of histone deacetylase 2 increases apoptosis and p21Cip1/WAF1 expression, independent of histone deacetylase 1. *Cell Death Differ*. **2005**, 12, 395-404.

58.) Harms, K.L.; Chen, X. Histone deacetylase 2 modulates p53 transcriptional activities through regulation of p53-DNA binding activity. *Cancer Res*. **2007**, 67, 3145-3152.

59.) Atsumi, A.; Tomita, A.; Kiyoi, H.; Naoe, T. Histone deacetylase 3 (HDAC3) is required to target promoters by PML-RARalpha as a component of the N-CoR co-repressor complex to repress transcription in vivo. *Biochem. Biophys. Res. Commun*. **2006**, 345, 1471-1480.

60.) Balasubramanian, S.; Ramos, J.; Luo, W.; Sirisawad, M.; Verner, E.; Buggy, J.J. A novel histone deacetylase 8 (HDAC8)-specific inhibitor PCI-34051 induces apoptosis in T-cell lymphomas. *Leukemia*. **2008**, 22, 1026-1034.

61.) Papeleu, P.; Vanhaecke, T.; Elaut, G.; Vinken, M.; Henkens, T.; Snykers, S.; Rogiers, V. Differential effects of histone deacetylase inhibitors in tumor and normal cells-what is the toxicological relevance? *Crit. Rev. Toxicol*. **2005**, 35, 363.

62.) (a) Butler, L.M.; Agus, D.B.; Scher, H.I.; Higgins, B.; Rose, A.; Cordon-Cardo, C.; Thaler, H.T.; Rifkind, R.A.; Marks, P.A.; Richon, V.M. Suberoylanilide hydroxamic acid, an inhibitor of histone deacetylase, suppresses the growth of prostate cancer cells in

vitro and in vivo. *Cancer Res*. **2000**, 60, 5165-5170. (b) Kelly, W.K.; O'Connor, O.A.; Marks, P.A. Histone deacetylase inhibitors: from target to clinical trials. *Expert Opin. Instig. Drugs*. **2002**, 11, 1695-1713.

63.) Munster, P.N.; Troso-Sandoval, T.; Rosen, N.; Rifkind, R.; Marks, P.A.; Richon, V.M. The histone deacetylase inhibitor suberoylanilide hydroxamic acid induces differentiation in human breast cancer cells. *Cancer Res*. **2001**, 61, 8492-8497.

64.) Deroanne, C.F.; Bonjean, K.; Servotte, S.; Devy, L.; Colige, A.; Clausse, N.; Blacher, S.; Verdin, E.; Foidart, J.M.; Nusgens, B.V.; Castronovo, V. Histone deacetylases inhibitors as anti-angiogenic agents altering vascular endothelial growth factor signaling. *Oncogene*. **2002**, 21, 427-436.

65.) Butler, L.M.; Agus, D.B.; Scher, H.I.; Higgins, B.; Rose, A.; Cordon-Cardo, C.; Thaler, H.T.; Rifkind, R.A.; Marks, P.A.; Richon, V.M. Suberoylanilide hydroxamic acid, an inhibitor of histone deacetylase, suppresses the growth of prostate cancer cells in vitro and in vivo. *Cancer Res*. **2000**, 60, 5165-5170.

66.) Qiu, L.; Kelso, M.J.; Hansen, C.; West, M.L.; Fairlie, D.P.; Parsons,P.G. Anti-tumour activity in vitro and in vivo of selective differentiating agents containing hydroxamate. *Br. J. Cancer*. **1999**, 80, 1252-1258.

67.) Richon, V.M.; Sandhoff, T.W.; Rifkind, R.A.; Marks, P.A. Histone deacetylase inhibitor selectively induces $p21^{WAF1}$ expression and gene-associated histone acetylation. *Proc. Natl. Acad. Sci. U.S.A.* **2000**, 97, 10014-10019.

68.) Sambucetti, L.C.; Fischer, D.D.; Zabludoff, S.; Kwon, P.O.; Chamberlin, H.; Trogani, N.; Xu, H.; Cohen, D. Histone deacetylase inhibition selectively alters the activity and

expression of cell cycle proteins leading to specific chromatin acetylation and antiproliferative effects. *J. Biol. Chem.* **1999**, 274, 34940-34947.

69.) (a) Marks, P.; Rifkind, R.A.; Richon, V.M.; Breslow, R.; Miller, T.; Kelly, W.K. Histone deacetylases and cancer: causes and therapies. *Nat. Rev. Cancer.* **2001**, 1, 194-202. (b) Gu, W.; Roeder, R.G. Acetylation of p53 sequence-specific DNA by acetylation of the p53 C-terminal domain. Cell. 1997, 90, 595-606. (c) Martinez-Balbas, M.A.; Bauer, U.M.; Nielsen, S.J.; Brehm, A.; Kouzarides, T. Regulation of E2F1 activity by acetylation. Embo J. 2000, 19, 662-671. (d) Marzio, G.; Wagener, C.; Gutierrez, M.L.; Cartwright, P.; Helin, K.; Giacca, M. E2F family members are differentially regulated by reversible acetylation. *J. Biol. Chem.* **2000**, 275, 10887-10892. (e) Kovacs, J.J.; Murphy, P.J.; Gaillard, S.; Zhao, X.; Wu, J.T.; Nicchitta, C.V.; Yoshida, M.; Toft, D.O.; Pratt, W.B.; Yao, T.P. HDAC6 regulates Hsp90 acetylation and chaperone-dependent activation of glucocorticoid receptor. *Mol. Cell* **2005**, 18, 601-607.

70.) Coffey, D.C.; Kutko, M.C.; Glick, R.D.; Butler, L.M.; Heller, G.; Rifkind, R.A.; Marks, P.A.; Richon, V.M.; LaQuaglia, M.P. The histone deacetylase inhibitor, CBHA, inhibits growth of human neuroblastoma xenografts in vivo, alone and synegeristically with All-Trans Retinoic Acid. *Cancer Res.* **2001**, 61, 3591-3594.

71.) Richon, V.M.; Emiliani, S.; Verdin, E.; Webb, Y.; Breslow, R.; Rifkind, R.A.; Marks, P.A. A class of hybrid polar inducers of transformed cell differentiation inhibits histone deacetylases. *Proc. Natl. Acad. Sci. U.S.A.* **1998**, 95, 3003-3007.

72.) Brinkmann, H.; Dahler, A.L.; Popa, C.; Serewko, M.M.; Parsons, P.G.; Gabrielli, B.G.; Burgess, A.J.; Saunders, N.A. Histone hyperacetylation induced by histone deacetylase inhibitors is not sufficient to cause growth inhibition in human dermal fibroblasts. *J. Biol. Chem*. **2001**, 276, 22491-22499.

73.) Kelly, W.K.; Richon, V.M.; O'Connor, O.; Curley, T.; MacGregor-Curtelli, B.; Tong, W.; Klang, M.; Schwartz, L.; Richardson, S.; Rosa, E.; Drobnjak, M.; Cordon-Cordo, C.; Chiao, J.H.; Rifkind, R.; Marks, P.A.; Scher, H. Phase I clinical trial of histone deacetylase inhibitor: suberoylanilide hydroxamic acid administered intravenously. *Clin. Cancer Res*. **2003**, 9, 3578-3588.

74.) Kelly, W.K.; O'Connor, O.A.; Krug, L.M.; Chiao, J.H.; Heaney, M.; Curley, T.; MacGregor-Cortelli, B.; Tong, W.; Secrist, J.P.; Schwartz, L.; Richardson, S.; Chu, E.; Olgac, S.; Marks, P.A.; Scher, H.; Richon, V.M. Phase I study of an oral histone deacetylase inhibitor, suberoylanilide hydroxamic acid, in patients with advanced cancer. *J. Clin. Oncol*. **2005**, 23, 3923-3931.

75.) Duvic, M.; Talpur, R.; Ni, X.; Zhang, C.; Hazarika, P.; Kelly, C.; Chiao, J.H.; Reilly, J.F.; Ricker, J.L.; Richon, V.M.; Frankel, S.R. Phase 2 trial of oral vorinostat (suberoylanilide hydroxamic acid, SAHA) for refractory cutaneous T-cell lymphoma (CTCL). *Blood*. **2007**, 109, 31-39.

76.) Piekarz, R. L.; Robey, R.; Sandor, V.; Bakke, S.; Wilson, W. H.; Dahmoush, L.; Kingma, D. M.; Turner, M. L.; Altemus, R.; Bates, S. E. Inhibitor of histone deacetylation,

depsipeptide (FR901228), in the treatment of peripheral and cutaneous T-cell lymphoma: a case report. *Blood*. **2001**, 98, 2865-2868.

77.) Sandor, V.; Bakke, S.; Robey, R. W.; Kang, M. H.; Blagosklonny, M. V.; Bender, J.; Brooks, R.; Piekarz, R. L.; Tucker, E.; Figg, W. D.; Chan, K. K.; Goldspiel, B.; Fojo, A. T.; Balcerzak, S. P.; Bates, S. E. Phase I trial of the histone deacetylase inhibitor, depsipeptide (FR901228, NSC 630176), in patients with refractory neoplasms. *Clin. Cancer Res.,* **2002**, *8*, 718-728.

78.) Harrison, S. J.; Quach, H.; Yuen, K. High response rates with the combination of bortezomib, dexamethasone and the pan-histone deacetylase inhibitor romidepsin in patients with relapsed or refractory multiple myeloma in a phase I/II clinical trial. *ASH Ann. Meet. Abstr.,* **2008**, *112*, 3698.

79.) Doss, H. H.; Jones, S. F.; nfante, J. R.; Spigel, D. R.; Willcutt, N.; Lamar, R.; Barton, J.; Keegan, M.; Burris III, H. A. A phase I trial of romidepsin in combination with gemcitabine in patients with pancreatic and other advanced solid tumors. *J. Clin. Oncol.,* **2008**, *26*(15S), 2567.

80.) Whitehead, R. P.; Rankin, C.; Hoff, P. M.; Gold, P. J.; Billingsley, K. G.; Chapman, R. A.; Wong, L.; Ward, J. H.; Abbruzzese, J. L.; Blanke, C. D. Phase II Trial of romidepsin (NSC-630176) in previously treated colorectal cancer patients with advanced disease: a southwest oncology group study (S0336). *Invest. New Drugs,* **2008**, *27*, 469-475.

81.) Byrd, J. C.; Marcucci, G.; Parthun, M. R.; Xiao, J. J.; Klisovic, R. B.; Moran, M.; Lin, T. S.; Liu, S.; Sklenar, A. R.; Davis, M. E.; Lucas, D. M.; Fischer, B.; Shank, R.; Tejaswi, S. L.; Binkley, P.; Wright, J.; Chan, K. K.; Grever, M. R. A phase 1 and pharmacodynamic

study of depsipeptide (FK228) in chronic lymphocytic leukemia and acute myeloid leukemia. *Blood,* **2005**, *105*, 959-967.

82.) Schrump, D. S.; Fischette, M. R.; Nguyen, D. M.; Zhao, M.; Li, X.; Kunst, T. F.; Hancox, A.; Hong, J. A.; Chen, G. A.; Kruchin, E.; Wright, J. J.; Rosing, D. R.; Sparreboom, A.; Figg, W. D.; M. S. S. Clinical and molecular responses in lung cancer patients receiving romidepsin. *Clin. Cancer Res.,* **2008**, *14,* 188-198.

83.) Klimek, V. M.; Fircanis, S.; Maslak, P.; Guernah, I.; Baum, M.; Wu, N.; Panageas, K.; Wright, J. J.; Pandolfi, P. P.; Nimer, S. D. Tolerability, pharmacodynamics, and pharmacokinetics studies of depsipeptide (romidepsin) in patients with acute myelogenous leukemia or advanced myelodysplastic syndromes. *Clin. Cancer Res.,* **2008**, *14*, 826-832.

84.) Shah, M. H.; Binkley, P.; Chan, K.; Xiao, J.; Arbogast, D.; Collamore, M.; Farra, Y.; Young, D.; Grever, M. Cardiotoxicity of histone deacetylase inhibitor depsipeptide in patients with metastatic neuroendocrine tumors. *Clin. Cancer Res.,* **2006**, *12*, 3997-4003.

85.) Molife, L. R.; Attard, G.; Fong, P. C.; Karavasilis, V.; Reid, A. H.; Patterson, S.; Riggs Jr, C. E.; Higano, C.; Stadler, W. M.; McCulloch, W.; Dearnaley, D.; Parker, C.; de Bono, J. S. Phase II, two-stage, single-arm trial of the histone deacetylase inhibitor (HDACi) romidepsin in metastatic castration-resistant prostate cancer (CRPC). *Ann. Oncol.,* **2009**, *21*, 109-113.

86.) Shah, M. H.; Villalona-Calero, M. A.; Marcucci, G.; Byrd, J.C.; Grever, M.R. HDAC inhibitors and cardiac safety. *Clin. Cancer Res.,* **2007**, *13,* 1068.

87.) Prince, H. M.; Bishton, M. J.; Harrison, S. J. Clinical studies of histone deacetylase inhibitors. *Clin. Cancer Res.,* **2009**, *15*, 3958-3969.

88.) http://www.fda.gov/NewsEvents/Newsroom/PressAnnouncements/ucm 189629.htm, **2009**.

89.) Vansteenkiste, J.; Van Cutsem, E.; Dumez, H.; Chen, C.; Ricker, J.L.; Randolph, S.S.; Schöffski, P. Early phase II trial of oral vorinostat in relapsed or refractory breast, colorectal, or non-small cell lung cancer. Invest. New Drugs. 2008, 26, 483-488.

90.) Woyach, J.A.; Kloos, R.T.; Ringel, M.D.; Arbogast, D.; Collamore, M.; Zwiebel, J.A.; Grever, M.; Villalona-Calero, M.; Shah, M.H. Lack of therapeutic effect of the histone deacetylase inhibitor vorinostat in patients with metastatic radioiodine-refractory thyroid cancer. J. Clin. Endocrinol. Metab. 2009, 94, 164-170.

91.) Eyüpoglu, I.Y.; Hahnen, E.; Tränkle, C.; Savaskan, N.E.; Siebzehnrübl, F.A.; Buslei, R.; Lemke, D.; Wick, W.; Fahlbusch, R.; Blümcke, I. Experimental therapy of malignant gliomas using the inhibitor of histone deacetylase MS-275. *Mol. Cancer Ther.* **2006**, 5, 1248-1255.

92.) Botti, E.; Mercurio, C.; Spallone, G.; Di Stefani, A.; Gabellini, M.; Orlandi, A.; Chimenti, S.; Minucci, S.; Costanzo, A., Histone deacetylases as new therapeutical targets for the treatment of Non-Melanoma Skin Cancer: results of phase I/IIa trial with topical DAC060. *J. Invest. Dermatol.* **2011,***131*, S46-S46.

93.) De Souza, R.; Zahedi, P.; Allen, C. J.; Piquette-Miller, M., Polymeric drug delivery systems for localized cancer chemotherapy. *Drug Deliv.* **2010,***17* (6), 365-375.

94.) National Cancer Institute (NCI). Topical Romidepsin in Treating Patients With Stage I or Stage II Cutaneous T-Cell Non-Hodgkin's Lymphoma. In: ClinicalTrials.gov [Internet].

Bethesda (MD): National Library of Medicine (US). 2000- [cited 2011 October 11]. Available from: http://clinicaltrials.gov/show/NCT00477698 NLM Identifier: NCT00477698.

95.) Arap, W.; Pasqualini, R.; Ruoslahti, E. Cancer treatment by a targeted drug delivery to tumor vasculature in a mouse model. *Science*. **1998**, 279, 377-380.

96.) Gabizon, A.; Catane, R.; Uziely, B.; Kaufman, B.; Safra, T.; Cohen, R.; Martin, F.; Huang, A.; Barenholz, Y. Prolonged circulation time and enhanced accumulation in malignant exudates of doxorubicin encapsulated in polyethylene-glycol coated liposomes. *Cancer Res*. **1994**, 54, 987-992.

97.) Mamot, C.; Drummond, D.C.; Noble, C.O.; Kallab, V.; Guo, Z.; Hong, K.; Kirpotin, D.B.; Park, J.W. Epidermal growth factor receptor-targeted immunoliposomes significantly enhance the efficacy of multiple anticancer drugs in vivo. *Cancer Res*. **2005**, 65, 11631-11638.

98.) Allen, T.M.; Cullis, P.R. Drug delivery systems: entering the mainstream. *Science*. **2004**, 303, 1818-1822.

99.) (a) Montero, A.; Beierle, J.M.; Olsen, C.A.; Ghadiri, M.R. Design, synthesis, biological evaluation, and structural characterization of potent histone deacetylase inhibitors based on cyclic alpha/beta-tetrapeptide architectures. *J. Am. Chem. Soc*. **2009**, 131, 3033-3041. (b) Oyelere, A.K.; Chen, P.C.; Guerrant, W.; Mwakwari, S.C.; Hood, R.; Zhang, Y.; Fan, Y. Non-peptide macrocyclic histone deacetylase inhibitors. *J. Med. Chem*. **2009**, 52, 456-468. (c) Furumai, R.; Komatsu, Y.; Nishino, N.; Khochbin, S.; Yoshida, M.; Horinouchi, S. Potent histone deacetylase inhibitors built from trichostatin A and

cyclic tetrapeptide antibiotics including trapoxin. *Proc. Natl. Acad. Sci. U.S.A*. **2001**, 98, 87-92.

100.) Marchion, D.C.; Bicaku, E.; Daud, A.I.; Richon, V.; Sullivan, D.M.; Munster, P.N. Sequence-specific potentiation of topoisomerase II inhibitors by the histone deacetylase inhibitor suberoylanilide hydroxamic acid. *J. Cell Biochem*. **2004**, 92, 223-237.

101.) Tsai, S.C.; Valkov, N.; Yang, W.M.; Gump, J.; Sullivan, D.; Seto, E. Histone deacetylase interacts directly with DNA topoisomerase II. *Nat. Genet*. **2000**, 26, 349-353.

CHAPTER 2

Linear Aryltriazolyl HDAC Inhibitors

The promise of HDAC inhibitors is due largely to their ability to broadly arrest cancer growth of nearly all transformed cell types through mechanisms including cell cycle arrest, differentiation, inhibition of angiogenesis, and apoptosis.[1,2] Recent validation through the FDA approvals of suberoylanilide hydroxamic acid (SAHA) and depsipeptide (FK-228) has underscored the promise of HDAC inhibitors as a viable treatment option.[3] Both are treatment options for cutaneous T-cell lymphoma, a debilitating hematological malignancy. In spite of the success of these HDACi, there are still questions over the viability of HDACi as a treatment option, specifically against solid tumors.[4] Consequently, much of the current research focuses on improving the pharmacokinetic and pharmacodynamic properties of current HDACi. The classical HDACi pharmacophore consists of three structural motifs: a zinc-binding group (ZBG), a hydrophobic linker, and a surface recognition cap group (Figure 2-1a). The ZBG interacts with the Zn^{2+} ion at the base of the active channel[5], while the linker group fills the channel, and the cap group interacts with surface residues near the rim of the channel. The most common ZBG for HDACi is the hydroxamate group. Several modifications of the ZBG have yielded other modestly successful groups, such as benzamides, α-ketoesters, electrophilic ketones, mercaptoamide, and phosphonates.[6] Consequently, the cap group has become an attractive feature to modify in order to generate more potent and selective HDACi.

2.1 Design of Aryltriazolylhydroxamates

Current HDACi surface recognition groups are linked to the linker group through hydrogen bond acceptor and donor groups, such as keto and amide groups (Figure 2-1b). The lack of preference seen in the diversity of these HDACi suggests that more pharmacokinetically/ pharmacodynamically desirable and more synthetically tractable groups could be incorporated to simplify the molecular design and creation of novel HDACi. It was proposed that the 1,2,3-triazole group could be a good candidate for an isostere of the keto and amide linker groups and facilitate better inhibition through increased hydrogen bonding.[7]

(a)

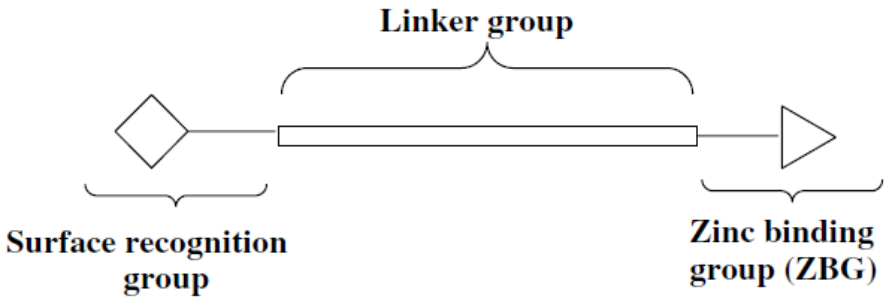

(b)

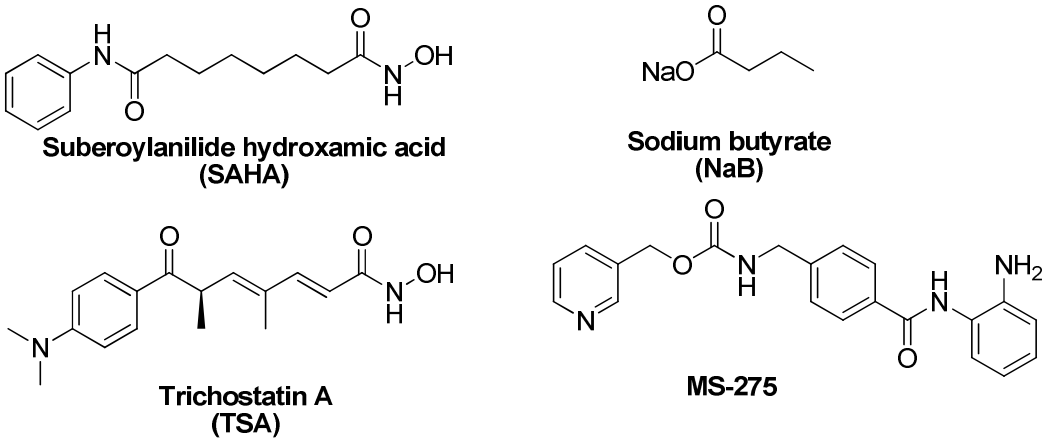

Figure 2-1: Classical HDACi pharmacophore (**a**) and selected examples of current HDACi (**b**).

2.2 In Vitro HDAC Inhibition by SAHA-like Aryltriazolylhydroxamates

Initial synthesis was carried out using the structure of SAHA as a template in order to directly compare the effects of replacement of the amide linker with a triazole group in SAHA-like aryltriazolylhydroxamates (Table 2-1b).[7] In addition to incorporating the triazole group, the methylene linker was also varied in order to better assess the optimal linker chain length for HDAC inhibition. The compound panel was assayed for *in vitro* HDAC inhibition using the Fluor de Lys assay, which uses HeLa nuclear extract as a source of HDAC enzymes, specifically class I HDACs 1 and 2, in conjunction with a fluorescent acetyl-lysine substrate. Compound **4a** had no discernable HDAC inhibition, while **4b-4d** showed a linker length-dependent anti-HDAC activity. In order to investigate the effects of triazole ring replacement, inhibition values for SAHA were compared to **4c**, which most closely approximates the length of SAHA. This revealed a 4.5 fold potentiation in HDAC inhibition compared to SAHA. Moreover, an extension of the linker by one methylene group (**4d**) further increased the potency over six fold compared to SAHA. Overall, the nanomolar range of inhibition values showed that the triazole group is not only a viable attachment option for the linker, but also that the ideal linker length is 5 or 6 methylene groups long.

Table 2-1: *In vitro* inhibition data for SAHA-like aryltriazolylhydroxamates.

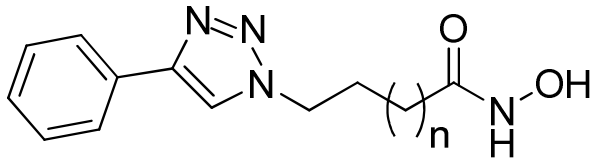

4a-d

Compound	n	IC_{50} (nM)[a]
4a	1	N.D.[b]
4b	2	110.0
4c	3	14.2
4d[c]	4	9.6
SAHA	-	65.0

(a) Half-maximal inhibition values (IC_{50}) were the mean of 3 independent experiments using the Fluor de Lys assay.

(b) N.D. = nondeterminable.

(c) Compound synthesized by Dr. Vishal Patil **4a-c** synthesized by Dr. Bob Chen SAHA and was used as a HDACi control.

In order to further interrogate the potential of triazole-based HDACi, a diverse compound panel was synthesized to evaluate the structure activity relationship (SAR) inherent to substitution of the aromatic the cap group. Linker lengths of five and six methylenes were used following the chain length-dependent inhibition pattern observed in **4a-d**. Introduction of an *N,N*-dimethylamino group, similar to the cap group of TSA (Figure 2-1b), resulted in a five methylene-linked compound that was comparable in HDAC inhibition to TSA (5nM IC_{50}) and 25 fold more active than the corresponding six methylene-linked compound (Table 2-2, comparing **7a** and **7b**). Conversely, nitrogen substitution within the aromatic ring (**7c-f**) did not

increase HDAC inhibition relative to **4c** and **4d**, but HDACi activity did vary depending on the location of the nitrogen substitution with the 2-pyridyl derivative **7e** being the most active. Increasing the linker length of the 2-pyridyl derivative further increased the potency (**7f** vs. **7e**), similar to the trend observed in **4c** and **4d**. Likewise, methyl substitution on the aromatic ring lent a preference toward *ortho* substitution (**7g**-**7i**). Interestingly, this trend is reversed with methoxy substitution on the ring, with *para*-substituted **7j** being the most potent and *ortho* substitution the least (**7j-l**). It is possible that the *para*-substituted preference observed is due to the increased steric bulk of the methoxy group as this trend has been seen in methoxy substitution on SAHA-like HDACi linked through a ketone group.[8] Attenuation in activity was further observed with the bisortho methoxy-substituted compound **7m**, reinforcing the theory that methoxy-substituted compounds are sterically constrained.

Substitution with biphenyl ring systems in compounds **7o-t** demonstrates variable anti-HDAC activity with a 50 fold preference for *meta* substitution of the biphenyl group over para substitution (**7o** vs. **7p**), and *ortho* substitution resulting in the lowest activity. Introduction of nitrogen potentiated *para*-biphenyl compounds with **7s** having nearly identical activity to **7p**, while a clear preference for five methylene linkers was observed, regardless of biphenyl substitution or attachment.

Substitution with fused six-six ring systems including naphthalenes and quinolines also resulted in potent HDACi activities. Parallel with the activities of pyridine compounds **7c-e**, the 2-quinoline derivative **7w** is more active than 7-quinoline analog **7x**, underscoring the selectivity for *ortho*-substitution with aromatic cap groups that contain nitrogen. The marked preference for a five methylene linker in naphthalene compound **7u** over the six methylene-linked **7v** further highlighted the preference for shorter linkers in large cap group compounds.

Table 2-2: *In vitro* HDAC inhibition data for aryltriazolylhydroxamates **7a-y**.

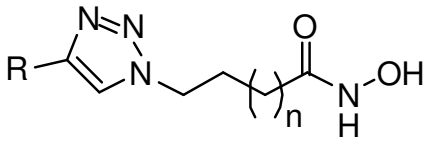

7a-y

Compound	R	n	IC_{50} (nM)	Compound	R	n	IC_{50} (nM)
7a	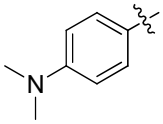	3	4.3	**7n**	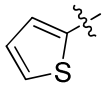	3	31.7
7b	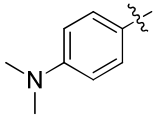	4	106.1	**7o**	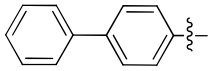	3	52.4
7c		3	287.2	**7p**	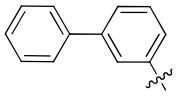	3	1.9
7d	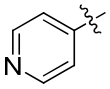	3	112.5	**7q**	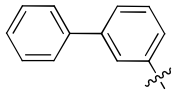	4	5.4
7e	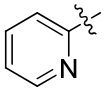	3	67.6	**7r**	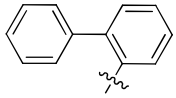	3	162.6
7f	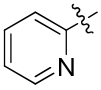	4	23.9	**7s**	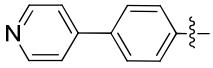	3	2.3
7g	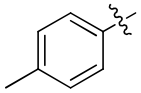	3	43.4	**7t**	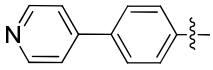	4	16.6
7h	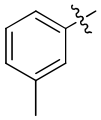	3	31.9	**7u**	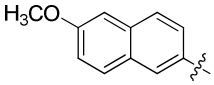	3	1.8
7i	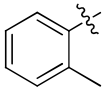	3	17.4	**7v**	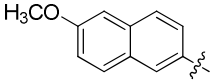	4	15.3
7j	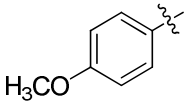	3	2.09	**7w**	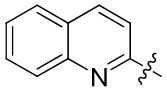	3	2.1

Compound	R	n	IC_{50} (nM)	Compound	R	n	IC_{50} (nM)
7k	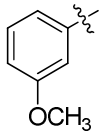	3	13.9	**7x**	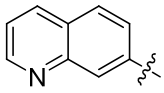	3	151.5
7l	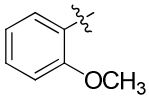	3	76.0	**7y**	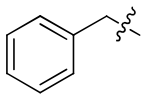	2	N.D.[a]
7m	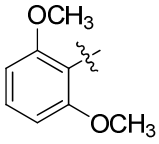	3	315.9	**SAHA**	-	-	65

Compounds synthesized by Dr. Bob Chen and Dr. Vishal Patil

In addition to SAHA, TSA was used as a control, with an IC_{50} of 5 nM.

All data represent the mean value of at least three independent experiments using the Fluor de Lys assay.

[a] N.D., nondeterminable within the tested concentration range (0.5-1000 nM)

Finally, the placement of the triazole ring was shown to be immensely important due to the lack of activity of **7y**. Compounds **4c** and **7y** are isomeric compounds with the same number of carbon atoms separating the cap group and hydroxamate. While **4c** is directly attached to the triazole ring, the triazole of **7y** is displaced toward the hydroxamate by one methylene. The low activity of **7y** demonstrates the importance of the positioning of the triazole ring and offers indirect evidence that the triazole ring plays an active role in binding within the active site channel.

2.2.1 Molecular Docking of Aryltriazolylhydroxamate HDACi

In order to better understand the structural basis of the broad disparity in HDAC inhibition values of aryltriazolylhydroxamates, molecular docking was performed using a validated docking program (AutoDock).[9-11] Compounds were docked with histone deacetylase-like protein (HDLP), chosen due to its high conservation of active site residues relative to class I HDACs.[12] In addition, crystal structures for HDLP bound with the HDACi SAHA and TSA are available for public use. All docking experiments were carried out on AutoDock 3.5 to the specifications of Lu *et al*[11] and the crystal structures of HDLP bound with SAHA and TSA, two known HDACi, are available in the public domain[12], aiding in validation.

SAHA (IC_{50} = 65 nM), **7o** (IC_{50} = 52 nM), **7p** (IC_{50} = 1.9 nM), and **7u** (IC_{50} = 1.8 nM) were all independently docked to HDLP, revealing binding preferences for two different pockets on the enzyme surface (Figure 2-2). Four possible binding pockets have been identified on the surface of HDLP to which binding could enhance inhibition.[10] Compounds **7o** and **7u** bind to the designated pocket 1, while SAHA and **7p** bind to pocket 2. The 1,4-biphenyl ring of **7o** adopted a coplanar orientation in its interaction with pocket 1, presumably with the stacking interactions of pocket 1 directing toward the co-planar geometry. This assumption is reinforced due to the similar orientation adopted by **7u** with its flat, fused six-six ring cap group. Conversely, **7p** adopted a nonplanar conformation with its 1,3-biphenyl cap group in order to bind to pocket 2. Upon closer inspection, the consequence of **7o** adopting the coplanar conformation in pocket 1 is that a kink is introduced into the linker chain. This has the effect of extracting the hydroxamate away from the zinc, offering an explanation for the reduced potency of **7o** compared to the analog **7p**.

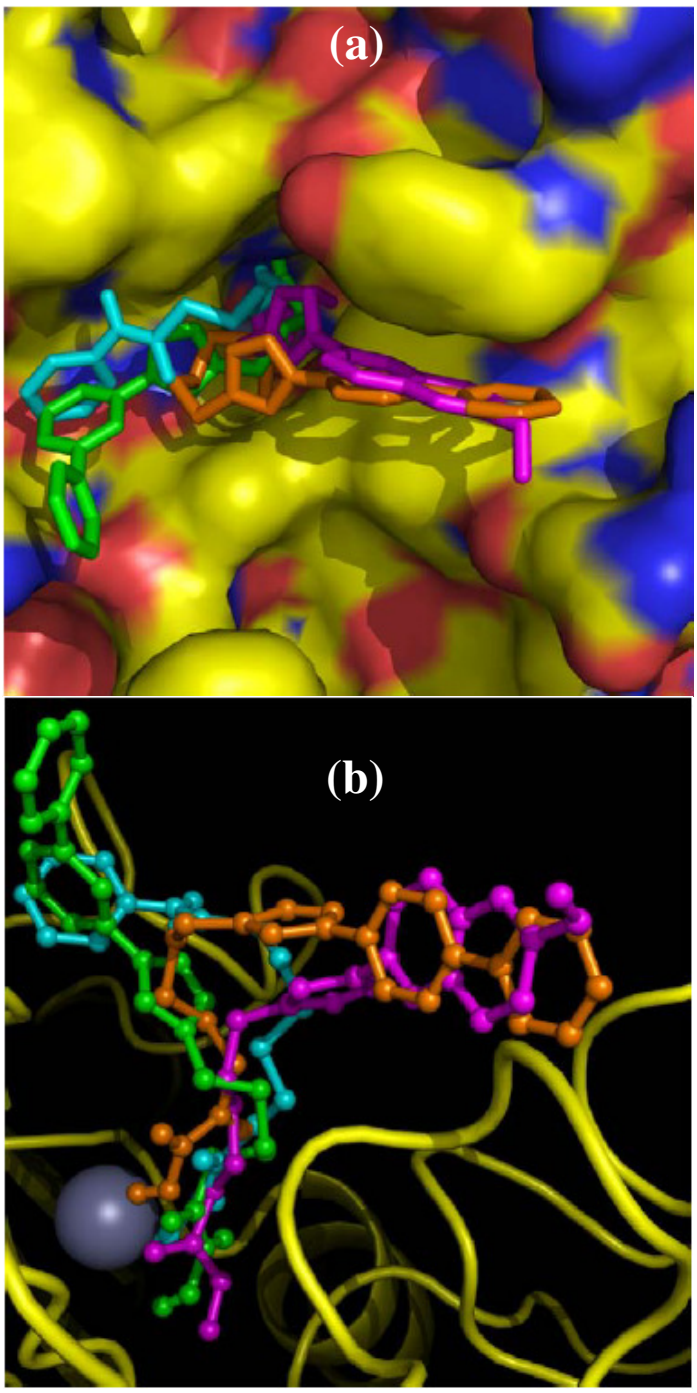

Figure 2-2: Molecular docking of aryltriazolylhydroxamates. SAHA (blue), **7o** (orange), **7p** (green), and **7u** (magenta) to HDLP using AutoDock 3.05, viewed with Pymol. (a) surface of HDLP near the active site; (b) transverse view of aryltriazolylhydroxamates coordinating active site zinc ion with active site residues visible nearby. Docking performed by Dr. Bob Chen.

2.3 Anticancer Activity of Aryltriazolyl HDACi

To screen for the anticancer activity of the aryltriazolyl HDACi, we tested selected compounds against DU-145 prostate cancer cells, a cell line known to respond to HDAC inhibition.[13] Compounds **7s**, **7u**, **7v**, and **7w** were evaluated along with the HDACi standard SAHA using both trypan blue exclusion and the MTS assay to qualitatively and quantitatively measure the effects of compound exposure for 72 hours on cell viability.[14,15] Treatment of DU-145 cells with SAHA gave an IC_{50} measurement around 2.1 μM in close agreement with literature values reported under similar experimental conditions.[16] Compounds **7s**, **7u**, **7v**, and **7w** were selected as lead compounds based on the potency of their inhibition of *in vitro* HDAC activity (Table 2-2). All compounds demonstrated low micromolar IC_{50} values ranging from 2.2 to 8.0 μM, with **7w** inhibiting prostate cancer cell growth at a level near that observed by SAHA. Overall, these results demonstrated the suitability of the triazole ring as a linking moiety in aryltriazolyl HDACi, a novel class of HDAC inhibitors.

2.4 Conclusion

These results have demonstrated the suitability of the 1,2,3-triazole ring as a surface recognition cap group-linking moiety in SAHA-like aryltriazolyl HDACi. A preference for five or six methylene-linker chains was observed in the SAR of these compounds. Moreover, several compounds have been identified that rival or exceed SAHA's *in vitro* HDAC inhibition. A subset of these inhibitors also arrests the growth of DU-145 prostate cancer cells. It is possible that these compounds will also possess enhanced *in vivo* activity compared with HDACi with keto-amide linkages, due to resistance of the triazole to metabolic degradation.[17]

Table 2-3: Cell growth inhibition for lead compounds of the **7** series of HDACi.

Compound	HeLa N.E. IC_{50} (nM)	DU-145 IC_{50}[a] (μM)	DU-145 IC_{50}[b] (μM)
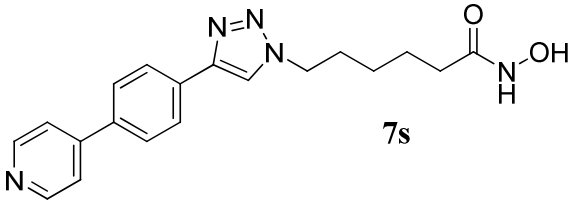 **7s**	2.3	4.72	3.07
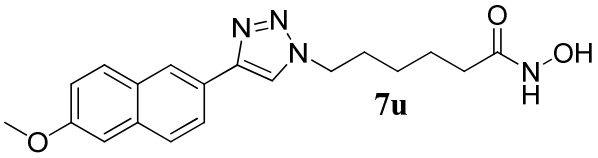 **7u**	1.8	3.95	2.6
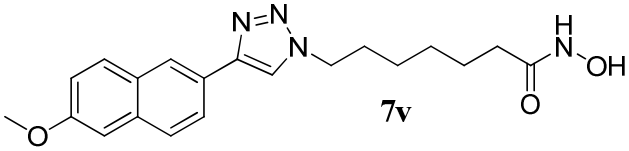 **7v**	15.3	7.76	3.99
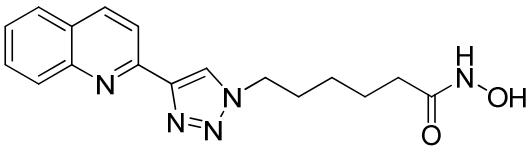 **7w**	2.1	2.25	2.46
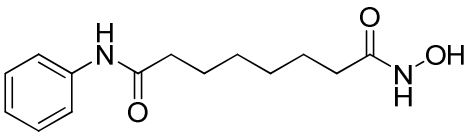 **SAHA**	65.0	2.12	2.11

SAHA was used as a control for all listed values.

[a] Cellular IC_{50} values were determined by trypan blue exclusion.

[b] Cellular IC50 values were determined using the MTS Assay (Promega).

2.5 Experimental Procedures

2.5.1 In Vitro HDAC Inhibition Assay

All inhibitors were screened for HDAC inhibition using the HDAC Fluorescent Activity Assay/Drug Discovery Kit (*Fluor de Lys* AK-500*,* Biomol [now Enzo Biosciences]). All compounds were solubilized in DMSO to a stock concentration of 10mM, from which test dilutions were made in DMSO. All kit reagents were stored at -80°C and thawed on ice shortly before the experiment. All experiments were performed in black 96-well microplates. First, compounds were diluted to 10X test concentrations in distilled water, and 5µl of each test concentration was added to test wells. This was then diluted with 5µl of assay buffer (50 mM Tris-HCl, pH 8.0, 137 mM NaCl, 2.7 mM KCl, 1 mM $MgCl_2$) in each well. Control wells received an equal volume of assay buffer. HeLa extract, as provided, was diluted 30X in assay buffer and 15µl was added to all wells. The fluorogenic substrate was then diluted to 40µM and 25µl was added to all wells and allowed to incubate at room temperature for 15 minutes. HDAC reactions were stopped with 100µl of a developer/TSA mixture. Fluorescence was assayed after 20 minutes at excitation and emission wavelengths of 360 nm and 460 nm, respectively. *In vitro* IC50 values were calculated using a graph of log(concentration) vs. logit(fluorescence).

2.5.2 Cell Viability Experiments

Human prostate carcinoma cells (DU-145 were obtained from the American Type Culture Collection (Manassas, VA). Cultures were grown in Eagles Minimal Medium (EMEM) containing L-glutamine (5 mM), sodium pyruvate (1 mM), sodium bicarbonate (1500 mg/L), and 10% fetal bovine serum. Cell cultures were maintained at 37°C with 5% CO_2. SAHA, and all other HDACi tested were dissolved in DMSO at a stock concentration of 10 mM and stored at -

80°C. Cells were passaged and allowed to grow for 24 hours prior to the addition of compounds. All compounds were diluted to appropriate test concentrations (0.5 – 10 μM) in complete medium and added to cultures for a duration of 72 hours. Viability was assessed by trypan blue exclusion as well as by mitochondrial activity via the MTS Assay (Promega).

2.6 References

1) Marks, P.A.; Richon, V.M.; Rifkind, R.A. Histone deacetylase inhibitors: inducers of differentiation or apoptosis of transformed cells. *J. Natl. Cancer Inst*. **2000**, 92, 1210-1216.

2) Bolden, J.E.; Peart, M.J.; Johnstone, R.W. Anticancer activities of histone deacetylase inhibitors. *Nat. Rev. Drug Disc*. **2006**, 5, 769-784.

3) (a) FDA approves vorinostat (Zolinza) for the treatment of cutaneous manifestations of cutaneous T-cell lymphoma (CTCL) http://www.fda.gov/cder/Offices/OODP/whatsnew/vorinostat.htm (b) www.fda.gov/NewsEvents/Newsroom/PressAnnouncements/2009/ucm189629.htm

4) Garber, K. HDAC inhibitors overcome first hurdle. *Nat. Biotechnol*. **2007**, 25, 17-19.

5) (a) Vannini, A.; Volpari, C.; Filocamo, G.; Casavola, E.C.; Brunetti, M.; Renzoni, D.; Chakravarty, P.; Paolini, C.; De Francesco, R.;Gallinari, P.; Steinkühler, C.; Di Marco, S. Crystal structure of a eukaryotic zinc-dependent histone deacetylase, human HDAC8, complexed with a hydroxamic acid inhibitor. *PNAS*, **2004**, 101, 15064-15069. (b) Somoza, J.R.; Skene, R.J.; Katz, B.A.; Mol, C.; Ho, J.D.; Jennings, A.J.; Luong, C.; Arvai, A.; Buggy, J.J.; Chi, E.; Tang, J.; Sang, B.C.; Verner, E.; Wynands, R.; Leahy, E.M.; Dougan, D.R.; Snell, G.; Navre, M.; Knuth, M.K.; Swanson, R.V.; McRee, D.E.;

Tari, L.W. Structural snapshots of human HDAC8 provide insights into the class I histone deacetylases. *Structure*, **2004**, 12, 1325-1334. (c) Schuetz, A.; Min, J.; Allali-Hassani, A.; Schapira, M.; Shuen, M.; Loppnau, P.; Mazitschek, R.; Kwlatkowski, N.P.; Lewis, T.A.; Maglathin, R.L.; McLean, T.H.; Bochkarev, A.; Plotnikov, A.N.; Vedadi, M.; Arrowsmith, C.H. Human HDAC7 harbors a class IIa histone deacetylase-specific zinc binding motif and cryptic deacetylase activity. *J. Biol. Chem.* **2008**, 283, 11355-11363.

6) Miller, T.A.; Witter, D.J.; Belvedere, S. Histone deacetylase inhibitors. *J. Med. Chem.* **2003**, 46, 5097-5116.

7) Chen, P.C.; Patil, V.; Guerrant, W.; Green, P.; Oyelere, A.K. Synthesis and structure-activity relationship of histone deacetylase (HDAC) inhibitors with triazole-linked cap group. *Bioorg. Med. Chem.* **2008**, 16, 4839-4853.

8) Woo, S.H.; Frechette, S.; Abou Khalil, E.; Bouchain, G.; Vaisburg, A.; Bernstein, N.; Moradei, O.; Leit, S.; Allan, M.; Fournel, M.; Trachy-Bourget, M.C.; Li, Z.; Besterman, J.M.; Delorme, D. Structurally simple trichostatin A-like straight chain hydroxamates as potent histone deacetylase inhibitors. *J. Med. Chem.* **2002**, 45, 2877-2885.

9) Morris, G.M.; Goodsell, D.S.; Halliday, R.S.; Huey, R.; Hart, W.E.; Belew, R.K.; Olson, A.J. Automated docking using a Lamarckian genetic algorithm and empirical binding free energy function. *J. Comput. Chem.* **1998**, 19, 1639-1662.

10) Wang, D.F.; Wiest, O.; Helquist, P.; Lan-Hargest, H.Y.; Wiech, N.L. On the function of the 14 Å long internal cavity of histone deacetylase-like protein: implications for the design of histone deacetylase inhibitors. *J. Med. Chem.* **2004**, 47, 3409-3417.

11) Lu, Q.; Wang, D.S.; Chen, C.S.; Hu, Y.D.; Chen, C.S. Structure-based optimization of phenylbutyrate-derived histone deacetylase inhibitors. *J. Med. Chem*. **2005**, 48, 5530-5535.

12) Finnin, M.S.; Donigian, J.R.; Cohen, A.; Richon, V.M.; Rifkind, R.A.; Marks, P.A; Breslow, R.; Pavletich, N.P. Structures of a histone deacetylase homologue bound to the TSA and SAHA inhibitors. *Nature* **1999**, 401, 188-193.

13) Butler, L.M.; Agus, D.B.; Scher, H.I.; Higgins, B.; Rose, A.; Cordon-Cardo, C; Thaler, H.T.; Rifkind, R.A.; Marks, P.A.; Richon, V.M. Suberoylanilide hydroxamic acid, an inhibitor of histone deacetylase, suppresses the growth of prostate cancer cells *in vitro* and *in vivo*. *Cancer Res*. **2000**, 60, 5165-5170.

14) Mosmann, T. Rapid colorimetric assay for cellular growth and survival: application to proliferation and cytotoxicity assays. *J. Immunol. Methods* **1983**, 65, 55-63.

15) Freshney, R. (1987) Culture of Animal Cells: A Manual of Basic Technique, p. 117, Alan R. Liss, Inc., New York.

16) Suzuki, T.; Nagano, Y.; Kouketsu, A.; Matsuura, A.; Maruyama, S.; Kurotaki, M.; Nakagawa, H.; Miyata, N. Novel inhibitors of human histone deacetylases: design, synthesis, enzyme inhibition, and cancer cell growth inhibition of SAHA-based non-hydroxamates. *J. Med. Chem*. **2005**, 48, 1019-1032.

17) Pedersen, D.S.; Abell, A. 1,2,3-triazoles in peptidomimetic chemistry. *Eur. J. Org. Chem*. **2011**, 13, 2399-2411.

CHAPTER 3

Dual Targeted Inhibitors of Topoisomerase and Histone Deacetylase

Several rational pharmacological strategies, including vaccination, gene therapy, immunotherapy, and new target identification and validation, have emerged for the treatment of metastatic diseases. In spite of this progress, chemotherapy remains the primary treatment option of choice for most cases of cancer. However, nearly all chemotherapeutic agents suffer from severe toxicities, as well as a range of undesirable side effects. To address these problems, the cancer treatment of the future will incorporate, within a single molecule, elements that allow for simultaneous targeting of multiple therapeutic targets, while maintaining lower side effects.[1-3] This realization has continued to spawn immense efforts in the literature. Studies directed toward identifying multivalent ligands that are promising pharmacological agents that may be more efficacious for various human diseases than highly selective single-target drugs are ongoing in several academic and pharmaceutical laboratories.[4-7] A subset of these studies has revealed that balanced modulation of a small number of targets may have superior efficacy and fewer side effects than single-target treatments.[1,7,8]

Epigenetic control has become widely accepted as a mechanism for cellular regulation.[9-11] Specifically, HDAC enzymes have generated much interest in cancer therapeutic literature because of their known associations with many oncogenes and tumor suppressors, leading to altered expression patterns, and have consequently become attractive targets for small-molecule inhibition.[12,13] HDACi have been shown to cause growth arrest, differentiation, and apoptosis in tumor cells and in animal models by inducing histone hyperacetylation and $p21^{waf1}$ expression.[14-17] Additionally, modulation of activities of HDACs alters the activity of a diverse range of

proteins, many of which are attractive therapeutic targets themselves, including p53, E2F, tubulin, and Hsp90.[18-22] HDAC inhibition has been clinically validated as a therapeutic strategy for cancer treatment with the FDA approvals of vorinostat (SAHA) and romidepsin (FK-228) for the treatment of cutaneous T-cell lymphoma.[23-25] However, a large number of the currently known HDACi have elicited only limited in vivo antitumor activities and have not progressed beyond preclinical characterizations.[26-28] HDACi that modulate the functions of additional intracellular targets, other than the various HDAC isoforms, may be able to ameliorate many of the shortcomings of current inhibitors.

3.1 Design of Dual-Targeted Topo II-HDAC Inhibitors

Because of the presence of large hydrophobic patches at the HDAC surface rim,[29,30] it is conceivable that appropriate conjugation of the surface recognition group of a prototypical HDACi to other hydrophobic antitumor pharmacophores could furnish a new class of bifunctional agents. To date, there exist only a few examples of this subtype of bifunctional HDACi-derived compounds.[31-33] Expansion of the repertoire of such bifunctional compounds could lead to broad acting, therapeutically viable anticancer agents.

An attractive starting point for the secondary target is the topoisomerase class of enzymes (Topo I and Topo II), which are validated targets for many small molecule inhibitors including clinically useful anthracyclines such as doxorubicin (DOX) and daunorubicin (DAU) (Figure 3-1) and camptothecins such as irinotecan and topotecan.[34] Topo inhibitors elicit anticancer activities primarily by stabilizing the DNA-enzyme cleavable complex through intercalation between DNA base pairs. However, DNA does not exist as a naked structure in the nucleus. It is noncovalently associated with histones to form the nucleosomes which make up chromatin

subunits. Agents, such as HDACi, that induce hyperacetylation of histone proteins complexed with DNA could increase the accessibility of DNA within chromatin and consequently potentiate the anticancer activities of Topo inhibitors.[35,36] Moreover, recent observations have shown that HDAC1, HDAC2, and Topo II colocalize *in vivo* as part of functionally-coupled complexes.[37,38] This evidence suggests that simultaneous Topo and HDAC inhibition could be a viable alternative approach in cancer therapy.

The following chapter will discuss the design and biological characterization of novel small molecules with dual-acting Topo II-HDAC inhibitory activities. Many of these conjugates inhibit HDAC and Topo II activities more potently than SAHA and daunorubicin, standard HDACi and Topo II inhibitors, respectively. Additionally, a subset of these compounds exhibited potent whole cell antiproliferative activities against representative breast, lung, and prostate cell lines. [Dr. William Guerrant, Dr. Vishal Patil, and Josh Canzoneri contributed to this work equally.]

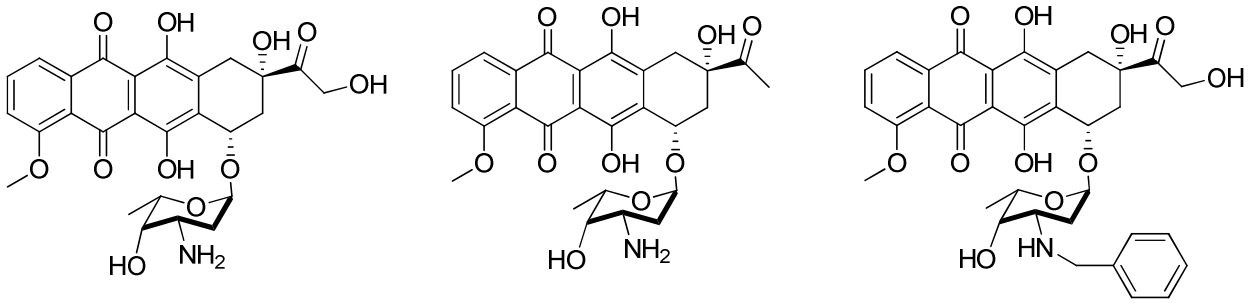

Figure 3-1: Representative structures of anthracyclines.

Anthracyclines are one of the most thoroughly studied classes of anticancer agents, with copious structure-activity relationship (SAR) data to aid in the design and characterization of

new anthracycline-containing compounds.[39-44] Specifically, *N*-benzylated anthracyclines, such as *N*-benzyl doxorubicin (AD-288)[42] (Figure 3-1), have enhanced Topo II inhibition activities, reduced cardiotoxicity, and reduced susceptibility to Pgp-mediated multidrug resistance.[45-47] We postulated that introduction of the HDACi through *N*-benzylation of the daunosamine sugar of DAU would be compatible with Topo II inhibition while possibly engendering the favorable attributes of *N*-benzylated anthracyclines to the resulting conjugates. In turn, the anthracycline moiety could serve two other purposes: (i) as a surface recognition cap group, allowing favorable orientation of the hydroxamic acid within the zinc binding pocket of HDAC, and (ii) as a delivery vehicle for HDACi through the nuclear-directed transport activity observed in interactions between anthracyclines and the proteasome.[43] On this basis, we designed two classes of conjugates: a direct DAU-SAHA conjugate and DAU-triazolyl hydroxamate conjugates (Figure 3-2). The latter conjugates were inspired by the previous work that showed that the triazole moiety could b incorporated in lieu of an amide bond as a surface recognition-connecting group in prototypical HDACi.[48]

3.2 *In Vitro* HDAC Inhibition

The HDAC inhibition of DAU-HDACi conjugates **7** and **12 a-d** was tested against HeLa nuclear extract HDACs using a cell-free assay (Fluor de Lys) as previously described.48 Overall, these compounds showed inhibition activities against HeLa nuclear extract HDACs, with potencies comparable to or exceeding SAHA (Table 3-1). It is of particular interest that compound **7** shows the same level of activity as SAHA. This suggests that the attachment of DAU does not impair the interaction between the HDACi component of the conjugate and the HDAC enzyme outer surface residues. It is also conceivable that the conjugate may adopt a

conformation whereby the anthracycline moiety can contribute positively to the interaction with the crucial HDAC active site or surface residues.

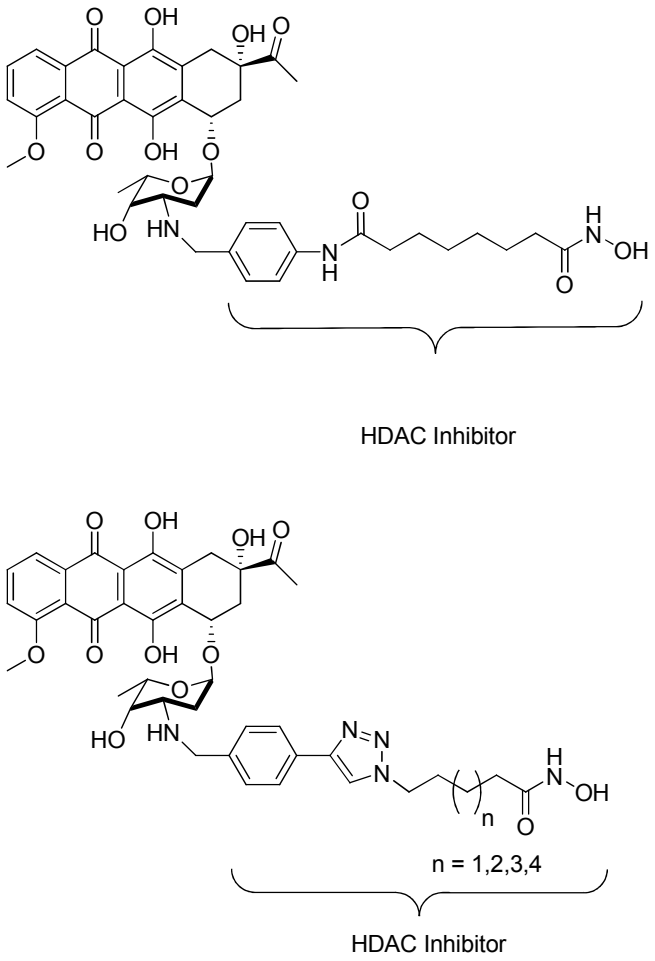

Figure 3-2: Design of dual-acting Topo II-HDAC inhibitors. All compounds were synthesized by Dr. Vishal Patil.

Table 3-1: *In vitro* HDAC inhibition of DAU-HDACi conjugates

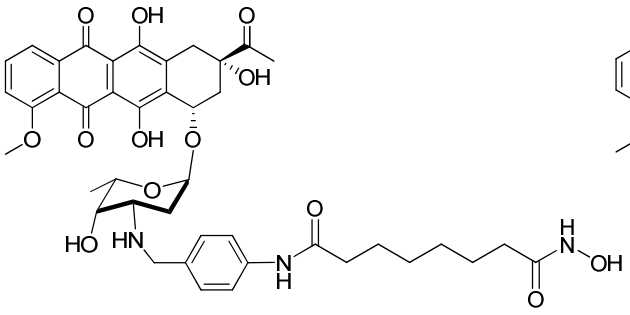

7

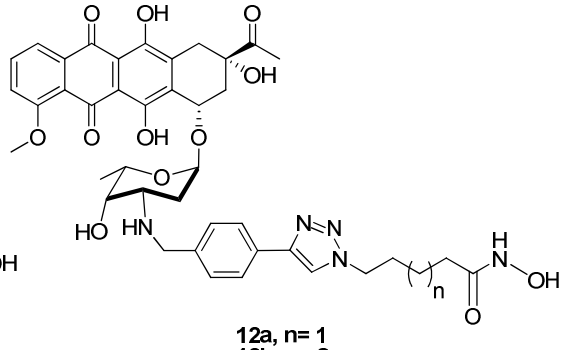

12a, n= 1
12b, n= 2
12c, n= 3
12d, n= 4

Compound	n	HeLa Nuclear Extract IC_{50}[a] (nM)	HDAC 1 IC_{50}[b] (nM)	HDAC 6 IC_{50}[b] (nM)	HDAC 8 IC_{50}[b] (nM)
SAHA		65.0	38±2	27±2	1989±156
DAU		N.D.	NT	NT	NT
7		64.7	47±3	20±1	220±21
12a	1	89.9	4600±240	555±36	N.D.
12b	2	1.6	54±3	30±2	4129±421
12c	3	0.9	8±0.4	20±0.4	710±43
12d	4	4.2	11±0.4	19±1	379±37

[a] Inhibition was assayed using the Biomol HDAC Fluorimetric Assay/Drug Discovery Kit.

[b] Data obtained through contracted arrangement with BPS Bioscience (San Diego, USA).

All triazole-linked conjugates potently inhibit HeLa nuclear extract HDACs with low to mid-micromolar IC_{50}'s. Among these conjugates, **12a** is the least active, closely followed by **12d**, which is about 20-fold more potent. Compounds **12b** and **12c** have the most potent anti-HDAC activity, with a slight preference for the six methylene-linked **12c**. Interestingly, the triazole-linked compound **12b** is 40-fold more potent than the amide-linked **7**, despite their similar linker length. Relative to the HDACi standard SAHA, **12c**, the most compound in this series, is 70-fold more potent (Table 3-1). These results showed that these conjugates followed a similar trend to that observed with aryltriazolyl HDACi.[48]

To probe for any HDAC isoform selectivity, possibly conferred by the complex anthracycline moiety acting as a surface recognition cap group, the DAU-HDACi conjugates were tested against selected recombinant HDACs – HDAC 1, HDAC 6, and HDAC 8. The pattern of HDAC inhibition of these compounds against HDAC 1 and HDAC 6 are similar to what we observed with the HeLa nuclear extract with few exceptions. Specifically, compounds **7** and **12b** have indistinguishable activity against HDAC 1 and HDAC 6 (Table 3-1). Additionally, **12a** which has a midnanomolar IC_{50} against HeLa nuclear extract is almost inactive against HDAC 1 (IC_{50} = 4.6 μM) while it maintains decent activity against HDAC 6 (IC_{50} = 0.6 μM). We are not sure of the cause of this disparity. In general, these compounds are weaker inhibitors of HDAC 8, with the exception of **7**, whose anti-HDAC 8 activity is only around 4-fold less that its anti-HDAC 1 activity (Table 1). This suggests that **7** is a more indiscriminant inhibitor of these HDAC enzymes, while the rest of the conjugates are more selective.

3.2.1 Molecular Docking of Dual-Targeted HDACi

To clarify the structural basis for the observed disparity in HDAC inhibition among compounds, we performed molecular docking using the AutoDock program .[48,49] Compounds were docked against a HDAC 1 homology model built from the human HDAC 2 X-ray structure (3MAX) coordinates.[50] The compounds with the least inhibitory activity (**12a**) and the best activity (**12c**) were docked in order to clearly delineate the basis of the ~600-fold difference in activities. Additionally, compound **7** was docked because of its distinct structural feature compared to **12a-d**, namely, the amide-coupled linker.

Interestingly, compounds **12a** and **12c**, differing only in linker length, do not bind to the same pocket but instead localize to two different pockets on the surface of HDAC 1(Figure 3-3a). It is possible that the hydroxyl group on the daunosamine sugar of **12c** makes hydrogen bonding contacts with the guanidinium group of Arg270 and that the linker chain more effectively positions the hydroxamate to the catalytic zinc by entering the active site through the top of the channel (Figure 3-3a and Figure 3-4c). In addition, two of the hydroxyl groups from the anthracycline ring of **12c** could take part in the H-bonding interaction with the backbone carbonyl group of Arg270 and the N-H group of Gly272. Conversely, compound **12** adopts a conformation to accommodate the shorter linker, consequently prohibiting H-bonding with Arg 270. Although many hydroxyl groups of **12a**'s anthracycline ring make potentially compensatory H-bonding contacts with the phenolic group of Tyr201 and the backbone carbonyl groups of Gly207 and Pro206 (Figure 3-4a &b), its binding pocket is more solvent-exposed compared to the binding pocket of **12c** (Fig 3-3a).

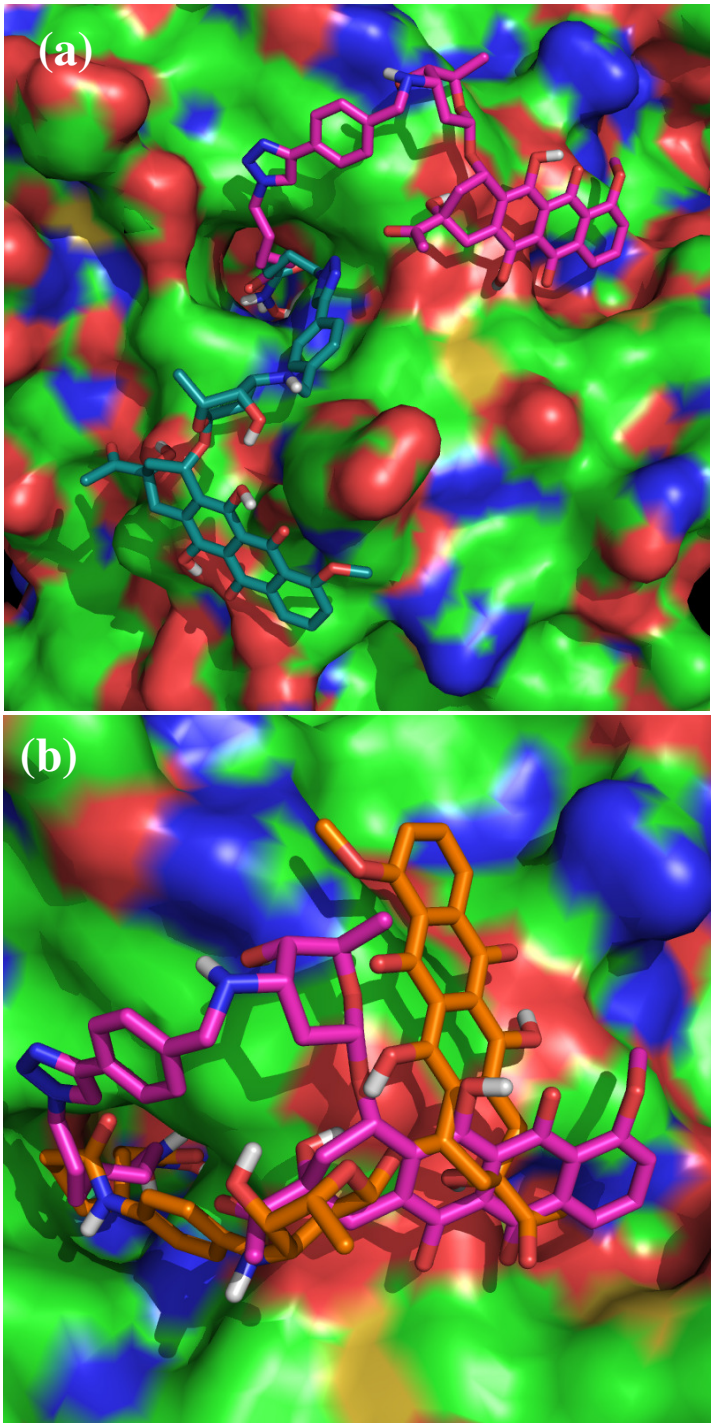

Figure 3-3: Docked structures of Topo II-HDACi conjugates at the HDAC 1 active site. (a) Superposition of low energy conformations of **12a** (teal) and **12c** (pink). (b) Overlay of low energy conformations of **12c** (pink) and **7** (orange). Docking performed by Dr. Vishal Patil.

The amide-linked compound **7** binds to a similar pocket, compared to **12c**, but it interacts with a different set of surface residues that contribute to its binding affinity. Unlike **12c** which enters the active site associating with the "top" of the hydrophobic channel, **7** interacts more so with the residues on the opposite side of the channel (Figure 3-3b). Consequently, the daunosamine hydroxyl group of **7** cannot interact with Arg270 similar to **12c**. In lieu of this interaction, the anthracycline ring of **7** may engage in H-bonding with the backbone carbonyl groups of Gly272, Gly268, and Thr304 on the enzyme surface rim (Figure 3-3b and Figure 3-4e,f). It is possible that the observed differences in the binding orientations of these compounds at the enzyme surface rim could account for the disparity in potencies against HDAC 1.

3.3 *In Vitro* Topo II Inhibition

To determine whether the DAU-HDACi conjugates retained their anti-Topo II activity, a cell-free DNA decatenation assay was used. Kinetoplast DNA (KDNA), a catenated network of mitochondrial DNA seen in trypanosomes, was used to quantify the conjugates' Topo II inhibition activity according to a literature protocol.[54,55] Figure 3-5 shows the results obtained from this study. KDNA and decatenated KDNA marker (lanes 1 and 2, respectively) were used as controls. Treatment of KDNA with Topo II for 10 minutes at 37°C resulted in extensive DNA decatenation (lane 3). As expected, the addition of 50 μM DAU to the decatenation experiment resulted in a severe impairment of DNA decatenation (comparing lanes 3 and 4). Relative to DAU, **12a** and **12d** have lower inhibition, with the worst overall inhibition shown by **12a**, the conjugate with the four methylene linker (lanes 7 and 8). Conjugates **12b** and **7** inhibited Topo II activity and comparable levels to that of DAU at the same concentration (lanes 6 and 9,

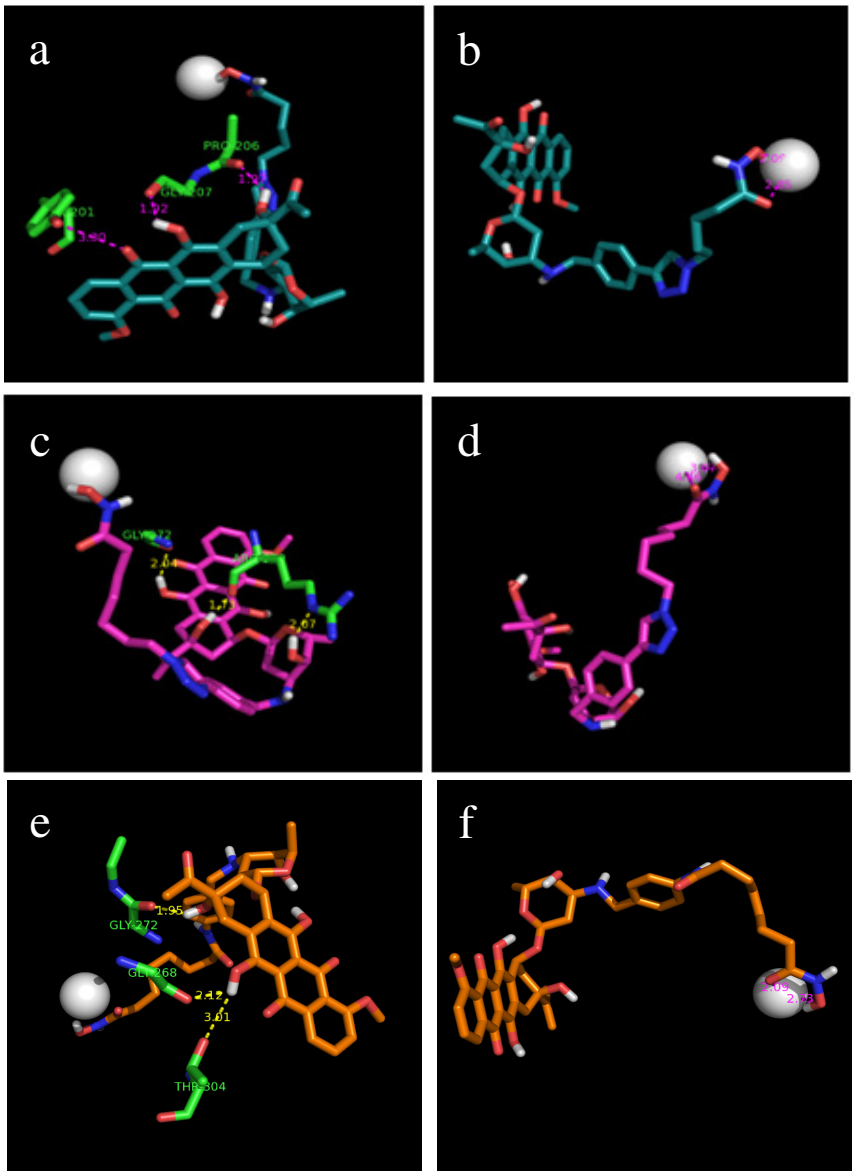

Figure 3-4: Docked structures of **12a** and **12c** within the active site of HDAC1. (a) Compound **12a** establishes H-bonding interactions between the anthracycline ring and Gly207, Pro206, Tyr201. (b) Orientation of compound **12a** near the catalytic zinc in the active site. (c) Compound **12c** establishes H-bonding interactions between the anthracycline ring and Arg270 and Gly272. (d) Orientation of compound **12c** near the catalytic zinc in the active site. (e) Docked structure of **7** reveals H-bonding interaction between the anthracycline ring and Gly272,Gly268, and Thr304. (f) Orientation of compound **7** near the catalytic zinc in the active site. All docking performed by Dr. Vishal Patil.

respectively). Notably, compound **12c** had enhanced Topo II inhibition compared to DAU, resulting in near total inhibition of decatenation at 50 μM (comparing lanes 4 and 5). In total, these results show that the Topo II inhibition activity of DAU is tolerant of an appropriate modification with HDACi groups, and as seen with **12c**, such groups could further enhance the Topo II inhibition activity of anthracycline derivatives. The molecular basis of the HDACi linker length-dependent enhancement of Topo II inhibition of the dual-acting conjugates is not entirely clear. It is plausible that the placement of the HDACi group of these conjugates within the minor groove of DNA, through the daunosamine sugar,[56] could further promote drug-DNA association, thereby enhancing the stability of the biologically relevant drug-DNA-Topo II ternary complex. Interestingly, **12c** also has the most potent inhibition activity against HDAC 1 (Table 3-1), thereby embodying both optimum anti-HDAC and Topo II inhibition activities under these cell free conditions.

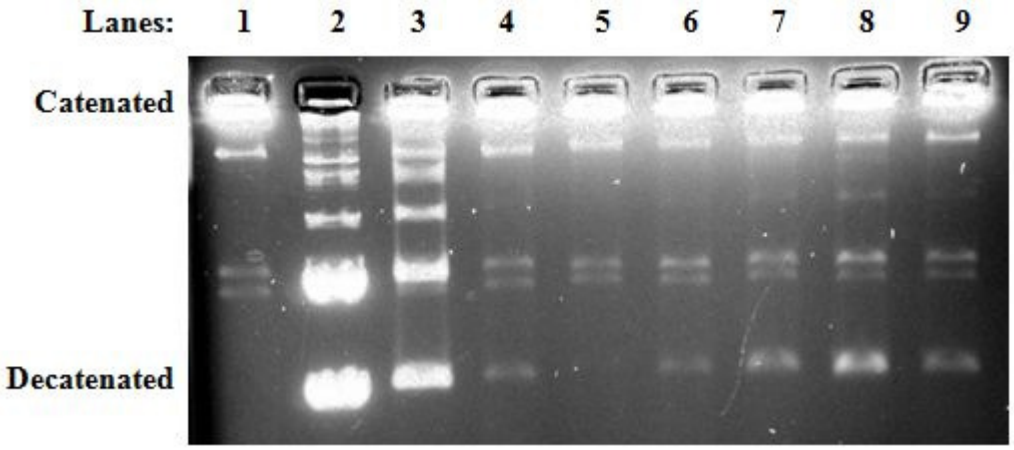

Figure 3-5: Decatenation by Topoisomerase II and inhibition with DAU-HDACi conjugates. Lanes 1-3: (1) KDNA, (2) decatenated KDNA marker, (3) KDNA and Topo II. Lanes 4-9: KDNA, Topo II and 50 μM (4) DAU, (5) **12c**, (6) **12b**, (7) **12d**, (8) **12a**, (9) **7**. Performed by Josh Canzoneri

3.4 Cancer Cell Growth Inhibition by Dual-Acting Topo II-HDACi

The prospect of biological activity against cancer cells was investigated through cell viability measurements of three human cancer cell lines treated with dual-acting Topo II-HDACi. IC_{50} values were quantified using the MTS assay, which measures the reductive capacity of functional mitochondria (Table 3-2). The positive control compounds DAU and SAHA inhibit the proliferation of these cell lines with IC_{50} similar to the values in the literature.[57,58] DAU shows a cell line-dependent cytotoxicity that varies by as much as 10-fold among the three cell lines while SAHA shows no such cell line-dependent effect (Table 3-2). Bifunctional compounds **12a-d** show linker length-dependent antiproliferative activities that closely match the trend of their anti-HDAC activities. Among the three cell lines investigated, these compounds decreased the viability of DU-145 the most, while they are the least cytotoxic to MCF-7. Although less pronounced than the effect seen with DAU, these compounds display cell line-dependent cytotoxicity as well. Nevertheless, the micromolar IC_{50} values and the traction with the anti-HDAC activities suggest that HDAC inhibition is the dominant mode of anti-proliferative activities in compounds **12a-d**. Specifically, the antiproliferative activities of **12c** and SAHA, compounds with similar linker length, are virtually indistinguishable against DU-145 and SK-MES-1 cell lines. This is surprising as **12c** displays the most potent HDAC and Topo II inhibition.

Interestingly, compound **7**, a true hybrid between SAHA and DAU, showed the best cytotoxicity of all the bifunctional inhibitors across all cell lines, possessing sub-micromolar activities. In fact, the cytotoxicity of **7** closely rivals that of DAU, and they are equipotent against MCF-7. This is contrary to the trend seen in cell-free assays of HDAC and Topo II inhibition. The potentiation of **7** within the cellular

Table 3-2: Inhibition of cancer cell viability by Topo II-HDACi

Compound	n	DU-145 IC_{50} (μM)[a]	SK-MES-1 IC_{50} (μM)[a]	MCF-7 IC_{50} (μM)[a]
7		0.13±0.06	0.47±0.02	0.99±0.21
12a	1	5.39±1.02	15.3±3.1	24.5±1.6
12b	2	1.61±0.29	4.68±0.75	13.4±1.85
12c	3	2.92±0.31	3.31±0.23	10.6±0.94
12d	4	2.06±0.33	2.61±0.11	14.8±1.6
DAU		0.09±0.002	0.17±0.09	0.95±0.05
SAHA		2.12±0.25	2.42±0.38	2.5±0.61

[a] Values are the average of two experiments performed in triplicate. IC_{50} values were determined using the MTS assay (Promega).

environment could be due to many factors, including the predominance of the Topo II inhibition character in dictating the bioactivity of **7**, the indiscriminant inhibition of multiple HDAC isoforms, or an alternate mechanism(s) that is unrelated to the inhibition of either target.

3.5 Modulation of Cellular Markers Consistent with HDAC Inhibition

3.5.1 p21 Upregulation and Histone Acetylation

To gain a better perspective of the molecular mechanisms behind the antiproliferative activities observed in response to these dual-acting inhibitors, we probed the effect of their exposure on the intracellular status of $p21^{waf1}$ (p21) in DU-145 cancer cells. p21 has been shown to be upregulated in response to HDACi treatment, as well as in a p53-independent response to DOX.[59,60] We dosed inhibitors at concentrations near the determined IC_{50} in DU-145 and evaluated protein expression status using western blotting (Figure 3-5). We controlled for equivalent protein loading using anti-actin antibody (Figure 3-5, bottom panel). As expected, SAHA results in marked upregulation of p21, even at 2.5 μM (top panel, lanes 2 and 3). However, neither DAU nor **7** shows noticeable upregulation in p21 expression compared to control levels (top panel, comparing lanes 4-7 to lane 1). This trend is reversed with **12b**, as a dose-dependent upregulation of p21 expression was observed (top panel, lanes 8 and 9). Relative to SAHA, however, the extent of p21 upregulation by **12b** is lower, though both were dosed at the same concentrations. Since these experiments were done at the IC_{50} of the respective compounds, these results may indicate that **7** and **12b** derive their cytotoxic activity primarily through Topo II and HDAC inhibition, respectively. Alternatively, the cytotoxic activity **7** could be due to perturbation of other intracellular HDAC inhibition markers.

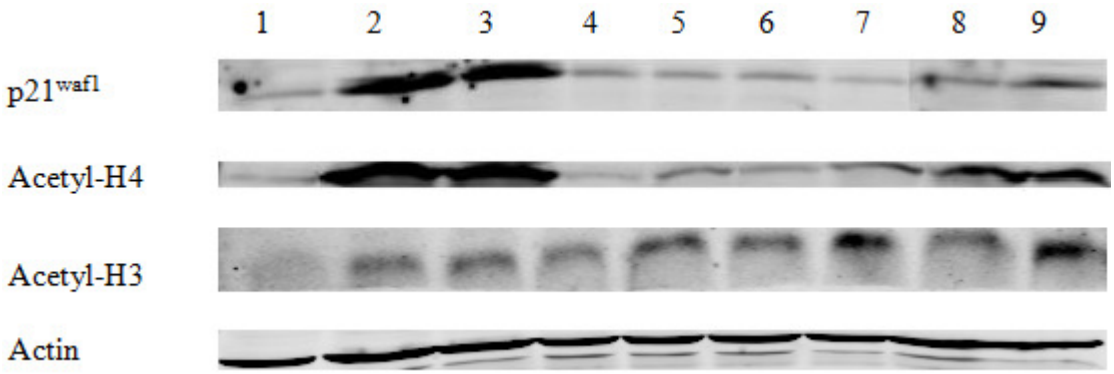

Figure 3-6. Immunoblot detection of cellular HDACi markers. DU-145 cells were dosed for 24 hours at the indicated concentrations to probe for acetylated histones H4 and H3, and $p21^{waf1}$. Actin was also probed to show equal loading of protein. Lane: (1) Control; SAHA (2) 2.5 µM, (3) 5 µM; DAU (4) 0.1µM, (5) 0.5 µM; **7** (6) 0.5 µM, (7) 1 µM; **12b** (8) 2.5 µM, (9) 5 µM.

To further investigate into the prospect of distinct mechanisms of action for **7** and **12b**, we probed for histone acetylation status in DU-145 cells exposed to the same drug concentrations used for p21 immunoblotting. Intracellular histone acetylation status is a more direct indicator of class I HDAC inhibition. SAHA shows a strong histone H4 acetylation (Figure 3-5, 2nd panel, lanes 2 and 3) while DAU and **7** display moderate dose-dependent change in acetylation at the concentrations tested (2nd panel, lanes 4 - 7). Compound **12b** shows a strong H4 acetylation, with levels close to that of SAHA, at both concentrations (2nd panel, lanes 8 and 9). The trend of the drug-induced perturbation of the acetylation state of H3, in core histones purified by acid extraction of DU-145 cell nuclear extract, is similar to that obtained for H4. Relative to the control, we observed distinct H3 acetylation in DU-145 cells exposed to the same

drug concentrations used for H4 immunoblotting (Figure 3-5, 3rd panel). These results provide evidence supporting the involvement of intracellular HDAC inhibition as part of the mechanisms of bioactivity of the dual-acting compounds **7** and **12b**.

3.5.2 Tubulin Acetylation

Additional data was sought in order to clarify the mechanisms involved in the antiproliferative activities and to delineate the disparity in enzyme inhibition versus antiproliferative activity. Tubulin was chosen as a target as it is acetylated by the cytoplamic HDAC6,[21,61,62] for which **7** and **12b** had nearly identical inhibition. Interestingly, inhibition of HDAC6-associated tubulin acetylation has been shown to enhance the cytotoxicity of DNA-damaging agents.[63] While most HDACi induce $p21^{waf1}$ overexpression, inhibition of tubulin deacetylation is compound specific,[64] potentially allowing for differentiation between the mechanisms and potencies of **7** and **12b**. Because tubulin acetylation in response to HDACi is a relatively early event [65], we dosed DU-145 cells for 4 hours with inhibitors at either IC_{50} concentrations (Table 2) or a high concentration (~5X IC_{50}). Immunoblotting revealed highly varied levels of tubulin acetylation among the inhibitors. DAU induced the lowest levels of acetylation, with IC_{50} concentration showing levels comparable with control and only a slight increase in response to higher concentration of drug (Figure 3-6, lanes 1-3). Compound **7** induced moderate levels of acetylation (Figure 3-6, lanes 4 and 5), while **12b** caused robust acetylation at 5X its IC_{50} (Figure 3-6, lanes 6 and 7). p21 expression at 4 hours remained low across all compounds tested, with no discernible induction relative to control (Data not shown).

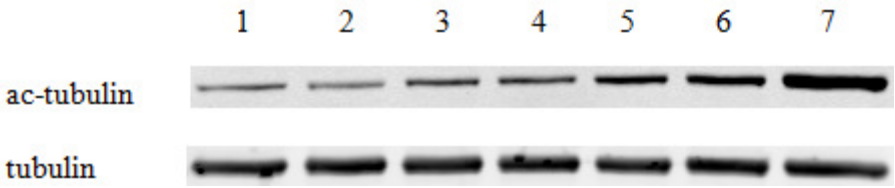

Figure 3-7: Tubulin acetylation in response to TopoII-HDACi. DU-145 cells were dosed for 4 hours with: (1) Control (0.1% DMSO), (2) DAU 90 nM, (3) DAU 500 nM, (4) **7** 130 nM, (5) **7** 500 nM, (6) **12b** 1.31 µM, (7) **12b** 10 µM.

3.6 Intracellular Topo II Inhibition

To obtain information about the intracellular fate of Topo II upon cell exposure to these dual-acting agents, we used an immunoblotting kit to assay compound-induced Topo II inhibition in an intracellular environment (Figure 3-7).[66] DU-145 cells were dosed with drug concentrations corresponding to cell growth inhibition IC_{50}'s while the control cells were dosed with vehicle (0.1% DMSO). The relative levels of stabilized Topo II-DNA cleavage complexes were determined for a 30 min drug treatment, as recommended by the manufacturer. Within this period, the control cells showed no significant amounts of Topo II inhibition, evidenced by the low levels of Topo II associated DNA (Figure 7a, lane 1). Cells treated with DAU and **12b** contained high levels of Topo II – DNA cleavage complexes, with **12b** showing a significantly higher amount (Figure 3-7a - lanes 2 vs. 4). This result suggests that **12b** could derive its cytotoxic activity, in part, from intracellular Topo II inhibition. Conversely, the levels of Topo II – DNA cleavage complexes in cells exposed to **7** is indistinguishable from that of the control cells (Figure 3-7a, lane 3), suggesting a minimal contribution of Topo II inhibition to the cytotoxic activity of **7** within this period. This observation is surprising in light of the seemingly

contradictory moderate effect of **7** on H4 acetylation (Figure 3-5), tubulin acetylation (Figure 3-6) and its potent cell growth inhibition activity (Table 3-2).

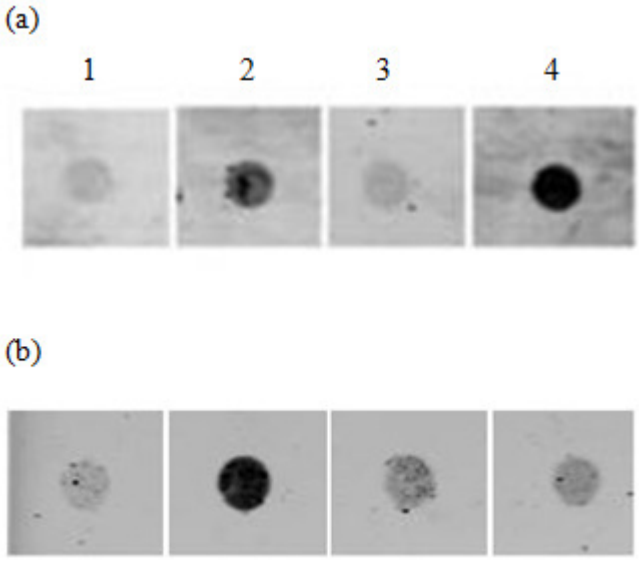

Figure 3-8: Intracellular Topo II inhibition. DU-145 cells were probed for stabilized DNA-Topo II cleavage complexes upon (a) 30 min treatment; (b) 72 h treatment with bifunctional compounds: (1) control, (2) 90 nM DAU, (3) 130 nM **7**, (4) 1.6 μM **12b**.

To elucidate any contribution Topo II inhibition could be adding to long-term inhibition of cell proliferation, Topo II cleavage complexes were assayed after 72 hours of treatment with compounds (Figure 3-7b). As expected, DAU treatment results in significant inhibition of Topo II activity relative to control levels (Figure 3-7b, comparing lanes 1 and 2). Compound **7** shows a measured increase in Topo II inhibition relative to control levels (Figure 3-7b, comparing lanes 1 and 3). Interestingly, we observed a drastic drop in the levels of stabilized Topo II-DNA

cleavage complexes upon cell exposure to **12b** for 72-hour (comparing lane 4 of Figures 3-7a and 3-7b). This result suggests that the Topo II inhibition activity of **7** increases with time while that of **12b** decreases. The persistence of the stabilized Topo II-DNA cleavage complexes over a longer period indicates that Topo II inhibition may contribute significantly to the mechanism of the antiproliferative activity of **7**.

3.7 Intracellular Localization of Dual-Acting Topo II-HDACi

HDAC1 and Topo II, are nuclear-localized targets of these bifunctional compounds, while HDAC6 is cytoplasmic. To determine whether decreased cell penetration could be one of the reasons for the difference in the potencies of compounds **7** and **12b**, we used confocal microscopy to visualize their intracellular localization (Figure 3-8). We exposed DU-145 cells to 1 μM of DAU, **7** and **12b**. After 4 hours incubation time, cells were monitored at 488nm, the excitation wavelength (λ_{ex}) of DAU, and we observed clear differences in the intracellular distribution profiles of the tested compounds. In agreement with previous study in the literature [67], DAU is localized within the nuclear and perinuclear regions of DU-145 cells. Although it shows a less nuclear localization, compound **7** is more widely distributed within the cytoplasm with evidence for perinuclear localization in similar to that of DAU. In contrast, **12b** shows a highly diminished intracellular distribution, with the bulk of the compound trapped in vesicle-like bodies within the cell (Figure 3-8). The relatively poor intracellular distribution of **12b** could be due to low cell membrane penetration or an enhanced pump-induced efflux of compound from within the cell.[68] We obtained a similar result with a lung tumor derived A549 cells (Figure 3-9). These results show that **7** and **12b** have different intracellular residency which

may affect access to their targets and consequently offer additional insight into underlying factors that could contribute to the disparity in the *in vitro* potency of these compounds.

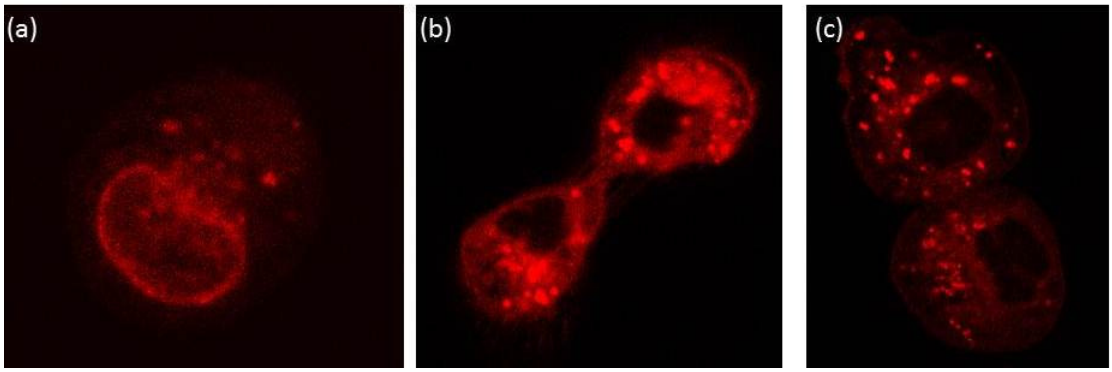

Figure 3-9: Intracellular distribution of dual-acting inhibitors in DU-145 cells. (a) DAU, (b) **7**, (c) **12b**. Cells were dosed at 1 μM for 4 hours with indicated compounds and visualized by confocal microscropy. Confocal microscopy by Josh Canzoneri/Will Guerrant.

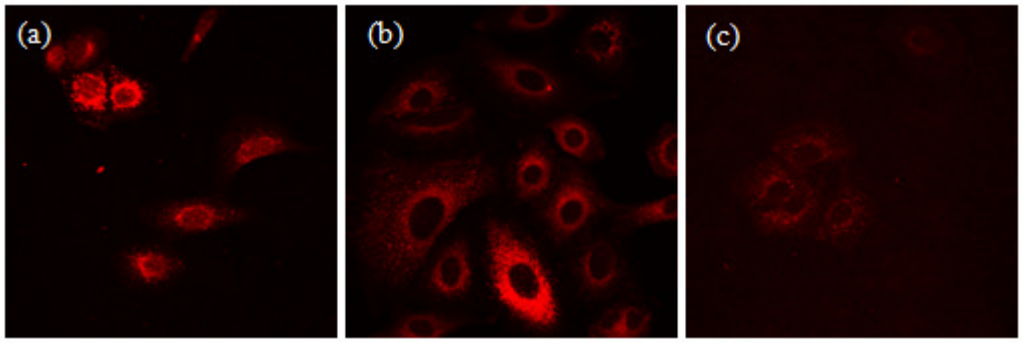

Figure 3-10: Intracellular distribution of dual-acting inhibitors in A549 lung cancer cells. (a) DAU, (b) **7**, (c) **12b**. A549 cells were dosed for 4 hours at 1 μM with the indicated compounds and visualized by confocal microscopy. Confocal microscopy by Josh Canzoneri.

3.8 Summary

There is evidence for the synergistic effect of combined Topo II and HDAC inhibitors on cancer.[38] However, this synergy is schedule dependent, hence traditional combination therapy involving Topo and HDAC inhibitors may be complicated by the inherent pharmacokinetic disadvantage of two separate drugs. To critically delineate the benefits of simultaneous Topo and HDAC inhibition in cancer therapy, it will be of interest to identify agents that possess Topo and HDAC inhibition activities within a single molecule. Toward this end, we have created dual-acting Topo II/HDAC inhibitors. A subset of these compounds potently inhibits the proliferation of representative cancer cell lines. When subjected to target-specific screening, these agents present both HDAC and Topo II inhibition signatures under cell-free conditions and in cell cultures. This observation suggests that the cytotoxic activities and potency of these dual-acting compounds could be dictated by either of the two anti-tumor pharmacophores. Specifically, results from HDAC and Topo inhibition studies; and p21, acetyl-H4, and acetyl-tubulin immunoblots highlight compound **7** as a moderate, yet sustained modulator of several intracellular targets important in tumor etiology. This may explain the superior antitumor activity of compound **7** relative to the other dual-acting agents disclosed in this study. It is, however, instructive to emphasize that the target validation experiments described herein are performed under different conditions at different incubation periods, so parsing out the specific contributions of the two targets to the bioactivity of these agents may not be direct.

Another target-independent factor which influences the bioactivity of the anthracycline-derived dual-acting agents is their cellular uptake and/or residency. In fact, diminished intracellular residency, occasioned by multidrug resistance protein (MRP) mediated efflux, is

one of the problems of an anthracycline-based chemotherapy regimen.[68] Compound **12b** shows a rapid on-set of HDAC and Topo II inhibition activities which may be quickly lost due to diminished intracellular residency. The poor intracellular distribution of **12b** may suggest that the triazole-containing compounds **12a-d** are prone to efflux, in a similar manner to the anthracycline template. Alternatively, it may be that **12a-d** are not easily up taken into the cell. Either of these limitations would compromise the bioactivity of **12a-d** and may explain their less than optimal cytotoxic activity, despite evidence for potent inhibition of Topo II and HDACs. Nevertheless, the amide-containing compound **7** is a lead that merits additional study due primarily to its good intracellular distribution and potency that rivals DAU. It will be of interest to know how **7** fares with respect to common deleterious side effects that have plagued anthracycline therapy.

The compatibility of the HDACi pharmacophore for addition of the large anthracycline moiety and the increase in activity against each target when DAU and HDACi were combined to form bifunctional Topo II-HDACi caused us to inquire whether combining Topo I and HDAC-inhibiting functionalities could furnish similar advantages. Topo I inhibitors are potent anticancer agents, causing DNA single strand breaks, cell cycle arrest and apoptosis,[69-73] but most importantly, HDACi have been shown to act synergistically with Topo I inhibitors, resulting in enhanced cancer apoptosis.[74] To investigate whether the same dual-targeted strategy would prove advantageous, dual-targeted compounds were designed using the camptothecin ring system and the linker and ZBG of SAHA-like HDACi (Figure 3-11).

(a)

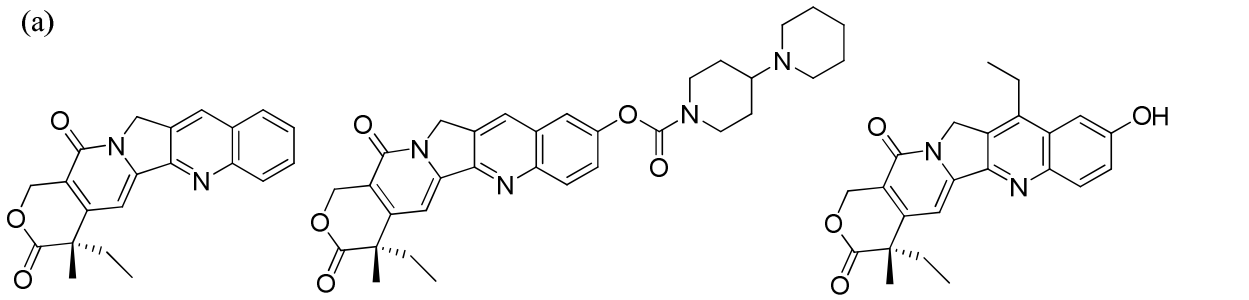

Camptothecin Irinotecan 7-ethyl-10-hydroxycamptothecin (SN-38)

(b)

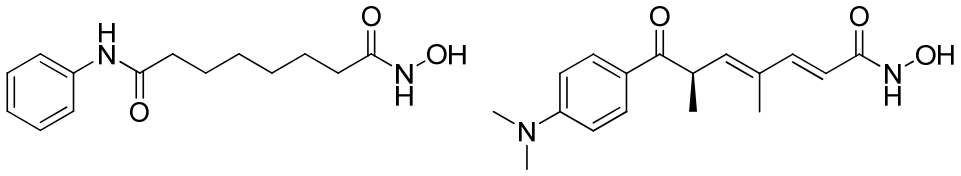

SAHA TSA

Figure 3-11: Representative structures of camptothecin inhibitors of Topo I (a), and (b) HDACi.

3.9 Design of dual-targeted Topo I-HDACi

The camptothecin family of Topo I inhibitors are potent anticancer drugs that form a ternary complex at the interface of the cleavage complex, inhibiting dissociation of Topo I from DNA. 10-hydroxycamptothecin and 7-ethyl-10-hydroxycamptothecin (SN-38) were chosen as the Topo I inhibiting templates for the design of dual-targeted Topo I-HDACi due to their promising activity against a range of tumor types. Also, both templates have demonstrated considerably more potency and less toxicity that the parent compound, camptothecin.[75-77] SAR studies on camptothecins have identified substitutions at the C-10 hydroxyl are tolerable[78] so additions of HDACi linkers through this position were performed using the 1,2,3-triazole ring linkage assayed previously (Figure 3-12).[48b] In this design, it was anticipated that the

camptothecin template might act as an aromatic surface recognition cap group, while retaining its Topo I inhibition activity. We introduced variations in the linker region to test the linker length-dependent potency of these bifunctional compounds. Linker lengths were chosen based on the optimal HDAC inhibition demonstrated by compounds with five and six methylene linkers in previous studies.[17,48,79]

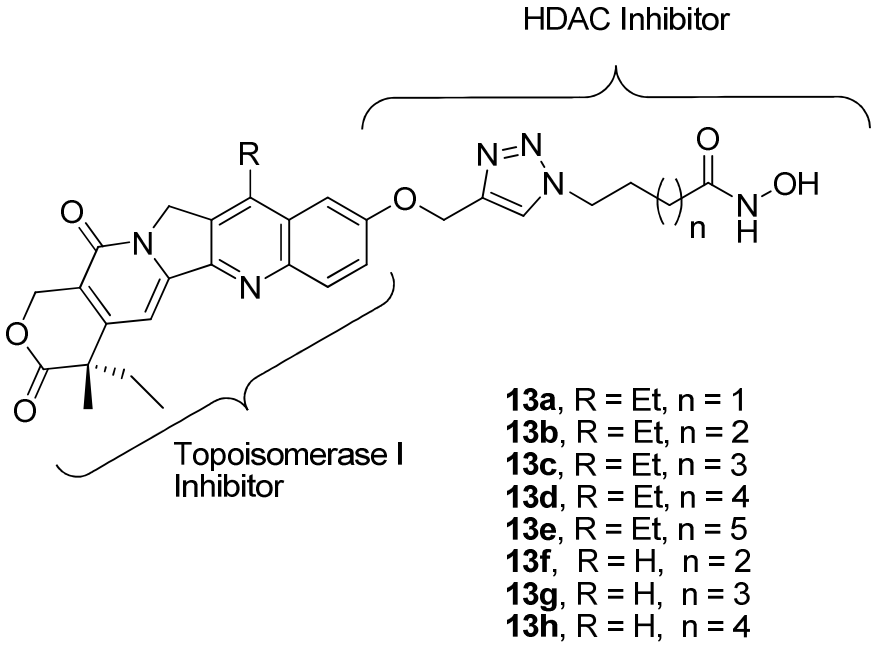

Figure 3-12: Design of dual-acting Topo I-HDACi.

Compounds synthesized by Daniel Yao (**13a-e**), Dr. Vishal Patil (**13f-h**)

3.10 *In vitro* HDACi activity

Building on previous observations regarding the linker length-dependent potency of triazole-linked HDACi, 7-ethyl-10-hydroxycamptothecin-derived compounds **13a-e** were screened for anti-HDAC activity using HeLa nuclear extract as previously described,[48] but with a slight modification. Camptothecin has a fluorescence emission close to the wavelength (460 nm)

of the fluorescence generated by cleavage of the assay substrate by HDAC. To circumvent this potential interference, control wells containing the same test concentrations were assayed similarly, but without HeLa nuclear extract, and the resulting fluorescence readings were subtracted from the experimental results. Compound **13a**, the shortest analogue with a three methylene linker separating the triazole ring and the hydroxamate moiety, has no measurable anti-HDAC activity at concentrations less than 10 μM (Table 3-3). The inactivity of **13a** may be due to the fact that its linker is too short to effectively position its hydroxamate moiety within the active site while maintaining the crucial surface residue contacts. Conversely, compounds **13b-e** displayed linker length-dependent HDAC inhibition activities with compound **13d**, an analogue with a six methylene linker, having inhibition activities comparable to SAHA (Table 3-3). The anti-HDAC activities of these compounds followed linker length-dependence similar to what we observed for other aryltriazolyl HDACi.[48b]

In order to elucidate the contribution of the ethyl group at the C-7 position toward HDAC inhibition, camptothecin-derived compounds **13f-h** were synthesized and assayed for anti-HDAC activity. The linker lengths of these compounds were chosen based on the optimal HDAC inhibition demonstrated by 7-ethyl-10-hydroxycamptothecin derived compounds **13b-d**. A comparison of the anti-HDAC activities of **13b-d and 13f-h**, against the HeLa cell nuclear extract HDACs, reveals that pairs with the same linker length have nearly identical HDAC inhibition activity (Table 3-3). These results suggest that the presence or absence of the ethyl group at the C-7 of the camptothecin ring system has no significant effect on the inhibition of HeLa cell nuclear extract HDACs. As expected, SN-38 has no measurable HDAC inhibition activity. For both sets of compounds, the best inhibition activity was observed in compounds with a six methylene linker. Furthermore, these compounds inhibited HeLa nuclear extract

HDACs with activities comparable to the standard HDACi, SAHA. This result suggests that the camptothecin ring is a compatible cap group for a dual-targeted HDACi, perhaps facilitating HDAC inhibition through interactions with enzyme surface residues, consistent with the accepted mode of inhibition.

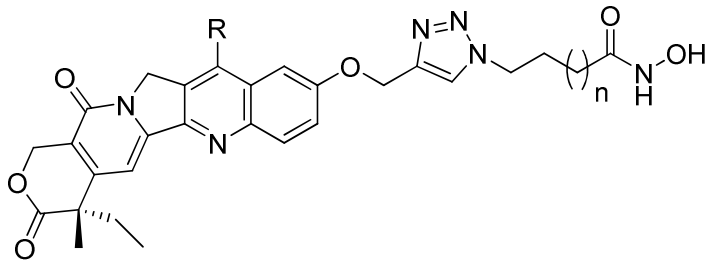

Compound	n	R	HeLa N.E. IC_{50} (nM)
13a	1	$-CH_2CH_3$	N.D.
13b	2	$-CH_2CH_3$	155.4
13c	3	$-CH_2CH_3$	120.7
13d	4	$-CH_2CH_3$	64.65
13e	5	$-CH_2CH_3$	212.3
13f	2	-H	144.5
13g	3	-H	112.2
13h	4	-H	56.2
SN-38	-	-	N.D.
SAHA	-	-	65.0

N.D. – nondeterminable within the tested concentration range, 1 nM-10 μM; N.E. –nuclear extract.

Table 3-4: HDAC inhibition of dual-targeted Topo I-HDACi against distinct isoforms.

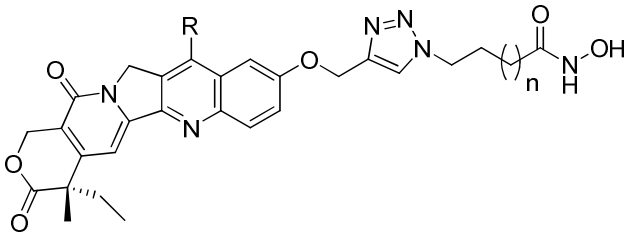

Compound	n	R	HDAC1 IC_{50} (nM)	HDAC 6 IC_{50} (nM)	HDAC 8 IC_{50} (nM)
13a	1	$-CH_2CH_3$	N.D.	85 ± 34	1726 ± 577
13b	2	$-CH_2CH_3$	NT	NT	NT
13c	3	$-CH_2CH_3$	129 ± 33	42 ± 6	N.D.
13d	4	$-CH_2CH_3$	50 ± 7	36 ± 5	N.D.
13e	5	$-CH_2CH_3$	369 ± 111	75 ± 34	2599 ± 475
13f	2	-H	116 ± 40	260 ± 40	N.D.
13g	3	-H	N.T.	N.T.	N.T.
13h	4	-H	37 ± 7	81 ± 26	1046 ± 316
SN-38	-	-	N.T.	N.T.	N.T.
SAHA	-	-	38 ± 2	27 ± 2	294 ± 35

N.D.-nondeterminable within the tested concentration range, 1 nM – 10 μM; N.T. – not tested; Data obtained through agreement with BPS Bioscience.

To obtain additional evidence for the specific mode of HDAC inhibition, isoform selectivity was investigated by testing selected compounds against pure HDAC1, HDAC6, and HDAC8 (Table 3-4). The pattern of anti-HDAC activities against HDAC1 and HDAC6 mirrored what was observed with HeLa nuclear extract results with one exception. The three methylene-linked compound **13a** is inactive against HDAC1 while it maintains low nanomolar and submicromolar IC_{50}'s against HDAC6 and HDAC8, respectively. In general, these compounds

are more selective for HDAC6 with modest to no activity against HDAC8. The preference and stronger activity against HDAC6 over HDAC1 could also provide an alternate explanation for the molecular mechanisms behind the inhibition data against HeLa nuclear extract, which is a rich source of HDACs 1 and 2.[80,81]

3.11 In Vitro Topo I Inhibition

We performed a cell-free DNA plasmid relaxation assay, according to a literature protocol, in order to determine the Topo I inhibition activity of these Topo I-HDACi conjugates.[82,83] In this assay, a supercoiled plasmid is incubated with Topo I in the presence or absence of Topo I inhibitors. Reactions are terminated by addition of SDS, which denatures Topo I. Reaction mixtures are then electrophoresed in an agarose gel and DNA is visualized using a nucleic acid dye. Stabilized cleavage complexes that are covalently bound to DNA will inhibit migration of DNA in the gel significantly more, relative to unbound, relaxed DNA. SN-38 was used as a positive control for Topo I inhibition and all compounds were tested at 50 μM (Figure 3-13). The 7-ethyl-10-hydroxycamptothecin-derived compounds **13a-e** inhibited Topo I as demonstrated by the reduction in relaxed plasmid and the increase in nicked plasmid compared to uninhibited Topo I (Figure 3-13a, lanes 4-8 vs. 2). Furthermore, there was little apparent drop in activity relative to SN-38 (lane 3). **13f-h** inhibited Topo I-induced plasmid relaxation with similar activities to each other, but with lesser activities relative to SN-38 (Figure 3-13b, lanes 4-6 vs. 3). The difference in inhibitory activities between **13a-e** and **13f-h** was not unexpected and could be explained by the greater potency of SN-38 over camptothecin in inhibiting Topo I.[84,85] Contrasting with HDAC inhibition, the modification at the C-7 position is a significant determinant of Topo I inhibition. These results, taken together with the HDAC

inhibition data, showed that these dual-targeted Topo I-HDACi can function to inhibit either target enzyme and conjugation of the two inhibiting moieties does not preclude the activities of either parent compound significantly.

(a)

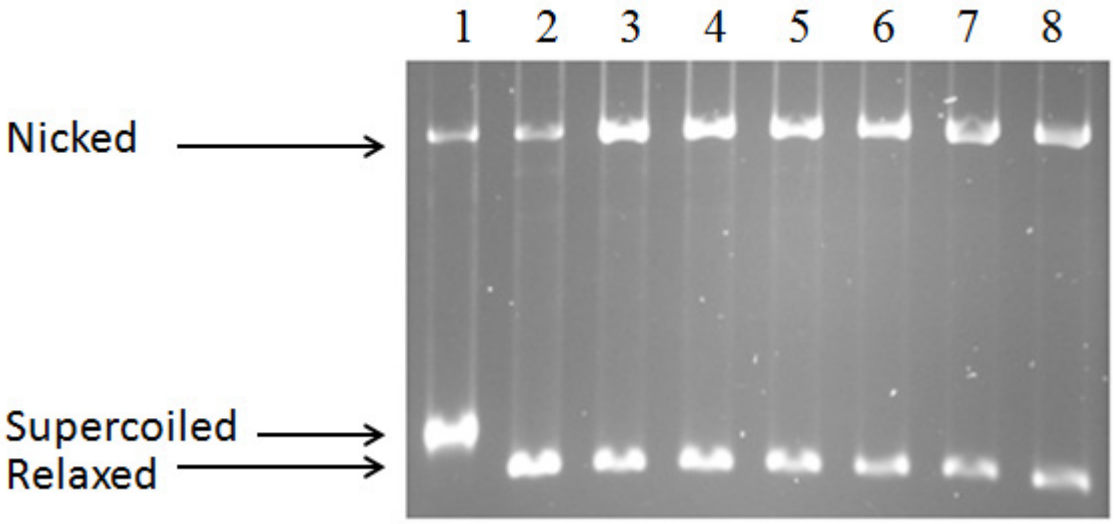

(b)

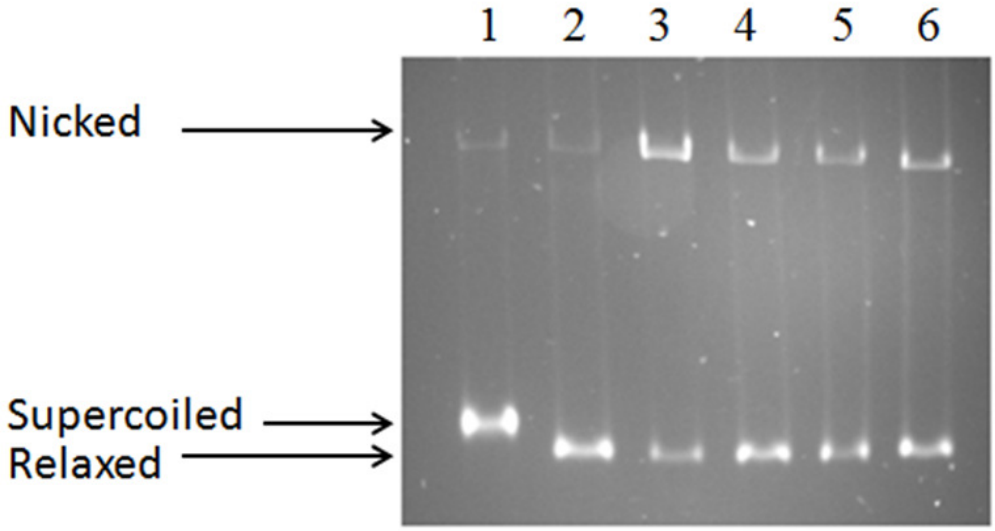

Figure 3-13: Topoisomerase I-induced plasmid relaxation assay.

(a) (Lane 1) PBR322 plasmid DNA; (Lane 2) DNA and Topo I; Lanes 3-8: DNA, Topo I and 50 μM: (3) SN-38; (4) **13a**; (5) **13b**; (6) **13c**; (7) **13d**; (8) **13e**.

(b) (Lane 1) PBR322 plasmid DNA; (Lane 2) DNA and Topo I; (Lanes 3-6) DNA, Topo I, and 50 μM: (3) SN-38; (4) 13f; (5) 13g; (6) 13h. Performed by Josh Canzoneri.

3.12 Anticancer activity of Topo I-HDACi

To examine the preliminary effects of these dual-acting inhibitors on cancer cell proliferation, they were screened against the DU-145 prostate cancer cell line and the inhibition of cell viability was measured. SN-38 and SAHA were used as positive controls with SN-38 potently inhibiting DU-145 viability in the mid-nanomolar range, while SAHA's IC_{50} was higher, in the low micromolar range. Compound **13a-e** displayed linker length-dependent anticancer activities with a five methylene linker proving optimal for inhibiting viability (Table 3-5). Compound **13a**, with the shortest linker of three methylenes, possessed the least potent activity against DU-145.

Conversely, compounds **13f-h** displayed indistinguishable anticancer activities with IC_{50}'s around 2 μM. Comparatively, most of the 7-ethyl-10-hydroxycamptothecin-based compounds are less active than their10-hydroxycamptothecin-based congeners. One exception is compound **13c** which showed anticancer activity that it identical to that of **13g**, its direct analog. More importantly, the micromolar activities suggest that HDAC inhibition may be the dominating mode of the anticancer activities of **13 a-h**.

Table 3-5: Anticancer activity of Topo I-HDACi

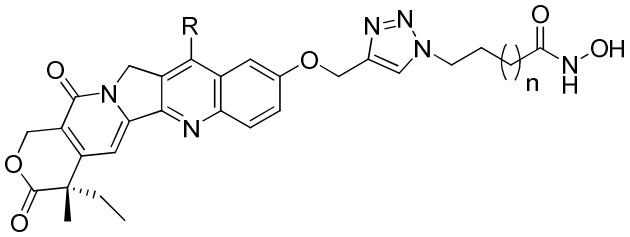

Compound	n	R	IC_{50} (μM)
13a	1	$-CH_2CH_3$	6.27
13b	2	$-CH_2CH_3$	4.25
13c	3	$-CH_2CH_3$	2.05
13d	4	$-CH_2CH_3$	3.11
13e	5	$-CH_2CH_3$	3.51
13f	2	-H	2.50
13g	3	-H	1.95
13h	4	-H	2.03
SN-38	-	-	0.11
SAHA	-	-	2.12

All values are the mean of two experiments performed in triplicate as measured by the MTS assay (Promega). DU-145 was dosed for 72 hours with drug.

3.13 Immunoblotting of $p21^{waf1}$ levels in response to Topo I-HDACi.

Since the anticancer activities displayed by Topo I-HDACi against DU-145 appeared to be driven by HDACi-based mechanisms, we profiled the contribution of intracellular HDAC inhibition through the level of $p21^{waf1}$ expression. Compounds **13c** and **13g** were used, premised

on the fact that they are representative examples from the two Topo I inhibiting templates with identical anticancer activities. Inhibitors were dosed at concentrations near the determined $1C_{50}$'s in DU-145 and $p21^{waf1}$ expression was probed via immunoblot (Figure 3-14). Equivalent protein loading was demonstrated using an anti-actin antibody (Figure 3-14, top panel). Both SAHA and SN-38[86] resulted in marked upregulation of $p21^{waf1}$ expression levels with 24 hour treatment (Figure 3-14, bottom panel, lanes 2-5). Gratifyingly, we observed that the dual-acting Topo I-HDACi **13c** caused a dose-dependent increase in $p21^{waf1}$ expression (Figure 3-14, bottom panel, lanes 6 and 7). Moreover, **13g** resulted in substantial upregulation of $p21^{waf1}$ expression with levels comparable to SN-38 (Figure 3-14, bottom panel, lanes 8 and 9). These results provide an initial molecular basis for the observed anticancer activity of Topo I-HDACi. It is unknown at present how much of the $p21^{waf1}$-dependent anticancer activity is contributed by each inhibiting moiety as both SAHA and SN-38 significantly increased $p21^{waf1}$ expression. Subsequent investigation into the expression levels of other cellular markers could clarify the driving force behind the cellular effects observed.

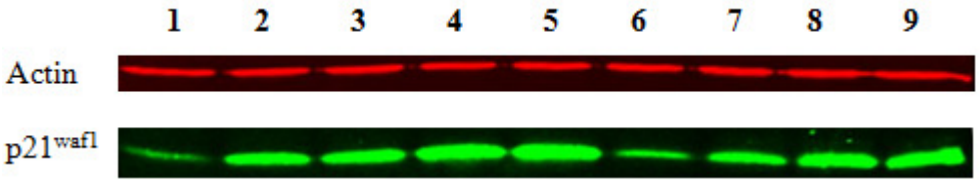

Figure 3-14: Immunoblot of $p21^{waf1}$ expression changes in response to Topo I-HDACi.
Lanes: (1) Control, (2) **SAHA**, 2.5 μM, (3) **SAHA** 5.0 μM, (4) **SN-38**, 0.1 μM, (5) **SN-38** 0.5 μM, (6) **13c**, 2.5 μM, (7) **13c**, 5.0 μM, (8) **13g**, 2.5 μM, (9) **13g**, 5.0 μM. DU-145 cells were treated for 24 hours with inhibitors.

3.14 Summary

A new class of dual-targeted Topo I-HDACi has been created from camptothecin and SAHA-like templates. Two types of camptothecin templates were used and both were connected through their 10-hydroxy moieties to alklyltriazolyl hydroxamates that we have shown possess enhanced HDAC inhibition activity.[48b] Results from *in vitro* and whole cell studies showed that these compounds possess inhibition activities against both target enzymes and inhibit the growth of DU-145 prostate carcinoma cells. Relative to the camptothecin standard SN-38, the functionalization of the 10-hydroxy moiety presented no observable deleterious effect on the Topo I inhibition by 7-ethyl-10-hydroxycamptothecin-derived conjugates **13a-e** and only minor attenuation in the inhibitory activities of 10-hydroxycamptothecin-derived conjugates **13f-h** at the concentration tested (50 μM). Despite their potent Topo I inhibition activities in cell-free DNA plasmid relaxation assays, these compounds displayed anticancer activities against DU-145 cells at levels more comparable to the HDACi standard SAHA. One plausible explanation for this observation is that the functionalization of the 10-hydroxy moiety may negatively impact the binding of these conjugates to Topo I as crystallographic evidence suggests that the 10-hydroxy group is involved in a hydrogen bonding interaction with a water molecule oxygen at the Topo I active site.[87] Alternatively, the ability of these conjugates to interact with other tumor growth-inhibiting secondary targets of camptothecins[88,89] may be compromised.

Overall, these compounds show promise as potent anticancer agents with the potential to broadly arrest tumor growth by inhibiting two essential enzymes. Further work is needed to better elucidate the specific mechanisms responsible for the activities of these compounds. Several avenues for investigation could achieve this aim. First, the intracellular Topo I inhibition

could be profiled by immunoblotting of stabilized cleavable complexes to determine the relative contribution of Topo I inhibition to the overall anticancer activity. Also, since camptothecins are fluorescent, their subcellular localization [90]could be easily determined. The specific subcellular distribution of these compounds could be used to form indirect conclusions about the mechanisms underlying their anticancer activities and also serve as a basis for their differences in activity relative to each other. Furthermore, the HDACi mechanisms involved could be further probed via histone acetylation blots and, since these compounds were isoform selective towards HDAC6, tubulin acetylation could be investigated. Finally, second generation conjugates that retain the 10-hydroxy moiety on the camptothecin template could be used to profile whether addition of the HDACi moiety through the C-10 hydroxy group decreases efficacy by negatively affecting Topo I binding. If this is the case, an alternate design may prove better suited to Topo I inhibition, and possibly HDAC inhibition as well.

3.15 Experimental

3.15.1 In Vitro HDAC Inhibition

In vitro HDAC inhibition was assayed using the HDAC Fluorimetric Assay/Drug Discovery Kit as previously described.[48] Briefly, 15 μL of HeLa nuclear extract was mixed with 5 μL of 10× compound and 5 μL of assay buffer. In order to control for anthracycline fluorescence, an extra set of control wells were used in which compounds were diluted to HDAC test concentrations and assayed as normal, but without HeLa nuclear extract. Fluorescence values generated in these wells were subtracted from test well means to eliminate fluorescent contribution from the anthracycline. This method was also used for camptothecin-derived compounds. Fluorogenic HDAC substrate (25 μL) was then added, and reaction was allowed to

proceed for 15 min at room temperature and then stopped by addition of a developer containing TSA. Fluorescence was monitored after 15 min at excitation and emission wavelengths of 360 and 460 nm, respectively. IC_{50} values were determined using logit plots.

3.15.2 In Vitro Topo II Decatenation Assay (Josh Canzoneri)

The decatenation of KDNA was assayed according to TopoGen protocol in order to determine topoisomerase II activity. The substrate KDNA (200ng) and 50µM drug were combined in assay buffer (50 mM Tris–HCl, pH 8, 120 mM KCl, 10 mM $MgCl_2$, 0.5 mM ATP, 0.5 mM dithiothreitol, 300ug/ml bovine serum albumin (BSA)) and incubated for 10 min on ice. Next, 1 U of topoisomerase II was added and the reaction was allowed to proceed for 10 min at 37°C. The reaction was quenched via the addition of loading buffer (1% sarkosyl, 0.025% bromophenol blue, and 5% glycerol), and was then analyzed by electrophoresis on a 1% agarose gel in TBE buffer (89 mM Tris, 89 mM borate, and 2 mM Na–EDTA, pH 8.3) for 3.5 h at 40 V. The gel was stained with SYBR Green I (Molecular Probes) for 30 min and was visualized under UV illumination and photographed on an AlphaImager.

3.15.3 Cell Culture and Viability

DU-145 prostate carcinoma and SK-MES-1 non-small cell lung carcinoma was obtained from ATCC (Manassass, VA) and maintained in the recommended growth mediums. MCF-7 breast cancer cells were a generous gift from Dr. Donald Doyle. All cell lines were maintained in a 37°C incubator with a 5% CO_2 environment. All compounds to be tested were dissolved to a concentration of 10 mM in DMSO and stored at -80°C. Cells were passaged 24 h prior to cell viability experiments. For cancer cell viability experiments, cells were dosed for 72 h and viability was determined both by Trypan Blue staining and/or through the use of the MTS assay

(Promega) according to manufacturer's instructions. Control wells were dosed with fresh media containing 0.1% DMSO.

3.15.4 Intracellular Topo II Inhibition

DU-145 cells were probed for Topo II inhibition with an *in vitro* blotting kit designed to show relative amounts of stabilized Topo II-DNA cleavage complexes (Topoisomerase II *In Vivo* Link Kit, Topogen). Briefly, cells were dosed with Topo II-HDACi's at concentrations pertaining to their respective IC_{50} values for cell viability inhibition. Control cells were dosed with 0.1% DMSO to take into account DMSO from stock solutions of drug. As recommended in the protocol instructions, cells were dosed for 30 minutes, counted, and lysed with 1% sarkosyl. Alternately, DU-145 cells were dosed for 72 hours, counted, and equalized with the cell count from the 30 min incubation before subsequent lysis. Lysate was collected, loaded on a CsCl gradient, and subjected to centrifugation at 31,000 RPM at room temperature for 12 hours. Aliquots of the gradient separations were then taken and the Topo II-DNA cleavage complexes were identified via absorbance at 260 nm. Aliquots were then loaded into a slot blotting device and subjected to vacuum to load proteins onto a nitrocellulose membrane. Immunoblotting using the Odyssey Imaging System (LiCor Biosciences) revealed Topo II levels associated with the stabilized DNA complexes.

3.15.5 Immunoblotting of $p21^{waf1}$ and Histone Acetylation

DU-145 prostate cancer cells were passaged 24 h prior to the experiment. Compounds to be tested were diluted in the growth medium so that the final concentration of DMSO was 0.1% and control cells were dosed with fresh media containing 0.1% DMSO. Cells were dosed for 24 h, then washed twice with ice-cold PBS, and lysed on the culture plate at 4°C for 5 min with

RIPA buffer containing protease inhibitors. Lysates were mixed repeatedly by pipetting and centrifuged at 14,000 X g for 15 minutes at 4°C. Supernatant was saved and protein concentration was quantified using the Bio-Rad Protein Assay (Bio-Rad) with BSA as the standard. For histone samples, the nuclear pellet was saved after centrifugation and washed with RIPA buffer. Pellets were resuspended in 0.2 N HCl and acid extracted overnight at 4°C. Samples were centrifuged at 6500 x g for 10 minutes at 4°C and the supernatant was saved and protein content was quantified using the Bio-Rad Protein Assay.

Loading buffer was added and protein samples were incubated at 100°C for 10 min before electrophoresis. Proteins were then transferred to a nitrocellulose membrane for 1 h, followed by blocking overnight in a 1:1 mixture of Odyssey Blocking Buffer (LiCor Biosciences) and PBS. Membranes were incubated with primary and secondary antibodies, both diluted in 1:1 Odyssey Blocking Buffer/PBS. Membranes were scanned on the Odyssey infrared imaging system (LiCor Biosciences) using both 700 nm and 800 nm channels simultaneously at 169 μm resolution and analyzed on the imaging software.

3.15.6 Immunoblotting of Tubulin Acetylation

DU-145 cells were passaged 24 hours prior to dosing. Compounds were diluted such that cells, including controls, were exposed to no more than 0.1% DMSO. Cells were dosed for 4 hours before lysis in RIPA buffer with protease inhibitors. Lysates were vortexed and centrifuged at 14,000 RPM at 4°C for 15 minutes. Supernatants were removed and protein concentration was assayed using the Bio Rad Protein Assay with BSA as a standard. Electrophoresis and immunoblotting were performed as described above. Rabbit anti-tubulin (Sigma) and mouse anti-acetyl tubulin (Invitrogen) were used to probe the membrane after

blocking with Odyssey Blocking buffer (Li Cor). Li Cor near-infrared secondary antibodies were used to image the blot with the Odyssey infrared imaging system at 700 and 800 nm.

3.15.7 Intracellular Localization of Topo II-HDACi (Josh Canzoneri)

Cells were plated on glass coverslips in 35mm dishes 24 h before the experiment. They were then incubated with fresh media containing the indicated compounds at concentration of 1 µM. After 4 hours, cells were washed with PBS Cover slips were then mounted and viewed under a confocal microscope (DAU λ_{ex} = 488nm,; Zeiss LSM 510 UV confocal microscope).

3.14.8 Topo I-induced DNA Plasmid Relaxation Assay (Josh Canzoneri)

The drug-induced formation of cleavable complexes was conducted in 10 mM Tris-HCl, pH 7.9, 1 mM EDTA, 0.15 M NaCl, 0.1% BSA, 0.1 mM spermidine, 5% glycerol. A 250-ng aliquot of pBR322 plasmid DNA (NEB) was mixed with the drug of interest and allowed to equilibrate at room temperature for 20 minutes. Next, reactions were placed on ice and 4 U of human topoisomerase I (Topogen) was added to a 20-ml total mixture volume. Each sample was incubated at 37°C for 30 minutes, then the formation of complexes was terminated by the addition of 2 ml of 10% SDS and 2 ml of 0.5 mg/ml Proteinase K (Ambion). The mixtures were subsequently incubated for 30 minutes at 37°C, then mixed with 2 ml of loading solution (25% bromophenol blue, 50% glycerol) and extracted with 20 ml of 24:1 chloroform/isoamyl alcohol. Samples were then analyzed by electrophoresis for 16 hours at 30 V on a pre-run (1 h at 30V) 1% agarose gel in TAE buffer (40 mM Tris-acetate, 1 mM EDTA, pH 8.0, containing 0.5 mg/ml ethidium bromide). After electrophoresis, the gel was stained with a 1:10,000 dilution of SYBR Green (Molecular Probes) in TE buffer (10 mM Tris-HCl, 1 mM EDTA, pH 8.0) at 4°C for 30

minutes on a rocker, and was then digitally photographed under transillumination with 300-nm UV light.

3.16 References

1.) Morphy, R.; Kay, C.; Rankovic, Z. From magic bullets to designed multiple ligands. *Drug Discov Today.* ***2004,*** 9, 641-651.

2.) Morphy, R.; Rankovic, Z. Designed Multiple Ligands. An Emerging Drug Discovery Paradigm. *J. Med. Chem.* **2005**, 48, 6523–6543.

3.) Frantz, S. Drug discovery: Playing dirty. *Nature.* **2005,** 437, 942-943**.**

4.) Roth, B. L.; Sheffler, D. J.; Kroeze, W. K. Magic shotguns versus magic bullets: Selectively non-selective drugs for mood disorders and schizophrenia. *Nat. Rev. Drug Discov*. **2004,** 3, 353-359.

5.) Hopkins, A. L.; Mason, J. S.; Overington, J. P. Can we rationally design promiscuous drugs? *Curr. Opinion Struct. Biol*. **2006**, 16, 127-136

6.) Cmeserly, P.; Agoston, V.; Pongor, S. The efficiency of multi-target drugs: The network approach might help drug design. *Trends Pharmacol. Sci.* **2005***,* 26, 178-182.

7.) Fray, M.J; Bish, G.; Brown, A.D.; Fish, P.V.; Stobie, A.; Wakenhut, F.; Whitlock, G.A. *N*-(1,2-Diphenylethyl)piperazines: A new class of dual serotonin/noradrenaline reuptake inhibitor. *Bioorg. Med. Chem. Lett.* **2006**, 16, 4345-4348.

8.) Neumeyer, J.L.; Peng, X.; Knapp, B.I.; Bidlack, J.M.; Lazarus, L.H.; Salvadori, S.; Trapella, C.; Balboni, G. New opioid designed multiple ligand from Dmt-Tic and Morphinan pharmacophores. *J.Med. Chem.* **2006**, 49, 5640-5643.

9.) Jones, P. A.; Baylin, S. B. The epigenomics of cancer. *Cell.,* **2007,** 128, 683-692.

10.) Kouzarides, T. Chromatin modifications and their function. *Cell.* **2007,** 128, 693-705.

11.) Shilatifard, A. Chromatin modifications by methylation and ubiquitination: implications in the regulation of gene expression. *Ann. Rev. Biochem.* **2006,** 75, 243-269.

12.) Ropero, S; Esteller, M. The role of histone deacetylases (HDACs) in human cancer. *Mol. Oncol,* **2007**, 1, 19-25.

13.) Marks, P. A.; Richon, V. M.; Rifkind, R. A. Histone deacetylase inhibitors: inducers of differentiation or apoptosis of transformed cells. *J. Natl. Cancer Inst*. **2000**, 92, 1210-1216.

14.) Saito, A.; Yamashita, T.; Mariko, Y.; Nosaka, Y.; Tsuchiya, K.; Ando, T.; Suzuki, T.; Tsuruo, T.; Nakanishi, O. A synthetic inhibitor of histone deacetylase, MS-275, with marked *in vivo* antitumor activity against human tumors. *PNAS*. **1999**, 96, 4592-4597.

15.) Glick, R. D.; Swindemen, S. L.; Coffey, D. C.; Rifkind, R. A.; Marks, P. A.; Richon, V. M.; La Quaglia, M. P. Hybrid polar histone deacetylase induces apoptosis and CD95/CD95 ligand expression in human neuroblastoma. *Cancer Res*. **1999**, 59, 4392-4399.

16.) Butler, L. M.; Agus, D. B.; Scher, H. I.; Higgins, B.; Rose, A.; Cordon-Cardo, C.; Thaler, H. T.; Rifkind, R. A.; Marks, P.A.; Richon, V.M. Suberoylanilide hydroxamic acid, an inhibitor of histone deacetylase, suppresses the growth of prostate cancer cells *in vitro* and *in vivo*. *Cancer Res*. **2000**, 60, 5165-5170.

17.) Oyelere, A.K.; Chen, P.C.; Guerrant, W.; Mwakwari, S.C.; Hood, R.; Zhang, Y.; Fan, Y. Non-peptide macrocyclic histone deacetylases inhibitors. *J. Med. Chem*. **2009**, 52, 456-468.

18.) Gu, W and Roeder, RG. Activation of p53 sequence-specific DNA binding by acetylation of the p53 C-terminal domain. *Cell*. **1997**, 90, 595-606.

19.) Martinez-Balbás, M.A.; Bauer, U.M.; Nielsen, S.J.; Brehm, A.; Kouzarides, T. Regulation of E2F1 activity by acetylation. *EMBO J*. **2000**, 19, 662-671.

20.) Marzio, G.; Wagener, C.; Gutierrez, M.I.; Cartwright, P.; Helin, K.; Giacca, M. E2F family members are differentially regulated by reversible acetylation. *J. Biol. Chem*. **2000**, 275, 10887-10892.

21.) Hubbert, C.; Guardiola, A.; Shao, R.; Kawaguchi, Y.; Ito, A.; Nixon, A.; Yoshida, M.; Wang, X.F.; Yao, T.P. HDAC6 is a microtubule-associated deacetylase. *Nature*. **2002**, 417, 455-458.

22.) Kovacs, J.J.; Murphy, P.J.; Gaillard, S.; Zhao, X.; Wu, J.T.; Nicchitta, C.V.; Yoshida, M.; Toft, D.O.; Pratt, W.B.; Yao, T.P. HDAC6 regulates Hsp90 acetylation and chaperone-dependent activation of glucocorticoid receptor. *Mol. Cell*. **2005**, 18, 601-607.

23.) Mann, B.S.; Johnson, J.R.; Cohen, M.H.; Justice, R.; Padzur, R. FDA approval summary: vorinostat for treatment of advanced primary cutaneous T-cell lymphoma. *Oncologist*. **2007**, 12, 1247-1252.

24.) Grant, C.; Rahman, F.; Piekarz, R.; Peer, C.; Frye, R.; Robey, R.W.; Gardner, E.R.; Figg, W.D.; Bates, S.E. Romidepsin; a new therapy for cutaneous T-cell lymphoma and a potential therapy for solid tumors. *Expert Rev. Anticancer Ther*. **2010**, 10, 997-1008.

25.) Mwakwari, S.C.; Patil, V.; Guerrant, W.; Oyelere, A.K. Macrocyclic histone deacetylases inhibitors. *Curr. Top. Med. Chem*. **2010**, 10, 1423-1440.

26.) Kelly, W. K; O'Connor, O. A.; Marks, P. A. Histone deacetylase inhibitors: from target to clinical trials. *Expert. Opin. Investig. Drugs.* **2002**, 11, 1695-1713.

27.) Rosato, R. R.; Grant, S. Histone deacetylase inhibitors in clinical development. *Expert Opin. Invest. Drugs.* **2004**, 13, 21-38.

28.) Yoo, C. B.; Jones, P. A. Epigenetic therapy of cancer: past, present and future. *Nature Rev. Drug Discov.* **2006**, 5, 37-50.

29.) Finnin, M. S.; Donigian, J. R.; Cohen, A.; Richon, V.M.; Rifkind, R.A.; Marks, P.A.; Breslow, R.; Pavletich, N.P. Structures of a histone deacetylase homologue bound to the TSA and SAHA inhibitors. *Nature.* **1999**, *401*, 188–193.

30.) Wang, D.-F.; Wiest, O.; Helquist, P.; Lan-Hargest, H-Y; Wiech, N.L. On the function of the 14 Å long internal cavity of histone deacetylase-like protein: implication for the design of histone deacetylase inhibitors. *J. Med. Chem.* **2004**, *47*, 3409–3417.

31.) Chen, L.; Wilson, D.; Jayaram, H.N.; Pankiewicz, K.W. Dual inhibitors of inosine monophosphate dehydrogenase and histone deacetylases for cancer treatment. *J. Med. Chem.* **2007**, 50, 26, 6685-6691.

32.) Mahboobi, S.; Dove, S.; Sellmer, A.; Winkler, M.; Eichhorn, E.; Pongratz, H.; Ciossek, T.; Baer, T.; Maier, T.; Beckers, T. Design of chimeric histone deacetylase- and tyrosine kinase-inhibitors: a series of imatinib hybrids as potent inhibitors of wild-type and mutant BCR-ABL, PDGF-Rβ, and histone deacetylases. *J. Med. Chem.* **2009**, 52, 8, 2265-2279.

33.) Cai, X.; Zhai, H-X.; Wang, J.; Forrester, J.; Qu, H.; Yin, L.; Cheng-Jung, L.; Bao, R.; Qian, C. Discovery of 7-(4-(3-ethynylphenylamino)-7-methoxyquinazolin-6-yloxy)-N-hydroxyheptanamide (CUDC-101) as a potent multi-acting HDAC, EGFR, and HER2 inhibitor for the treatment of cancer. *J. Med. Chem.* **2010**, 53, 5, 2000-2009.

34.) Piccart-Gebhart, M. J. Anthracyclines and the tailoring of treatment for early breast cancer. *N. Engl. J. Med*. **2006**, 354, 2177-2179.

35.) Kim, M. S.; Blake, M.; Baek, J. H.; Kohlhagen, G.; Pommier, Y.; Carrier, F. Inhibition of histone deacetylase increases cytotoxicity to anticancer drugs targeting DNA. *Cancer Res.* **2003**, 63, 7291–7300.

36.) Catalano, M.G.; Fortunati, N.; Pugliese, M.; Poli, R.; Bosco, O.; Mastrocola, R.; Aragno, M.; Bocuzzi, G. Valproic acid, a histone deacetylase inhibitor, enhances sensitivity to doxorubicin in anaplastic thyroid cancer cells. *J. Endocrinol*. **2006**, 191, 2, 465-472.

37.) Johnson, C.A.; Padget, K.; Austin, C.A.; Turner, B.M. Deacetylase activity associates with topoisomerase II and is necessary for etoposide-induced apoptosis. *J. Biol. Chem.* **2001**, 276, 7, 4539-4542.

38.) Marchion, D.C.; Bicaku, E.; Daud, A.I.; Richon, V.; Sullivan, D.M.; Munster, P.N. Sequence-specific potentiation of topoisomerase II inhibitors by the histone deacetylase inhibitor suberoylanilide hydroxamic acid. *J. Cell Biochem*. **2004**, 92, 2, 223-237.

39.) Tewey, K.M.; Rowe, T.C.; Yang, L.; Halligan, B.D.; Liu, L.F. Adriamycin-induced DNA damage mediated by mammalian DNA topoisomerase II. *Science*. **1984**, 226, 466-468.

40.) Binaschi, M.; Bigioni, M.; Cipollone, A.; Rossi, C.; Goso, C.; Maggi, C.A.; Capranico, G.; Animati, F. Anthracyclines: selected new developments. *Curr. Med. Chem. Anticancer Agents*. **2001**, 1, 2, 113-130.

41.) Pommier, Y.; Schwartz, R.E.; Kohn, K.W.; Zwelling, L.A. Formation and rejoining of deoxyribonucleic acid double-strand breaks induced in isolated nuclei by antineoplastic intercalating agents. *Biochemistry*. **1984**, 23, 3194-3201.

42.) Kiyomiya, K.; Matsuo, S.; Kurebe, M. Proteasome is a carrier to translocate doxorubicin from cytoplasm into nucleus. *Life Sci*. **1998**, 62, 20, 1853-1860.

43.) Kiyomiya, K.; Matsuo, S.; Kurebe, M. Mechanism of specific nuclear transport of adriamycin: the mode of nuclear translocation of adriamycin-proteasome complex. *Cancer Res*. **2001**, 61, 2467-2471.

44.) Tong, G.L.; Wu, H.Y.; Smith, T.H.; Henry, D.W. Adriamycin analogs. 3. synthesis of N-alkylated anthracyclines with enhanced efficacy and reduced toxicity. *J. Med. Chem.* **1979**, 22, 912-918.

45.) Martín, B.; Vaquero, A.; Priebe, W.; Portugal, J. Bisanthracycline WP631 inhibits basal and Sp1-activated transcription initiated *in vitro*. *Nucleic Acids Res*. **1999**, 27, 3402-3409.

46.) Lothstein, L.; Israel, M.; Sweatman, T.W. Anthracycline drug targeting: cytoplasmic versus nuclear – a fork in the road. *Drug Resist. Updat*. **2001**, 4, 169-177.

47.) Gate, L.; Couvreur, P.; Nguyen-Ba, G.; Tapiero, H. N-methylation of anthracyclines modulates their cytotoxicity and pharmacokinetics in wild type and multidrug resistant cells. *Biomed & Pharmacotherapy*. **2003**, 57, 301-308.

48.) (a) Mwakwari, S.C.; Guerrant, W.; Patil, V.; Khan, S.I.; Tekwani, B.L.; Gurard-Levin, Z.A.; Mrksich, M.; Oyelere, A.K. Non-peptide histone deacetylases inhibitors derived from tricyclic ketolide skeleton. *J. Med. Chem*. **2010**, 53, 6100-6111.; (b) Chen, P.C.; Patil, V.; Guerrant, W.; Green, P.; Oyelere, A.K. Synthesis and structure-activity relationship of histone deacetylase (HDAC) inhibitors with triazole-linked cap group. *Bioorg. Med. Chem*. **2008**, 16, 4839-4853.

49.) Lu J., Yoshida O, Hayashi S., Arimoto H. Synthesis of rigidly-linked vancomycin dimers and their *in vivo* efficacy against resistant bacteria. *Chem. Commun.* **2007**, 251-253.

50.) Preobrazhenskaya, M. N.; Olsufyeva, E.N.; Solovieva, S.E.; Tevyashova, A.N.; Reznikova, M.I.; Luzikov, Y.N.; Terekhova, L.P.; Trenin, A.S.; Galatenko, O.A.; Treshalin, I.D.; Mirchink, E.P.; Bukhman, V.M.; Sletta, H.; Zotchev, S.B. Chemical modification and biological evaluation of new semi-synthetic derivatives of 28, 29-didehydronystatin A_1 (S44HP), a genetically engineered anti-fungal polyene macrolide antibiotic. *J. Med. Chem*. **2009**, 52, 189–196.

51.) Yang S., Lagu B., Wilson L. Mild and efficient Lewis acid-promoted detritylation in the synthesis of N-hydroxy amides: a concise synthesis of (-)-cobactin T. *J. Org. Chem.* **2007**, 72(21) 8123-8126.

52.) Morris, G.M.; Goodsell, D.S.; Halliday, R.S.; Huey, R.; Hart, W.E.; Belew, R.K.; Olson, A.J. Automated docking using a Lamarckian genetic algorithm and empirical binding free energy function. J. Comput. Chem. 1998, 19, 1639-1662.

53.) Estiu G.; Wiest, O. HDAC1 homology model, Personal Communication.

54.) Marini, J.C.; Miller, K.G.; Englund, P.T. Decatenation of kinetoplast DNA by topoisomerases. *J. Biol. Chem*. **1980**, 255, 11, 4976-4979.

55.) Sahai, B and Kaplan, *J.* A quantitative decatenation assay for type II topoisomerases. *Anal. Biochem*. **1986**, 156, 2, 364-379.

56.) Qu, X.; Wan, C.; Becker, H.C.; Zhong, D.; Zewail, A.H. The anticancer drug-DNA complex: femtosecond primary dynamics for anthracycline antibiotics function. *PNAS*. **2001**, 98, 25, 14212-14217.

57.) Kulp, S.K.; Chen, C.S.; Wang, D.S.; Chen, C.Y.; Chen, C.S. Antitumor effects of a novel phenylbutyrate-based histone deacetylases inhibitor, (*S*)-HDAC-42, in prostate cancer. *Clin. Cancer Res*. **2006**, 12, 5199-5206.

58.) Doyle, L.A.; Abruzzo, Y.W.; Krogmann, T.; Yongming, G.; Rishi, A.K.; Ross, D.D. A multidrug resistance transporter from human MCF-7 breast cancer cells. *PNAS*. **1998**, 95, 15665-15670.

59.) Richon, V.M.; Sandhoff, T.W.; Rifkind, R.A.; Marks, P.A. Histone deacetylase inhibitor selectively induces $p21^{WAF1}$ expression and gene-associated histone acetylation. *PNAS*. **2000**, 97, 18, 10014-10019.

60.) Gartenhaus, R.B.; Wang, P.; Hoffmann, P. Induction of the WAF1/CIP1 protein and apoptosis in human T-cell leukemia virus type I-transformed lymphocytes after treatment with adriamycin by using the p53-dndependent pathway. *PNAS*. **1996**, 93, 265-268.

61.) North, B.J.; Marshall, B.L.; Borra, M.T.; Denu, J.M.; Verdin, E. The human Sir2 ortholog, SIRT2, is an NAD^+-dependent tubulin deacetylase. *Mol. Cell.* **2003**, 11, 437-444.

62.) Schäfer, S.; Saunders, L.; Eliseeva, E.; Velena, A.; Jung, M.; Schwienhorst, A.; Strasser, A.; Dickmanns, A.; Ficner, R.; Schlimme, S.; Sippl, W.; Verdin, E.; Jung, M. Phenylalanine-containing hydroxamic acids as selective inhibitors of class IIb histone deacetylases (HDACs). *Bioorg. Med. Chem.*, **2008**, 16, 2011-2033.

63.) Namdar, M.; Perez, G.; Ngo, L.; Marks, P.A. Selective inhibition of histone deacetylases 6 (HDAC6) induces DNA damage and sensitizes transformed cells to anticancer agents. *PNAS*, **2010**, 107, 20003-20008.

64.) Blagosklonny, M.V.; Robey, R.; Sackett, D.L.; Du, L.; Traganos, F.; Darzynkiewicz, Z.; Fojo, T.; Bates, S.E. Histone deacetylases inhibitors all induce p21 but differentially cause tubulin acetylation, mitotic arrest, and cytotoxicity. *Mol. Cell Ther*., **2002**, 1, 937-941.

65.) Zhang, Y.; Li, N.; Caron, C.; Matthias, G.; Hess, D.; Khochbin, S.; Matthias, P. HDAC-6 interacts with and deacetylates tubulin and microtubules *in vivo*. *EMBO J*. **2003**, 22, 1168-1179.

66.) Gao, H.; Huang, K.C.; Yamasaki, E.F.; Chan, K.K.; Chohan, L.; Snapka, R.M. XK469, a selective topoisomerase IIβ poison. *Proc. Natl. Acad. Sci*. **1999**, 96, 12168-12173.

67.) Kiyomiya, K.; Satoh, J.; Horie,H. ;Kurebe, M.; Nakagawa, H.; Matsuo, S. Correlation between nuclear action of anthracycline anticancer agents and their binding affinity to the proteasome. *Int. J. Oncol.* **2002**, 21, 5, 1081-1085.

68.) Marbeuf-Gueye, C.; Ettori, D.; Priebe, W.; Kozlowski, H.; Garnier-Suillerot, A. Correlation between the kinetics of anthracycline uptake and the resistance factor in cancer cells expressing the multidrug resistance protein or the P-glycoprotein**.** *Biochim Biophys Acta.* **1999,** 1450, 3, 374-384

69.) Chen, A.Y. and Liu, L.F. DNA Topoisomerases: Essential Enzymes and Lethal Targets. *Annu. Rev. Pharmacol. Toxicol.* **1994,** 34, 191-218

70.) Froelich-Ammon, S.J. and Osheroff, N. Topoisomerase Poisons: Harnessing the Dark Side of Enzyme Mechanism. *J. Biol. Chem.* **1995,** 270, 21429-21432.

71.) Pommier, Y. DNA Topoisomerase I Inhibitors: Chemistry, Biology, and Interfacial Inhibition. *Chem. Rev.* **2009,** 109, 2894-2902.

72.) Hsiang, Y.H.; Lihou, M.G.; Liu, L.F. Arrest of Replication Forks by Drug-Stabilized Topoisomerase I-DNA Cleavable Complexes as a Mechanism of Cell Killing by Camptothecin. *Cancer Res.* **1989,** 49, 5077-5082.

73.) Matsukawa, Y.; Marui, N.; Sakai, T.; Satomi, Y.; Yoshida, M.; Matsumoto, K.; Nishino, H.; Aoike, A. Genistein Arrests Cell Cycle Progression at G2-M. *Cancer Res.* **1993,** 53, 1328-1331.

74.) Bevins, R. L.; Zimmer, S. G. It's about time: scheduling alters effect of histone deacetylase inhibitors on camptothecin-treated cells. *Cancer Res.* **2005**, 65 (15), 6957.

75.) Zhang, R.; Li, Y.; Cai, Q.; Liu, T.; Sun, H.; Chambless, B. Preclinical pharmacology of the natural product anticancer agent 10-hydroxycamptothecin, an inhibitor of topoisomerase I. *Cancer Chemother. Pharmacol*. **1998**, 41, 257.

76.) Chen, Z. S.; Furukawa, T.; Sumizawa, T.; Ono, K.; Ueda, K.; Seto, K.; Akiyama, S. I. ATP-dependent efflux of CPT-11 and SN-38 by the multidrug resistance protein (MRP) and it's inhibition by PAK-104P. *Mol. Pharmacol.* **1999**, 55, 921.

77.) Sugimori, M.; Ejima, A.; Ohsuki, S.; Uoto, K.; Mitsui, I.; Matsumoto, K.; Kawato, Y.; Yasuoka, M.; Sato, K.; Tagawa, H.; Terasawa, H.; Antitumor agents. VII. Synthesis and antitumor activity of novel hexacyclic camptothecin analogues. *J. Med. Chem.* **1994**, 37, 3033.

78.) (a) Leu, Y. L.; Chen, C. S.; Wu Y. J.; Chern J. W. Benzyl ether-linked glucuronide derivative of 10-hydroxycamptothecin designed for selective camptothecin-based anticancer therapy. *J. Med. Chem.* **2008**, 51, 1740. (b) Ulukan, H.; Swaan, P. W. Camptothecins: a review of their chemotherapeutic potential. *Drugs* **2002**, 62, 2039-2057.

79.) Guerrant, W.; Patil, V.; Canzoneri, J.C.; Oyelere, A.K. Dual targeting of histone deacetylase and topoisomerase II with novel bifunctional inhibitors. *J. Med. Chem.* **2012**, 55, 1465-1477.

80.) *HDAC Fluorimetric Assay/Drug Discovery Kit. AK-500 Manual. Fluorescent Assay System;* BIOMOL International, L.P.; Plymouth Meeting, PA, 2005.

81.) Ying, Y.; Taori, K.; Kim, H.; Hong, J.; Luesch, H. Total synthesis and molecular target of largazole, a histone deacetylase inhibitor. *J. Am. Chem. Soc*. **2008**, 130, 8455-8459.

82.) Madhavaiah, C.; Verma, S. Plasmid relaxation induced by copper metalated diglycine conjugates under heterogeneous reaction conditions. *Bioorg. Med. Chem. Lett*. **2003**, 13 923-926.

83.) Dexheimer, T.S.; Pommier, Y. DNA cleavage assay for the identification of topoisomerase I inhibitors. *Nat. Protoc*. **2008**, 3, 1736-1750.

84.) Kawato, Y.; Aonuma, M.; Hirota, Y.; Kuga, H; Sato, K. Intracellular roles of SN-38, a metabolite of the camptothecin derivative CPT-11, in the antitumor effect of CPT-11. *Cancer Res*. **1991**, 51, 4187-4191.

85.) Larsen, A.K.; Gilbert, C.; Chyzak, G.; Plisov, S.Y.; Naguibneva, I.; Lavergne, O.; Lesueur-Ginot, L.; Bigg, D.C.H. Unusual potency of BN 80915, a novel fluorinated E-ring modified camptothecin, toward human colon carcinoma cells. *Cancer Res*. **2001**, 61, 2161-2167.

86.) Motwani, M.; Jung, C.; Sirotnak, F.M.; She, Y.; Shah, M.A.; Gonen, M.; Schwartz, G.K. Augmentation of apoptosis and tumor regression by flavopiridol in the presence of CPT-11 in Hct116 colon cancer monolayers and xenografts. *Clin. Cancer Res*. **2001**, 7, 4209-4219.

87.) Staker, B.L.; Hjerrild, K.; Feese, M.D.; Behnke, C.A.; Burgin, Jr, A.B.; Stewart, L. The mechanism of topoisomerase I poisoning by a camptothecin analog. *PNAS* **2002**, 99, 15387-15392.

88.) Bredholt, T.; Dimba, E. A.O.; Hagland, H.R.; Wergeland, L.; Skavland, J.; Fossan, K.O.; Tronstad, K.J.; Johannessen, A.C.; Vintermyr, O.K.; Gjertsen, B.T. Camptothecin and khat (*Catha edulis* Forsk.) induced distinct cell death phenotypes involving modulation of c-$FLIP_L$, Mcl-1, procaspase-8 and mitochondrial function in acute myeloid leukemia cell lines. *Mol. Cancer* **2009**, 8, 101.

89.) Chatterjee, D.; Schmitz, I.; Krueger, A.; Yeung, K.; Kirchoff, S.; Krammer, P.H.; Peter, M.E.; Wyche, J.H.; Pantazis, P. Induction of apoptosis in 9-nitrocamptothecin-treated DU145 human prostate carcinoma cells correlates with de Novo Synthesis of CD95 and CD95 ligand and down-regulation of c-$FLIP_{short}$. *Cancer Res*. **2001**, 61, 7148-7154.

90.) Croce, A.C.; Bottiroli, G.; Supino, R.; Favini, E.; Zuco, V.; Zunino, F. Subcellular localization of the camptothecin analogues, topotecan and gimatecan. *Biochem. Pharmacol*. **2004**, 67, 1035-1045.

Chapter 4

Lung-Targeted Macrocyclic HDAC Inhibition

The promise of HDACi as a viable therapeutic strategy, evinced initially through the *in vitro* inhibition of multiple cancer cell types through multiple antiproliferative mechanisms and later with the FDA approvals of SAHA and FK-228, has recently been somewhat overshadowed with lingering questions about their applicability for the treatment of solid tumors.[1] Moreover, cardiac side effects, namely QTc prolongation observed with virtually every HDACi, and the cardiotoxicity observed in one clinical trial with FK-228 have been cause for concern.[1,2] Additionally, the discovery that different tumor types dysregulate specific HDAC isoforms[3] has made the design and validation of isoform-selective HDACi an attractive goal that has unfortunately been hampered by the lack of crystal structures for most HDAC enzymes.[4] Additionally, this approach has also been complicated by the discovery that certain HDAC enzymes are functionally redundant with others. A complimentary strategy to address these issues could be to design tissue-specific HDACi, which could target solid tumors of a particular tissue while limiting side effects caused by off-target residency.

Lung cancer is both the second most common cancer by incidence and accounts for the highest mortality in both sexes, making it an essential target for chemotherapeutic development.[5] Additionally, lung cancer is known to upregulate class I HDACs, specifically HDACs 1 and 3[3], and combined treatment with SAHA, carboplatin, and paclitaxel has shown promising *in vivo* responses over carboplatin, paclitaxel and placebo.[6] It is possible that a lung-targeted HDACi could inhibit the dysregulated HDAC isoforms, allowing for more precise definition of the

HDAC-specific contributions to the malignant phenotype, as well as selectively accumulating in concentrations conducive to effective treatment of solid lung tumors. We believed an appropriate framework to design lung-targeted HDACi could incorporate complex cap groups that could selectively interact with distinct HDAC isoforms while serving as a lung-targeting moiety.

4.1 Design of Lung-Targeted Macrocyclic HDACi

All HDACi currently reported, including the aryl hydroxamates, benzamides, short-chain fatty acids, electrophilic ketones, and macrocyclic peptides, fit the classical three-motif pharmacophoric model (Figure 2-1).[7] Of these, the macrocyclic peptide class of inhibitors possess the most complex cap groups, affording the greatest opportunity for modulating the biological activities of HDAC enzymes through isoform-selective inhibition. Although the cyclic-peptide HDACi possess potent nanomolar HDAC inhibition activities, their broader application in cancer therapy remains unproven.[7] One exception, FK-228, is currently FDA-approved for the treatment of cutaneous T-cell lymphoma and displays an selective inhibition profile for class I HDACs.[8,9]

The dearth of clinically-effective cyclic-peptide HDACi could arise in part due to developmental problems common to large peptides, such as poor oral bioavailability. In addition to the pharmacologically disadvantaged peptidyl backbone, cyclic-peptide HDACi offer limited opportunity for side chain modifications and are stereochemically constrained, in the case of the cyclic tetrapeptide HDACi.[10] Identification of nonpeptide macrocyclic HDACi could afford a novel class of compounds with more biologically favorable characteristics, as well as further enhance the understanding of the roles of specific interactions with residues on the outer surfaces

of HDAC enzymes. Most importantly, an appropriate peptidomimetic would need to retain efficacy as a cap group within the HDACi pharmacophore while selectively directing the small molecule toward lung tissue selectivity.

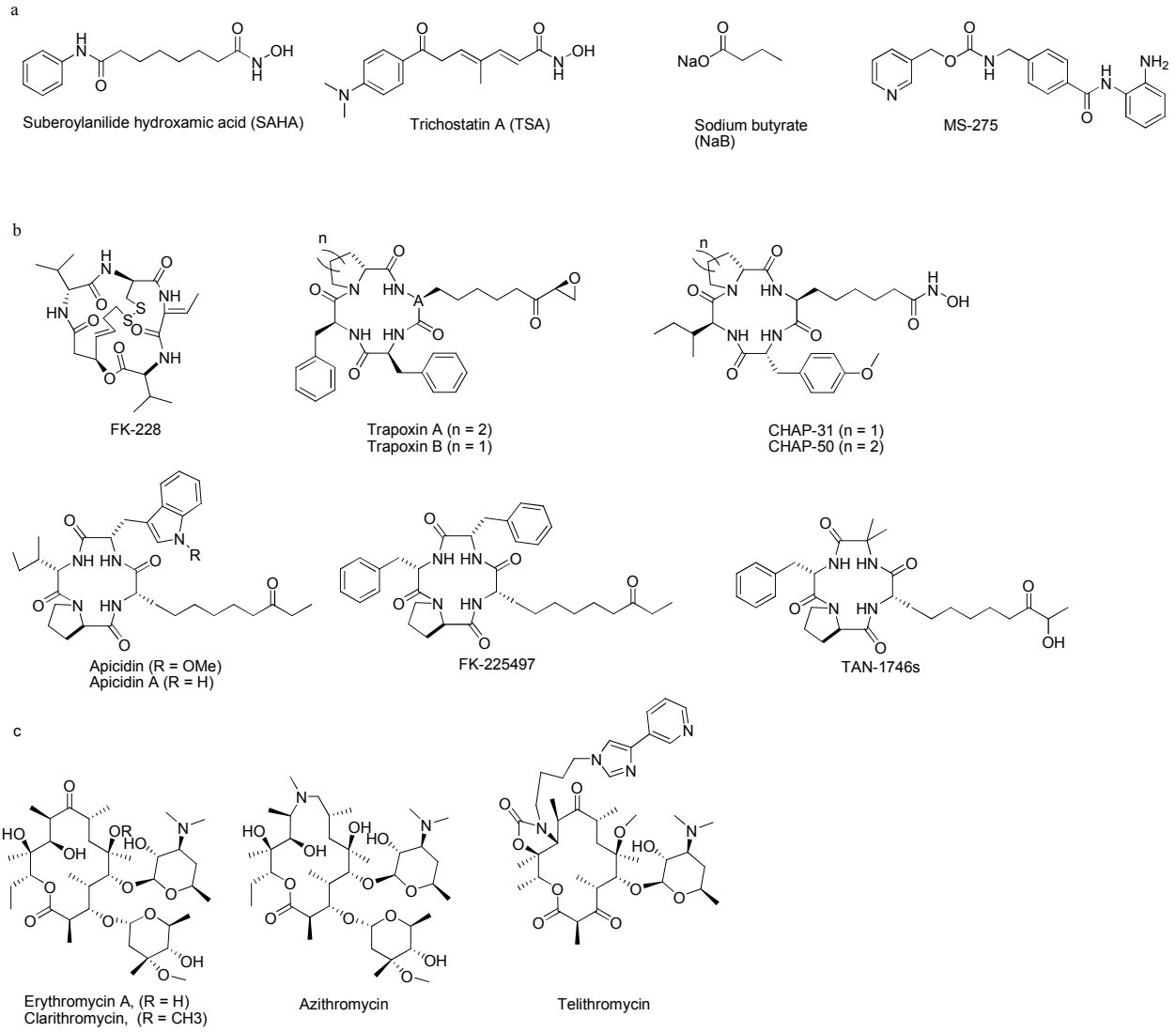

Figure 4-1: Selected examples of linear HDACi (a), representative cyclic-peptide HDACi (b), and representative macrolide antibiotics (c).

Macrolides are glycosylated polyketide antibiotics that have been in clinical use for more than 50 years for the treatment of respiratory tract infections (Figure 2-1). Macrolides also possess other pharmacologically favorable, non-antibiotic properties, such as anti-inflammatory and immunomodulatory effects, that make them promising candidates for the management of chronic diseases affecting airway inflammation.[11,12] Most importantly, macrolides possess favorable pharmacokinetic properties that distribute the drug to the lungs preferentially, possibly through a macrophage-dependent mechanism, in high and sustained concentrations.[13-16] Additionally, macrolides derived from the 6-*O*-methylerythromycin A ring have been reported to serve as nonpeptide surrogates for the peptide backbone of macrocyclic peptide luteinizing hormone-releasing hormone (LHRH) receptor agonists.[17] The advantageous pharmacology and peptidomimetic nature of macrolides fit optimally within a lung-targeted design and we hypothesized that an appropriate substitution of the cyclic peptide moiety of a prototypical cyclic-peptide HDACi with macrolide skeletons could generate a novel class of potent, nonpeptide, lung-targeted macrocyclic HDACi.

In order to test this hypothesis, a SAHA-macrolide conjugate was sought that would incorporate the 12-membered azalide ring of azithromycin as the macrolide template (Figure 2-1). The azithromycin skeleton is attractive due to its excellent pharmacokinetic profile and the ease of chemical transformation of key moieties on the skeleton.[18] The design approach necessitated attachment of the HDACi linker and ZBG to the macrolide remote from the macrocyclic ring, as we anticipated that a potential steric hindrance might occur at the HDAC active site due to the introduction of the azithromycin skeleton, a macrocyclic ring not optimized for HDAC binding. After studying the NMR[19] and 3D structure, the 3' amine was chosen as the position best suited for modification with a HDACi moiety as there are well established

transformations of the tertiary amine moiety,[17,18] and almost all modifications at this position attenuate antibacterial activity.[18b] Two compounds were synthesized with SAHA-like moieties attached at the 3' tertiary amine, macrocyclic depsipeptide **8** and the descladinose depsipeptide **10** (Figure 4-2).

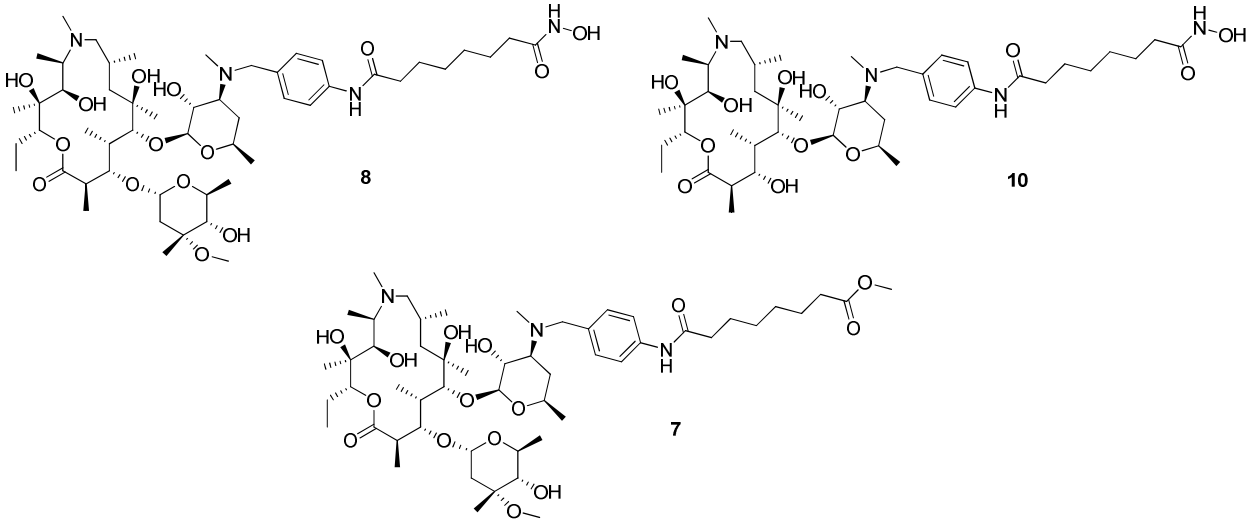

Figure 4-2: Structures of macrocyclic depsipeptides **8** and **10**, with methyl ester precursor, **7**. Synthesized by Dr. Yomi Oyelere.

4.2 *In Vitro* HDAC Inhibition by Macrocyclic HDACi

4.2.1 Inhibition of HeLa Nuclear Extract HDACs

The inhibition of HDAC by macrocyclic depsipeptides was assayed using a cell-free kit assay (Fluor de Lys, Biomol) which revealed concentration-dependent inhibition of HeLa nuclear extract, containing high concentrations of HDACs 1 and 2. Both **8** and **10** have identical anti-HDAC activity, with IC_{50} values in the low nanomolar range(Table 4-1). Conversely, compound **7**, the methyl ester precursor of **8**, is devoid of activity in this assay. This result

suggests that the azithromycin macrolide is an appropriate cap group substitute for that of typical cyclic-peptide HDACi. Additionally, it is possible that these compounds bind in an orientation that facilitates effective hydroxamate placement to chelate the Zn^{2+} ion while orienting the cladinose sugar away from enzyme residues, thus explaining the identical activities of **8** and **10**.

Table 4-1: *In vitro* HDAC inhibition of nonpeptide macrocyclic HDACi

Compound	HeLa Nuclear Extract (nM)[a]
7	N.D.
8	107.1
10	109.8
16a	91.6
16b	88.8
SAHA	65.0

[a] IC_{50} values were determined using the Biomol HDAC Fluorimetric Assay/Drug Discovery Kit. N.D. : not determinable.

We then initiated a structure-activity relationship (SAR) study on **8** and **10** in order to optimize the HDAC binding affinity of these compounds. The linker-cap group connecting moiety, macrolide skeleton, and linker length are three fragments that were altered in an attempt to arrive at optimal anti-HDAC activity. The AutoDock program[20] and the crystal structure of histone deacetylase-like protein (HDLP)[21] were both used the guide the structural optimization. In an earlier study, we demonstrated the utility of the 1,2,3-triazole ring as an alternative linker-cap group connection moiety in SAHA-like HDACi.[22] Accordingly, we tested the compatibility

of the triazole ring with the anti-HDAC activity of **8** and **10**, using the triazole-connected analogs **16a** and **16b**, respectively (Figure 4-2).

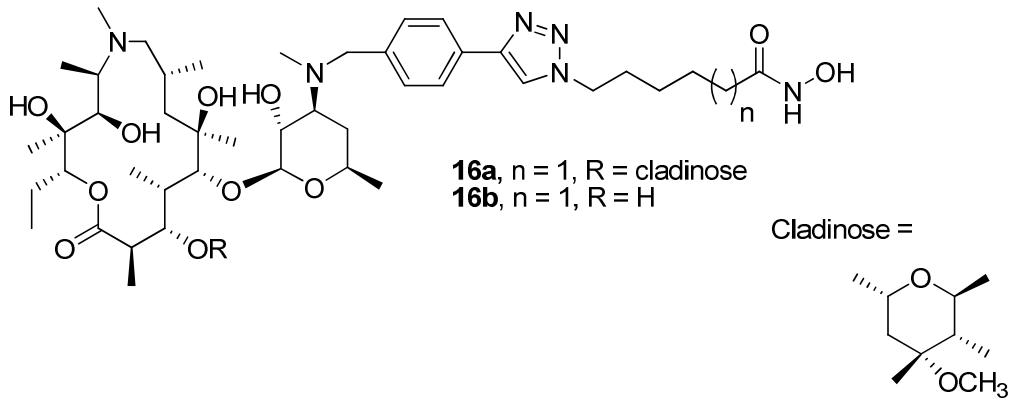

Figure 4-3: Azithromycin-based nonpeptide macrocyclic HDACi.

Synthesized by Drs. Yomi Oyelere and Bob Chen

Surprisingly, HDAC inhibition studies revealed that the triazolyl compounds **16a** and **16b** have virtually identical anti-HDAC activity as the amide compounds **8** and **10** (Table 4-1). This result contrasts with our previous observation that incorporation of the triazole ring led to an enhancement in anti-HDAC activity in SAHA-like HDACi.[22] To gain a greater understanding of the molecular interactions dictating the activities of these nonpeptide macrocyclic HDACi at the HDAC active site, **16b** was docked on HDLP using AutoDock as previously described.[20,22] HDLP was chosen because it shares conserved active site residues with class I HDACs.[21] Additionally, direct docking experiments using this structure or a HDAC1 homology model built from the same HDLP structure have given docking results with essentially the same quality and agreement with experimental data. Either of these approaches has been extensively used in the literature to interrogate the binding interactions of HDAC inhibitors at the enzyme active site.[20b,c]

Docked structures indicated interesting molecular surface complementarity between **16b** and the HDAC outer rim. Previous investigations have shown that there are four possible binding pockets on the HDLP surface whose interactions with the HDACi cap groups could enhance inhibitor binding activity.[20b] Compound **16b** adopts a docked structure that placed the macrolide macrocyclic ring in binding pockets 1 and 3 (Figure 4-3a). In addition, the hydrophobic parts of the macrolide ring optimally interact with the hydrophobic residues in pocket 1 and 3 while the hydrophilic groups orient away from the pocket's hydrophobic residues. Compared to the structure of SAHA, **16b** binds such that the hydroxamate is removed farther from the Zn^{2+} ion (Figure 4-3b). From this result, it was inferred that optimizing the length of the linker region could place the hydroxamate deeper in the channel to chelate the Zn^{2+} ion, thereby enhancing HDAC inhibition.

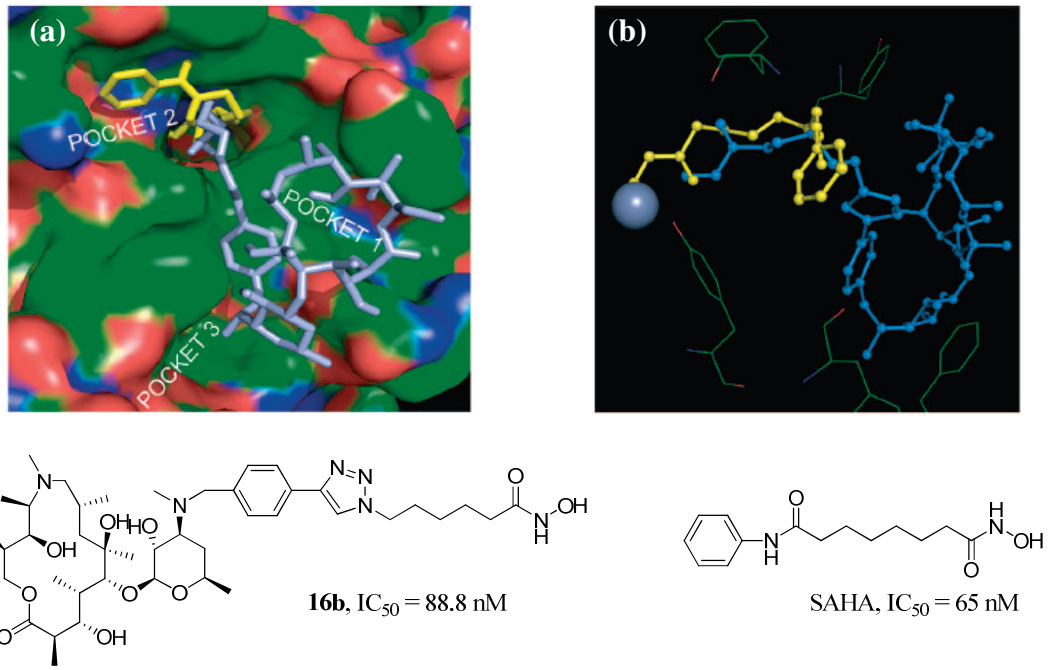

Figure 4-4: Docked structures of **16b** (blue) and SAHA (yellow) on the HDLP active site channel (a) and zinc ion. Docking by Dr. Bob Chen.

Based on the encouraging compatibility of the azithromycin macrolide ring as a HDACi cap group, further SAR studies focused on optimizing the linker chain and macrolide cap group. The 15-membered azithromycin macrolide was replaced with a 14-membered clarithromycin macrolide in **24a-d**, and the linker chain was lengthened for both sets of compounds (Figure 4-5). Further docking analyses of analogs of **16b** with longer methylene linker lengths revealed that **16d**, a six-methylene analog of **16b**, optimally interacts with the Zn^{2+} ion (Figure 4-6a). Interestingly, compound **24d**, an analog of **16d** in which the 15-membered azithromycin ring has been replaced with the 14-membered clarithromycin ring, shows a slight preference for the enzyme. Closer analysis of docked structures of **16d** and **24d** showed that the C12-C14 region of the larger 15-membered ring is about 0.5 Å closer to the phenyl ring of Phe338, a residue that defines one of the hydrophobic pockets (Figure 4-6b).

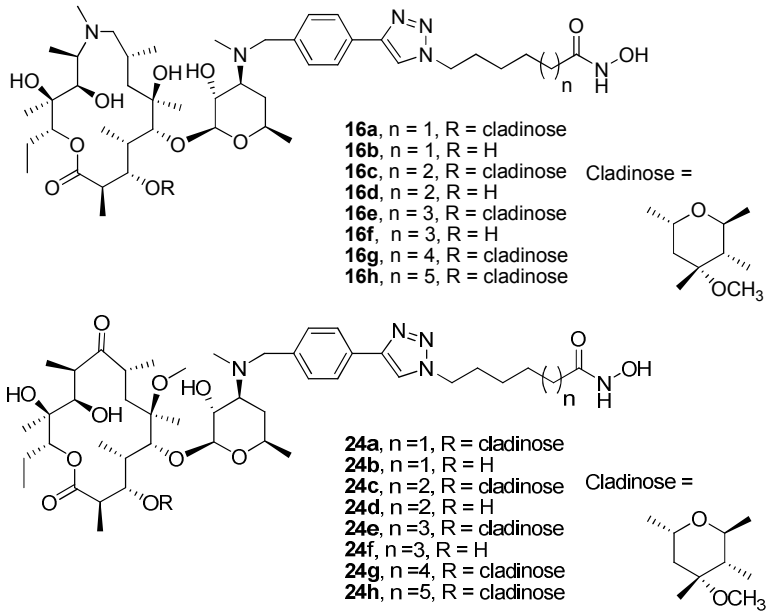

Figure 4-5: Nonpeptide macrocyclic HDACi based on azithromycin (**16** series) and clarithromycin (**24** series) macrolide skeletons. Synthesized by Dr. Bob Chen.

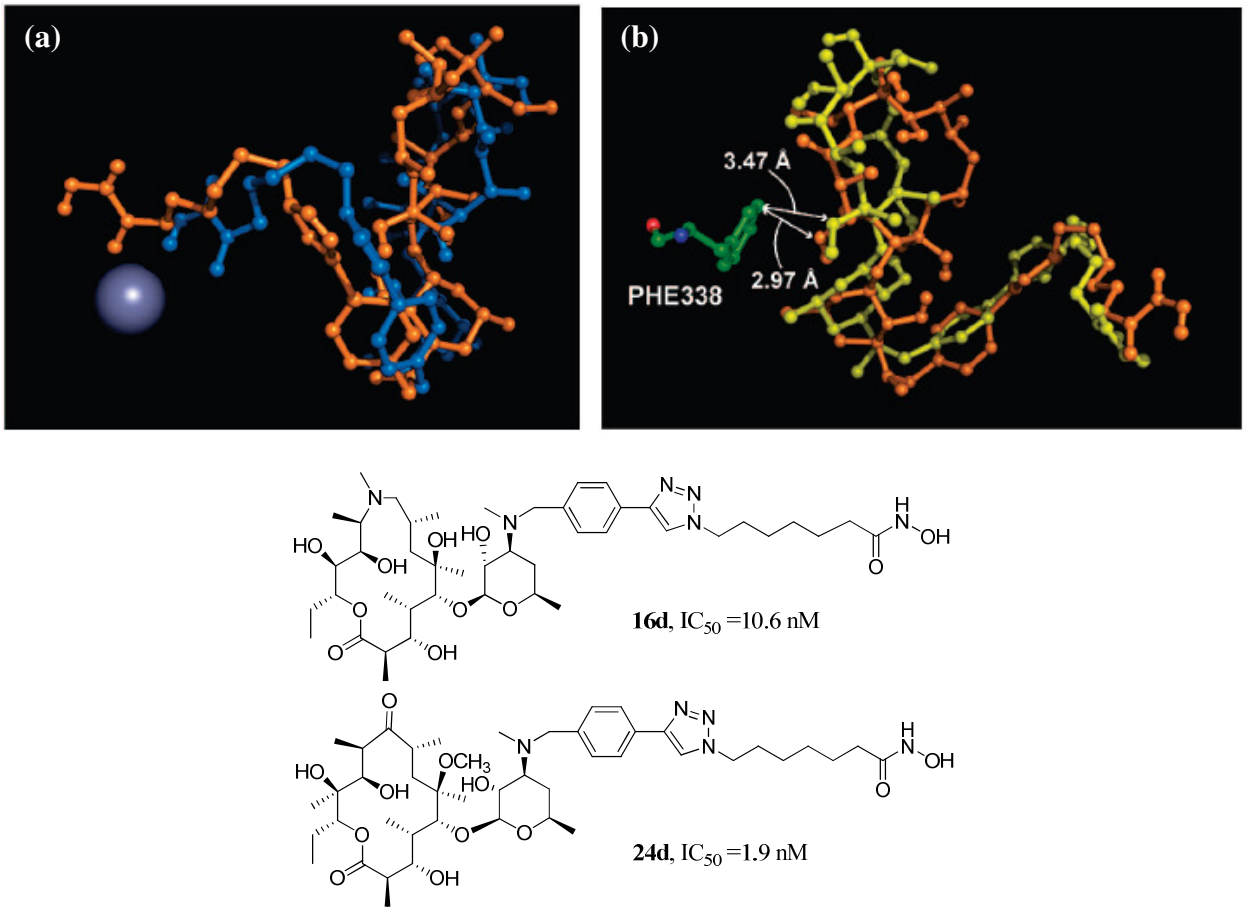

Figure 4-6: Docked structures of **16b** (blue) and **16d** (orange). Hydroxamate positioning (a). Macrolide ring interactions of **16d** (orange) and **24d** (yellow) with the HDLP surface (b). Docking by Dr. Bob Chen.

In order to experimentally test whether there is a preference for the 14-membered macrolide cap group, indicated through *in silico* results, compounds **16c-h** and **24a-h** were tested against HeLa nuclear extract to assay for anti-HDAC activity. HDAC inhibition results revealed activities that essentially parallel the in silico prediction (Table 4-2). The compounds displayed both linker-length and macrolide-type dependent HDAC inhibition activities. For both types of compounds, an increase in the linker length to a six-methylene linker conferred better anti-

HDAC activity. Further increases in linker length past six methylenes did not improve HDAC inhibition and were detrimental to function in longer linker lengths. For compounds with five- and six-methylene linkers, head-to-head comparisons revealed that the 14-membered compounds are around 2- to 5-fold better HDACi than their 15-membered counterparts (Table 4-2, compare **16d** and **24d**, for example). However, this preference dissipated with increasing linker lengths. This is presumably due to the relief of the steric clash between the macrocyclic ring and the phenyl ring of Phe338, along with less optimal cap group placement, conferred by the longer linkers.

4.2.2 HDAC8 Inhibition and Intra-Class I HDAC Selectivity

We then probed for evidence of HDAC isoform selectivity of the macrocyclic HDACi by testing for HDAC8 inhibition activity. HDAC8 was chosen because it is in the same class as HDACs 1 and 2, the principal HDACs contained in HeLa nuclear extract used to preliminarily determine anti-HDAC activity. Moreover, there are very few examples of HDAC inhibitors that are selective for HDAC isoforms within the same class; therefore use of HDAC8 allowed for a quick, yet rigorous assessment of HDAC isoform selectivity inherent to these compounds. Compared to SAHA, all nonpeptide macrocyclic HDACi tested were more selective for HDAC 1/2. In particular, six methylene-linked 14-membered compounds **24c** and **24d** are several-fold more selective than their 15-membered counterparts (Table 4-2). Although HDLP and HDAC8 share similar amino acid sequences and topology at the active site, X-ray crystallography data of HDACi bound to HDAC8 has revealed significant inhibitor-specific changes in the enzyme active site topology of HDAC8.[23] Our docking analysis operates in a rigid receptor mode, and is therefore incapable of capturing such crystallographically-observed ligand-induced changes.

Table 4-2: *In vitro* HDAC inhibition (IC_{50}) and isoform selectivity of nonpeptide macrocyclic HDACi.

Compound	HeLa Nuclear Extract (nM)[a]	HDAC 8 (nM)[b]	Isoform selectivity[c]
7	N.D.	NT	N.D.
8	107.1	6680	62
10	109.8	2320	21
16a	91.6	4730	51
16b	88.8	3740	42
16c	13.9	994	72
16d	10.6	1020	97
16e	58.9	7130	121
16f	72.4	6780	94
16g	145.5	11050	38
16h	226.7	N.D.	N.D.
24a	37.0	3990	108
24b	44.3	4750	107
24c	4.1	1890	462
24d	1.9	1390	743
24e	55.6	5880	106
24f	123.0	4420	36
24g	169.8	10550	56
24h	223.4	N.D.	N.D.
SAHA	65.0	1860	29

[a] IC_{50} values were determined using the Biomol HDAC Fluorimetric Assay/Drug Discovery Kit. [b] Values determined using the Fluor de Lys HDAC8 Fluorimetric Drug Discovery Kit. c Calculated by dividing the anti-HDAC8 IC_{50} by the anti-nuclear extract IC_{50}. N.D. : not determinable. NT: not tested.

Nevertheless, we docked **16b** on the HDAC8 structure reported by Somoza et al.[23] Contrasting with the docked structure on HDLP, the orientation of **16b** on HDAC8 is such that the linker and ZBG adopt a closed conformation at the entrance to the active site. In this conformation, the linker coiled around the macrocyclic ring and oriented the hydroxamate toward the Zn^{2+} ion, albeit much farther away than possible for any stabilizing interaction to occur (Figure 4-7). An alternate, lower energy conformation of **16b** oriented the hydroxamate away from the Zn^{2+} ion. Therefore, it is possible that the observed isoform selectivity may be due to the nonpeptide macrocyclic HDACi's inability to effectively induce active site conformational changes requisite for HDAC8-specific inhibitor binding to the active site.[24] HDAC8 activity has also been observed to depend on the sequence of its peptide substrate,[25] so it is also possible that enzyme inhibition, and consequently isoform selectivity, may depend on the specific substrate tested.

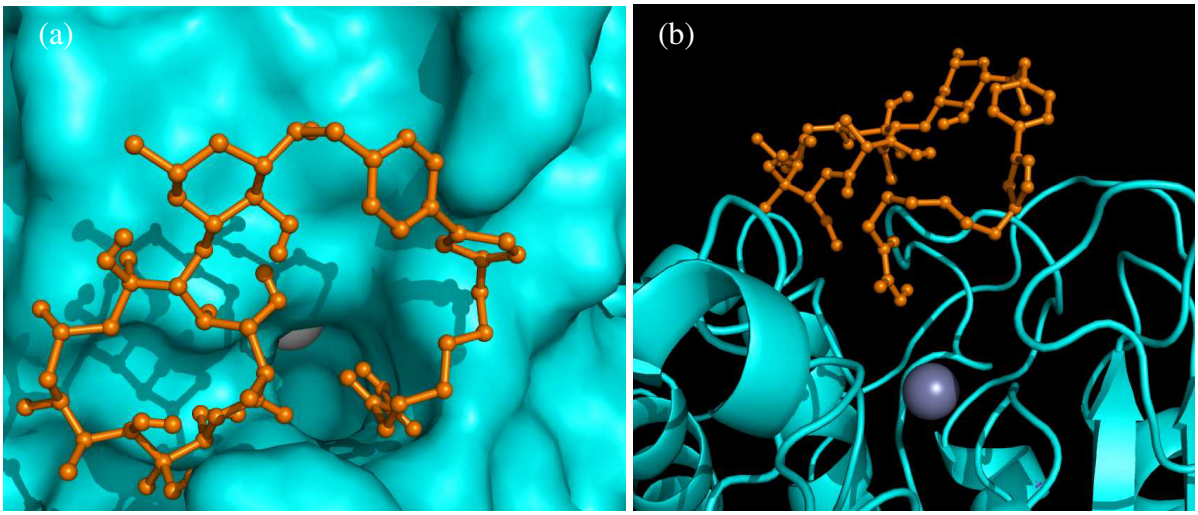

Figure 4-7: Docked structure of **16b** with HDAC8 surface (a) and active site (b). Docking experiment performed by Dr. Bob Chen.

4.2.3 HDAC6 Inhibition and Class I/II Isoform Selectivity

HDAC isoform selectivity of selected macrocyclic HDACi was further tested against HDAC6, a representative member of class II HDACs. Compounds **16c** and **16d**, and **24c** and **24d**, were chosen because they were the most potent 15- and 14-membered macrocyclic HDACi, representatively (Table 4-2). A cell-free HDAC6 inhibition assay was performed as recommended by the supplier (Biomol).[26] Contrary to SAHA, which inhibited HDACs 1/2 and HDAC6 equally, macrocyclic HDACi continued to display a preference for class I HDACs (Table 4-3). This observation is in agreement with the literature, suggesting that complex cap groups tend to promote isoform selectivity.[7,27]

Table 4-3: *In vitro* HDAC6 inhibition by macrocyclic HDACi.

Compound	HDAC1/2 IC_{50} (nM)[a]	HDAC6 IC_{50} (nM)	Isoform Selectivity[b]
16c	13.9	78.0	6
16d	10.6	117.4	11
24c	4.1	89.3	22
24d	1.9	148.5	78
SAHA	65.0	85.5	1

[a] HeLa Nuclear Extract comprised mainly of HDACs 1 and 2. [b] calculated by dividing the IC50 of HDAC6 by the IC50 of HDAC1/2. All data was obtained from the mean of two independent experiments in triplicate.

4.3 Cancer Cell Growth Inhibition

4.3.1 Inhibition of Cancer Cell Viability by Macrocyclic HDACi

The anticancer activity of macrocyclic HDACi was tested against three transformed cell lines: SK-MES-1 (human NSCLC), NCI-H69 (human SCLC), DU-145 (human prostate cancer). Table 4-4 shows the calculated IC_{50} values for each compound tested through trypan blue exclusion, as previously described.[28,22] The IC_{50} values obtained for SAHA closely agree with reported values under similar experimental conditions.[29] Macrocyclic methyl ester **7**, the precursor to compound **8** (Figure 4-2), has no effect on cell viability (data not shown), which may not be surprising since compound **7** has no HDAC inhibition activity (Table 4-1). Unexpectedly, macrocyclic depsipeptides **8** and **10** did not inhibit DU-145 in the tested concentration range (0.5 - 25 μM). Conversely, all triazole-linked macrocyclic HDACi inhibited all transformed cell lines tested. Specifically, compounds **16b**, **24c**, and **24d** are at least twice as potent as SAHA in DU-145 (Table 4-4), a cell line known to respond to HDACi.[30]

Gratifyingly, macrocyclic HDACi potently inhibit both lung cancer cell lines with a preference for 5 and 6 methylene linkers in 15- and 14-membered macrolide compounds. We selected these compounds as leads for further study in an *in vivo* model relevant for lung cancer chemotherapeutic validation. Most importantly, none of the tested macrocyclic hydroxamates show any growth inhibitory effects on either normal human primary lung fibroblasts or human mammary epithelial cell lines at concentrations up to 10 μM (Table 4-4). These data show that the macrocyclic compounds are selectively toxic to the transformed cells, a property often observed with HDACi.

Table 4-4: Cell growth inhibition data for nonpeptide macrocyclic HDACi[a].

Compound	SK-MES-1 (μM)	NCI-H69 (μM)	DU-145 (μM)	Lung Fibroblast (μM)	HMEC (μM)
8	NT	NT	>25	NT	NT
10	NT	NT	>25	NT	NT
16a	1.79	1.92	1.45	>10	>10
16b	1.68	1.77	1.24	>10	>10
16c	2.33	3.45	1.88	>10	>10
16d	2.56	3.01	1.97	>10	>10
16e	4.89	4.56	5.89	>10	>10
16f	4.67	3.99	5.68	>10	>10
16g	7.54	8.45	>10	>10	>10
24a	2.15	2.67	2.98	>10	>10
24b	1.95	1.92	3.29	>10	>10
24c	1.33	1.45	1.12	>10	>10
24d	1.28	1.49	1.05	>10	>10
24e	4.89	5.67	6.97	>10	>10
24f	4.45	5.09	5.78	>10	>10
24g	7.12	7.29	8.14	>10	>10
SAHA	2.42	2.06	2.12	>10	>10

[a] IC_{50} values were determined using trypan blue exclusion. Each value is obtained from the mean of two experiments performed in quadruplicate. NT: not tested.

4.3.2 Molecular Mechanisms for Macrocyclic HDAC Inhibition

An important biomarker that is primarily associated with intracellular HDAC inhibition is the expression level of the $p21^{waf1}$ gene. Upregulation of the $p21^{waf1}$ gene has generally been observed with cellular HDAC inhibition.[31,32] In an effort to understand the cellular mechanisms contributing to the observed anticancer activity of macrocyclic HDACi, we investigated the effect of **24d**, a representative macrocyclic HDACi on the expression level of $p21^{waf1}$ protein in SK-MES-1 cells. SAHA was used as a positive control for HDAC inhibition. Cells were exposed to HDACi for 8 hours and cellular $p21^{waf1}$ expression was quantified by immunoblotting. Results show a dose-dependent increase in $p21^{waf1}$ expression in response to HDACi treatment (Figure 4-8). This provided additional evidence that the likely mechanism of anticancer activity of nonpeptide macrocyclic hydroxamates is through intracellular HDAC inhibition.

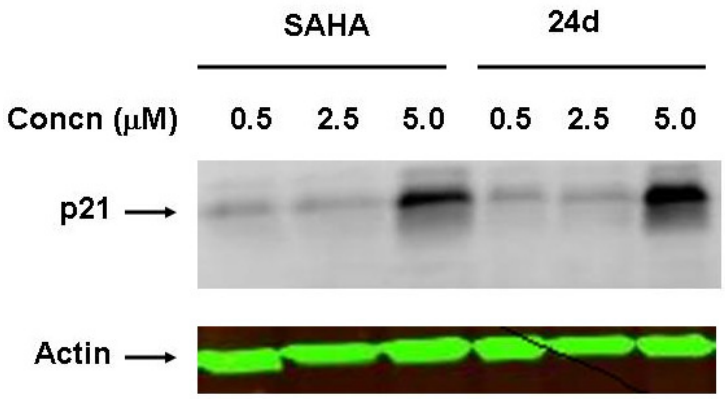

Figure 4-8: Immunoblot of $p21^{waf1}$ expression in response to macrocyclic HDACi.
SK-MES-1 cells were dosed for 8 hours with SAHA and 24d. Actin expression (green) was used as an indicator of equal protein loading.

4.4 *In Vivo* Lung Targeting by Macrocyclic HDACi

The robust HDAC inhibition and anticancer activity observed during *in vitro* screening of nonpeptide macrocyclic HDACi encouraged further progression into *in vivo* validation as a lung-targeted HDACi therapeutic. The 15-membered series of macrocyclic hydroxamates, specifically **16a** and **16c**, were chosen as lead compounds due to the validated lung targeting and accumulation properties of the azithromycin macrolide.[13-16] Male Balb/C mice were used for further screening of compounds that possessed promising tissue distribution profiles.

4.4.1 Maximum Tolerated Dose of Macrocyclic HDACi in Mice

Since azithromycin accumulates over time in the lungs,[33] it is possible that toxicity due to increasing *in vivo* concentrations of **16a** and **16c** could invalidate any antitumor activity these compounds could confer. To screen for *in vivo* toxicity, male Balb/C mice were injected intravenously with **16a** and **16c** at concentrations up to 100 mg/kg body mass daily, for five days. SAHA was used as a standard for HDACi activity. Animals were observed for signs of toxicity including loss of more than 10% body mass, hyperactive erratic behavior, difficulty moving, seizures, hunching, and squinting. No signs of stress were observed with either compound and all animals survived the five day injection with moderate weight gain (Figure 4-9). The lack of observable toxicity for all compounds assuaged concern over the accumulation of high concentrations of macrocyclic hydroxamates *in vivo*.

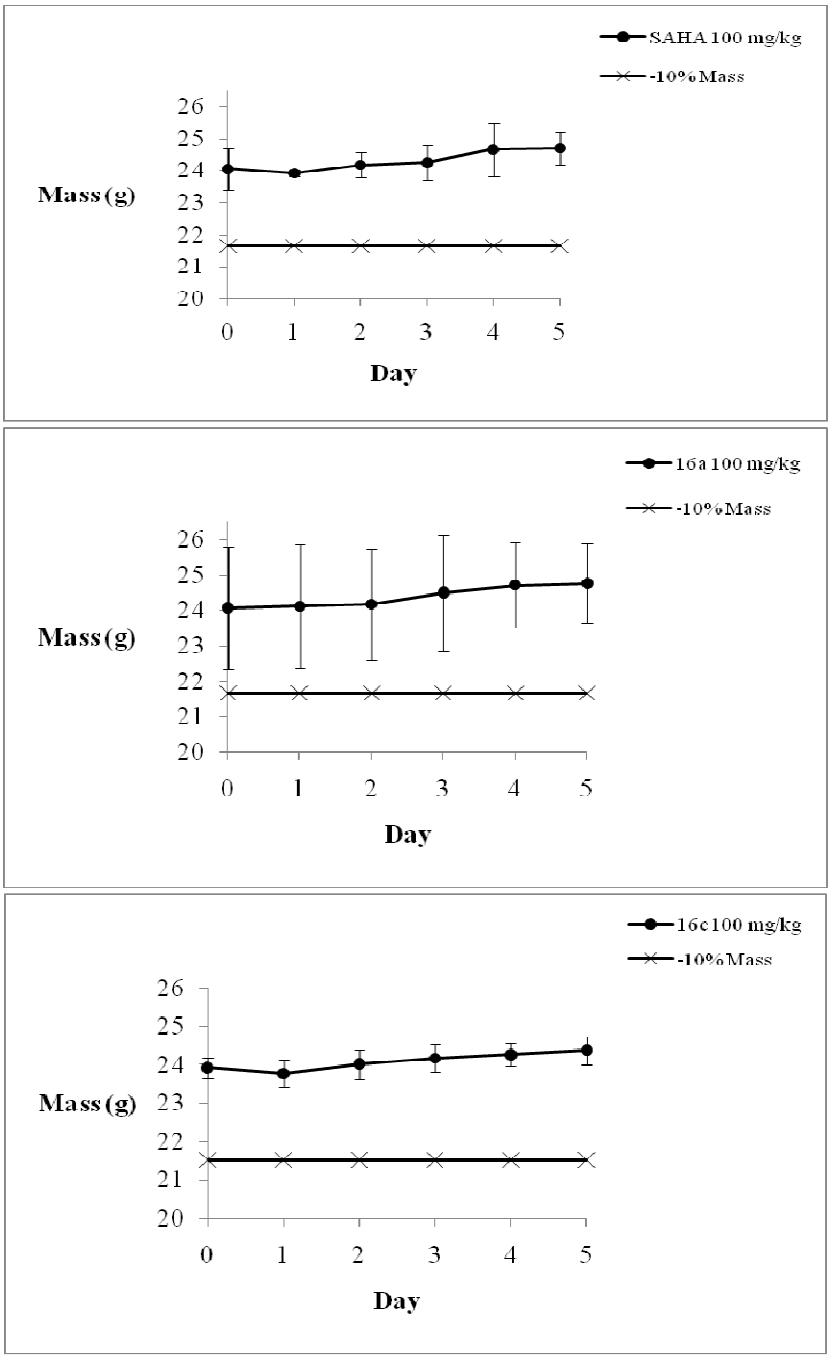

Figure 4-9: *In vivo* toxicity caused by macrocyclic HDACi treatment, measured by weight loss. Mice were weighed before injection of macrocyclic HDACi. Loss of 10% of age-adjusted mass was taken as an indicator of toxicity/stress that would require euthanasia. Error bars demonstrate 1 standard deviation above or below the mean mass of 3 mice, 7 weeks old.

4.4.2 Tissue Distribution of Radiolabeled Macrocyclic HDAC Inhibitors

The extent to which the macrolide cap group conferred *in vivo* lung-targeting and accumulation properties onto nonpeptide macrocyclic HDACi was investigated through a radioactive assay that we designed. Carbon-14 (^{14}C)-labeled analogs of **16a** and **16c** (**17a** and **17c**, respectively) were synthesized for a liquid scintillation-based assay to determine the tissue distribution of macrocyclic HDACi in the Balb/C mouse model (Figure 4-10). Isotopically-labeled ^{14}C-azithromycin was also synthesized for use as a lung-targeted control (Figure 4-11). Nonradioactive acetylated 15-membered macrocyclic hydroxamates (Figure 4-12) were also synthesized and tested in Balb/C mice as a toxicity control for the acetyl group addition to the macrolide scaffold. A five day dosing regimen of daily intravenous injections of nonradioactive acetylated compounds at 100 mg/kg in Balb/C mice caused no discernible toxicity (Figure 4-13). DMSO was used as a vehicle control for the acetylated compounds.

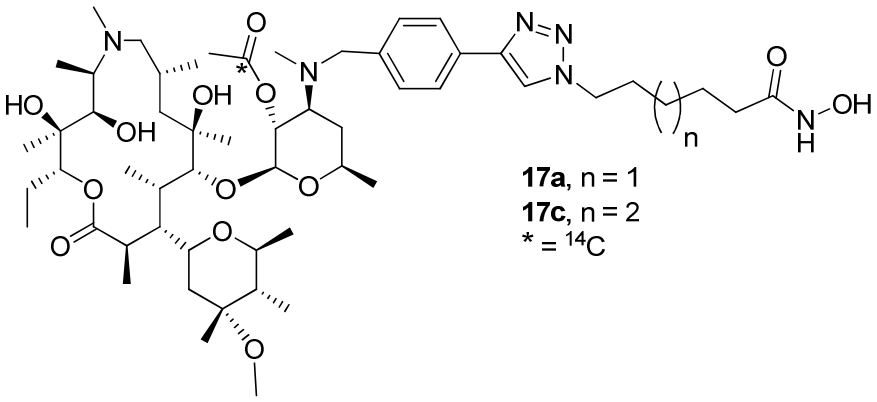

Figure 4-10: Radiolabeled 15-membered macrocyclic hydroxamates. Compounds were synthesized by Dr. Bob Chen.

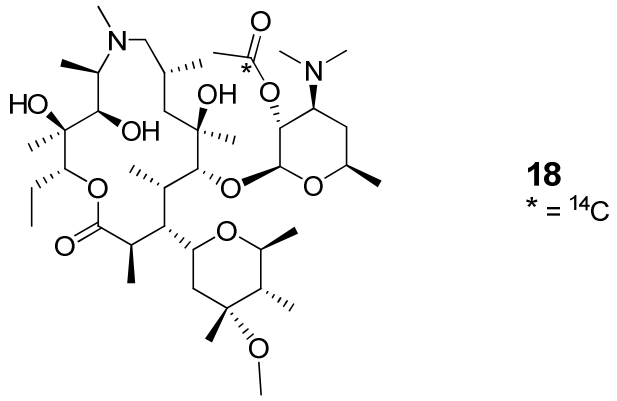

Figure 4-11: Compound 18 (^{14}C-azithromycin).

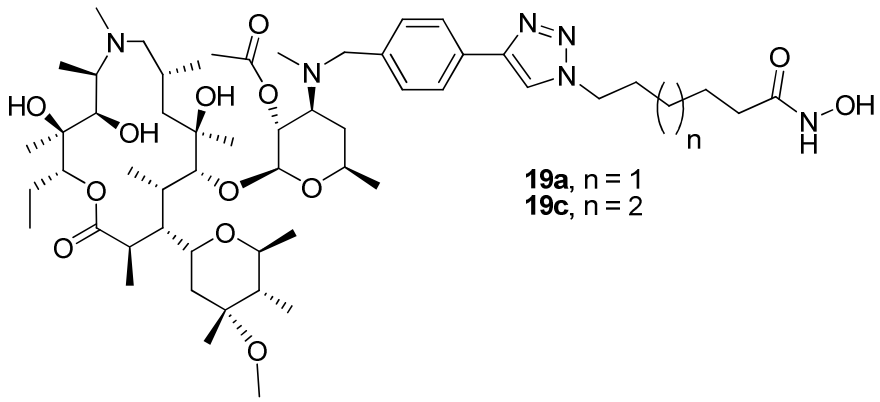

Figure 4-12: Acetylated 15-membered hydroxamates.

Synthesized by Dr. Bob Chen.

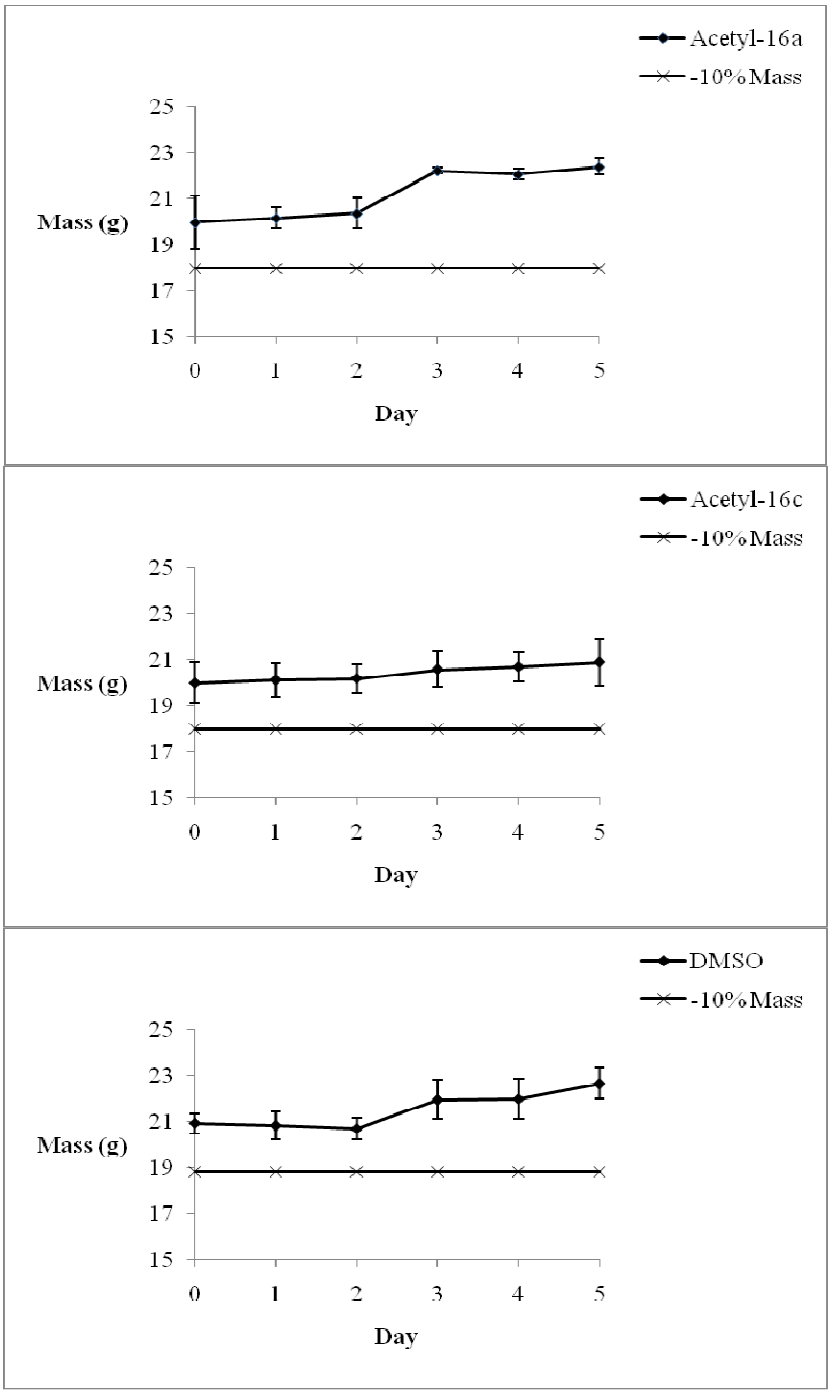

Figure 4-13: Acetylated 15-membered hydroxamates caused no discernible toxicity in Balb/C mice over 5 days, dosed intravenously with 100 mg/kg drug. Each point is the mean of three mice. Error bars show 1 standard deviation above and below the mean mass of 3 mice, 5 weeks old.

To determine the tissue distribution of radiolabeled macrocyclic HDACi, compounds **17a** and **17c** were injected intravenously into Balb/C mice for 8 hours and 24 hours at a concentration of 50 mg/kg. At the end of each timecourse, animals were sacrificed and relevant tissues and blood samples were removed. Blood samples were centrifuged in serum separator tubes to isolate the serum fraction and tissues were rinsed with saline to remove blood. Equal masses of tissues and volumes of serum were solubilized and the radioactive activity present was determined via liquid scintillation counting. The concentrations of radiolabeled macrocyclic HDACi present in each sample (Figure 4-14) were determined through comparison to calibration curves of each compound (shown in Appendix).

The resulting tissue distribution showed significant lung-targeting by macrocyclic HDACi, with **17c** preferentially accumulated in the lungs at both timepoints. For both compounds, lung concentrations remained approximately constant over the course of 8 to 24 hours (Figure 4-14). Both compounds also localized to the liver in high concentrations comparable to levels in the lungs. This result trends with literature reports of elevated liver concentrations of azithromycin several hours after treatment.[34] Biliary excretion through the liver is also the primary mode of elimination for azithromycin and mononuclear phagocyte system macrophages reside in the liver so it is possible that macrolide-loaded hepatic macrophages could account for high levels of liver localization, at least in part.[35,36] By contrast, levels of macrocyclic HDACi in serum and other tissues were relatively low, consistent with azithromycin's pharmacokinetic profile.[33,34,37,38]

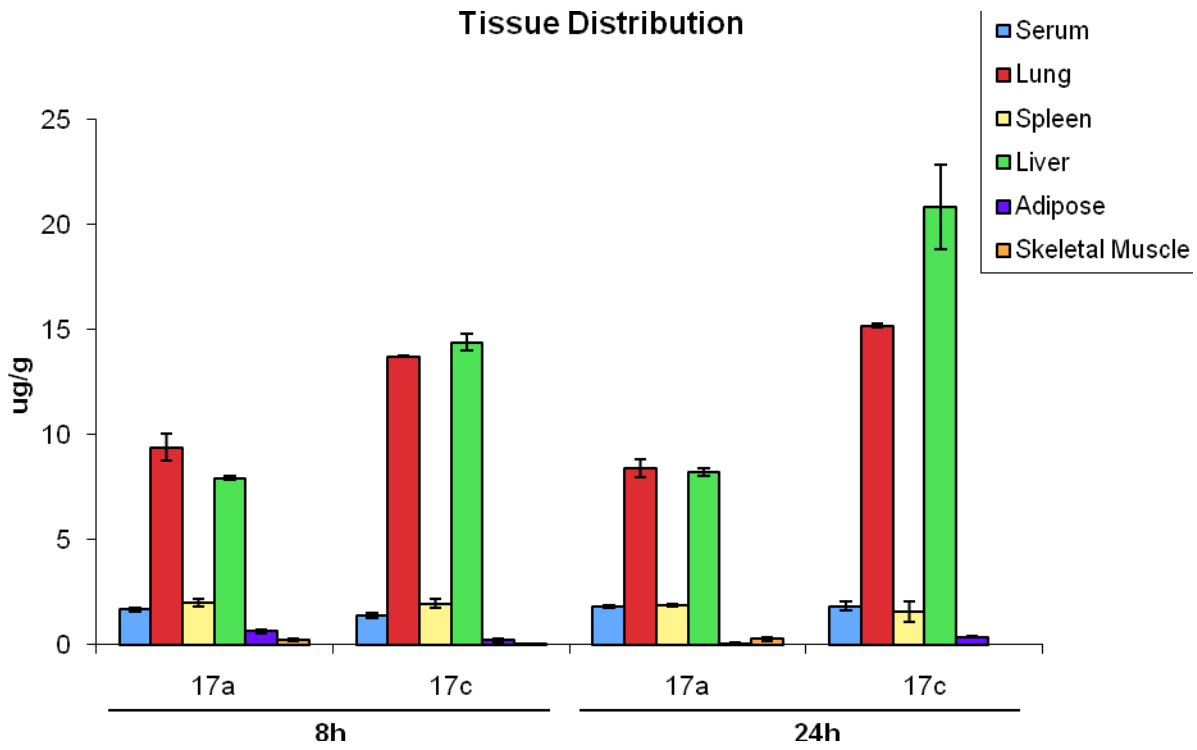

Figure 4-14: Biodistribution of radiolabeled macrocylic hydroxamates in relevant organs and blood fractions in Balb/C mice. Each bar represents the mean of 8 tissue or blood fraction samples. Error bars represent ± 1 standard deviation.

Radiolabeled azithromycin, by contrast, displayed remarkably higher tissue concentrations with significant concentrations localized to the lungs, liver, and spleen. This is consistent with the reported pharmacokinetics of unlabeled azithromycin.[34] Compared with radiolabeled macrocyclic HDACi, **18** localizes to the lungs in slightly higher concentrations that decrease somewhat over 16 hours. Levels of azithromycin in the liver were much higher compared to **17a** and **17c**, but these decreased over 16 hours as well. The most significant difference between the biodistributions of **17a/c** and **18** is the 25-fold increase in spleen residence of **18**. The spleen is a major organ of the mononuclear phagocyte system and contains

high concentrations of splenic macrophages that play roles in innate and aquired immune responses which could account for the increase in spleen concentrations.[39] Off-target adipose and heart tissues have low levels of **18**. This result suggests that attachment of the HDACi moiety abrogates, at least in part, the spleen-directed distribution properties of the parent macrolide and drastically reduces liver residence. Lung-targeted concentrations are not diminished significantly between **17c**, the better of the two radiolabeled macrocyclic HDACi, and **18**. The in vivo tissue distribution profile revealed through the liquid scintillation results suggest that nonpeptide macrocyclic HDACi could be used to treat lung cancer due to the unique pharmacokinetic properties conferred by the parent macrolide.

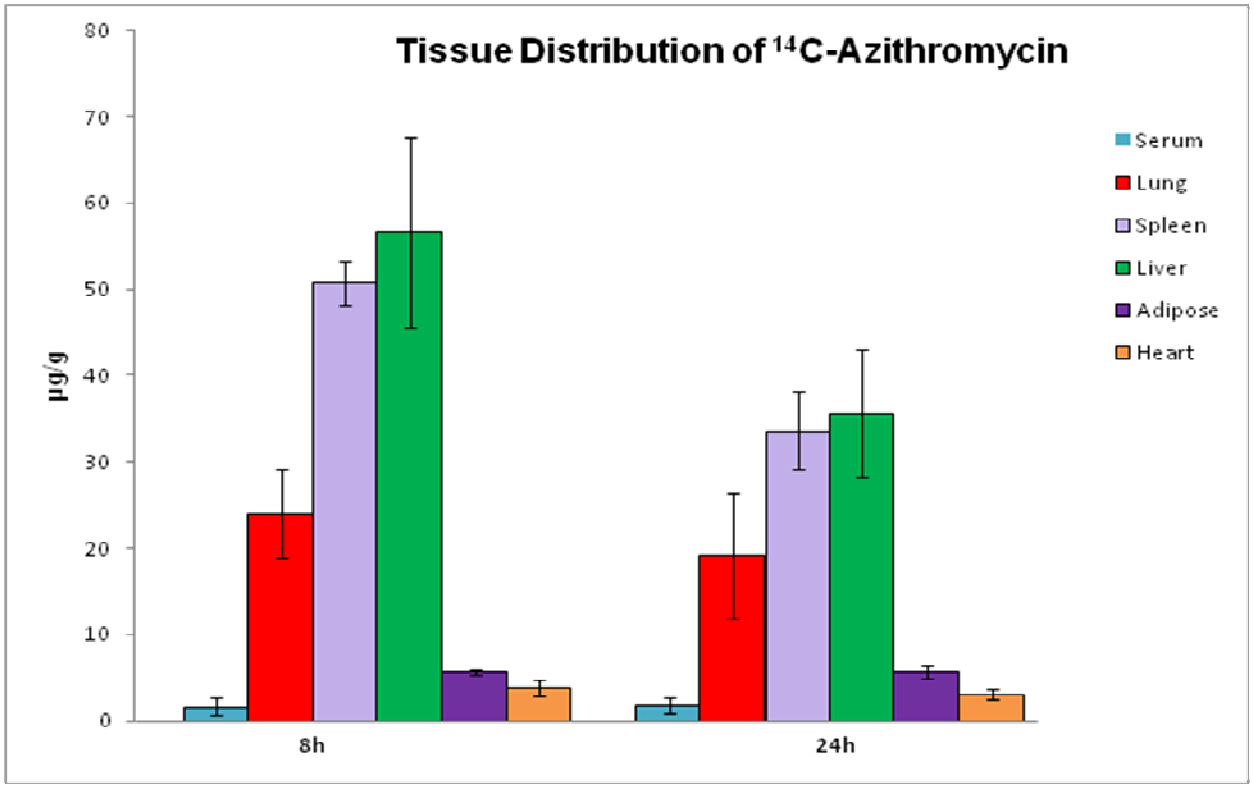

Figure 4-15: Biodistribution of radiolabeled azithromycin in relevant organs and blood fractions in Balb/C mice. All bars are the average of 8 tissue or blood fraction samples. Error bars represent one standard deviation above and below the mean.

4.5 Conclusion

The clinical efficacy of HDACi-based chemotherapies is greatly reduced in solid tumors. This shortcoming must be addressed for broader use and success of HDACi therapies. Targeted HDACi with distinct tissue distributions could more selectively concentrate in specific cancer-burdened tissues, focusing anticancer activity where it is needed and lowering side effects. The macrocyclic-peptide class of HDACi possesses the most complex cap-group moieties and offers

the best opportunity for specific modulation of HDACi biological activity. Replacement of the pharmacokinetically disadvantaged cyclic-peptide cap group with azithromycin and clarithromycin macrolide skeletons yielded potent nonpeptide macrocyclic HDACi. A subset of these compounds inhibited HeLa nuclear extract HDACs many fold more potently than SAHA and had low micromolar anticancer activities against lung cancer and prostate cancer. Moreover, nonpeptide macrocyclic HDACi caused no observable *in vitro* toxicity in normal human cells or in an animal model dosed for five days with a concentration of 100 mg/kg/day. Most importantly, azithromycin-based macrocyclic HDACi display a tissue distribution profile that mimics the parent macrolide, and targets the compounds selectively to lung and liver tissues, consistent with recorded pharmacokinetic profiles. These nonpeptide macrocyclic HDACi display great promise in overcoming the inefficacy of HDACi in treating solid tumors, harnessing lung-targeting conferred by the appended macrolide and potent anti-HDAC and anticancer activity.

The future direction of this project must center on challenging an *in vivo* lung tumor with these HDACi and evaluating their efficacy in order to validate that tissue-targeted HDACi can surpass the limitations that current agents have shown in the clinic. Ideally, an animal model that can be implanted with a lung tumor that can be detected and evaluated for growth inhibition will be used. It is essential that an orthotopic tumor implant be used to test the efficacy of nonpeptide macrocyclic HDACi, rather than a heterotopic tumor. The unique pharmacokinetic/delivery properties conferred on these compounds by the azithromycin skeleton may be dependent on lung-associated macrophages or other phagocytic cells.[33] Lewis lung carcinoma (LLC), a mouse lung cancer cell line has been chosen for initial *in vivo* anticancer activity experiments. This cell line has demonstrated in vivo responses to TSA treatment[40] and has been commonly used for

anticancer agent profiling.[41-43] Most importantly, LLC is significantly inhibited by **16c** in low micromolar concentrations (IC_{50} = 1.1 μM)(Figure 4-16).

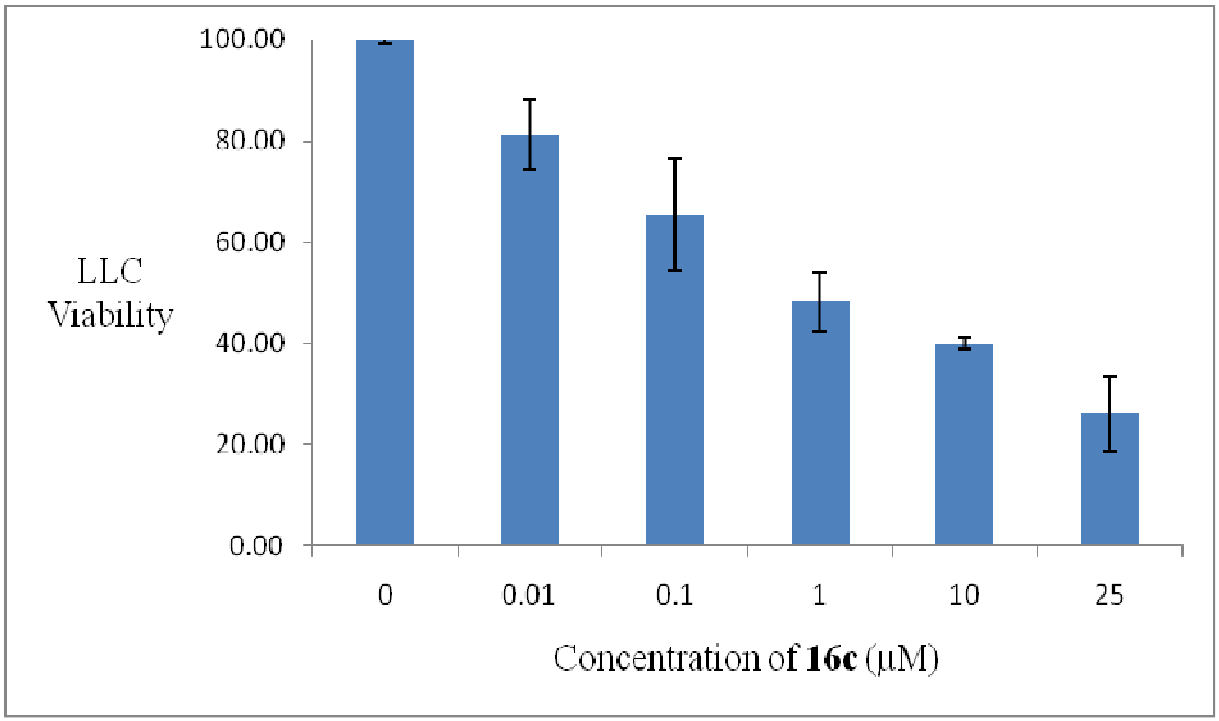

Figure 4-16: HDACi-induced decrease in LLC Viability. LLC cells were dosed for 72 hours with **16c**. Viability was determined using the MTS assay.

Two imaging strategies have been designed to facilitate observation of the tumor within a live mouse: (a) a stably-transfected luciferase-expressing LLC line for luminescent bioimaging, and (b) labeling of epidermal growth factor receptor (EGFR) on LLC with a near-infrared (NIR) probe for fluorescent imaging. The luciferase activity of the transfected LLC line correlates well with cell number when compared directly with MTS results (data not shown). Alternatively, the near-infrared probe has shown suitability in labeling these cells *in vitro* for the same end purpose (Figure 4-17). The resulting *in vivo* anti-lung cancer activity will determine the ultimate legacy

of these compounds, but one would think the successes shown so far will stimulate further investigation and design of tissue-targeted HDAC therapies.

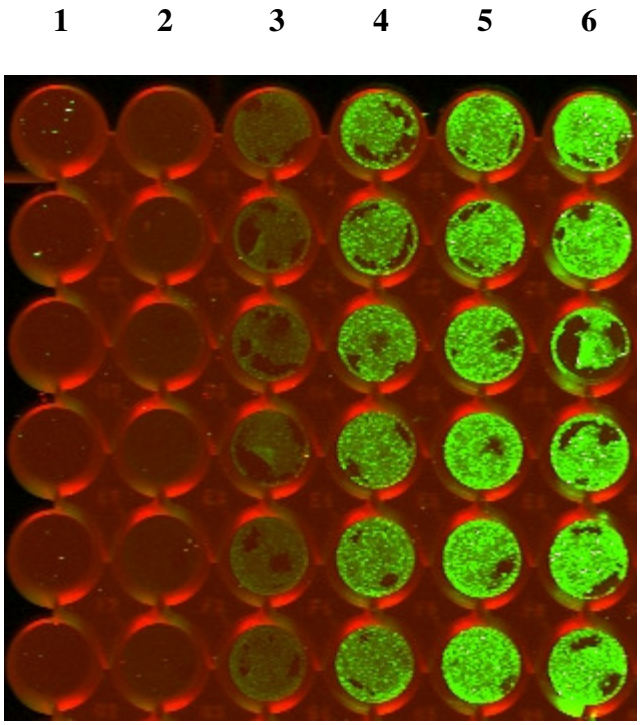

Figure 4-17: On-cell western blot of EGFR on LLC with a NIR probe. Wells: 1) Control, 2) 1 ng/ml, 3) 10 ng/ml, 4) 100 ng/ml, 5) 250 ng/ml, 6) 500 ng/ml. Cells were labeled with the 800CW-EGF NIR probe (LiCor) according to manufacturer's protocol.

4.6 Experimental Methods

4.6.1 In Vitro HDAC Inhibition

In vitro HDAC inhibition was assayed using the HDAC Fluorimetric Assay/Drug Discovery Kit. 15 μL of HeLa nuclear extract was mixed with 5 μL of 10× compound and 5 μL of assay buffer. Fluorogenic substrate (25 μL) was added, and reaction was allowed to proceed

for 15 min at room temperature and then stopped by addition of a developer containing TSA. Fluorescence was monitored after 15 min at excitation and emission wavelengths of 360 and 460 nm, respectively. IC_{50} values were determined using logit plots.

4.6.2 Cancer Cell Cytotoxicity

DU-145 prostate carcinoma, SK-MES-1 non-small cell lung carcinoma, and NCI-H69 small cell lung carcinoma were obtained from ATCC (Manassass, VA) and maintained in the recommended growth mediums. All cell lines were maintained in a 37°C incubator with a 5% CO_2 environment. All compounds to be tested were dissolved to a concentration of 10 mM in DMSO and stored at -80°C. Cells were passaged 24 h prior to cell viability experiments. For cancer cell viability experiments, cells were dosed for 72 h and viability was determined both by Trypan Blue staining and through the use of the MTS assay (Promega) according to manufacturer's instructions. Control wells were dosed with fresh media containing 0.1% DMSO.

4.6.3 Immunoblotting of $p21^{waf1}$

SK-MES-1 lung cancer cells were passaged 24 h prior to the experiment. Compounds to be tested were diluted in the growth medium so that the final concentration of DMSO was 0.1% and control cells were dosed with fresh media containing 0.1% DMSO. Cells were dosed for 8 h, then washed twice with ice-cold PBS, and lysed on the culture plate at 4°C for 5 min with RIPA buffer containing protease inhibitors. Lysates were mixed repeatedly by pipetting and centrifuged at 14,000 X g for 15 minutes at 4°C. Supernatant was saved and protein concentration was quantified using the Bio-Rad Protein Assay (Bio-Rad) with BSA as the standard. Loading buffer was added and protein samples were incubated at 100°C for 10 min

before electrophoresis. Proteins were then transferred to a nitrocellulose membrane for 1 h, followed by blocking overnight in a 1:1 mixture of Odyssey Blocking Buffer (LiCor Biosciences) and PBS. Membranes were incubated with primary antibodies, washed with 0.1% Tween-20 in PBS four times for 5 minutes each, and then incubated with secondary antibodies, followed by another four washing steps. Both sets of antibodies were diluted in 1:1 Odyssey Blocking Buffer/PBS. Membranes were scanned on the Odyssey infrared imaging system (LiCor Biosciences) using both 700 nm and 800 nm channels simultaneously at 169 μm resolution and analyzed on the imaging software.

4.6.4 In Vivo Lung Targeting

All Balb/C mice were obtained from Jackson Laboratories and housed according to protocol in the PRL. During experiments involving injections of HDACi, animals were observed at least twice daily for sign of distress that would require immediate euthanasia. All experiments were carried out using strict aseptic technique.

For jugular vein injections, used to intravenously inject HDACi or radiolabeled compounds, mice were prepared one day prior to the experiment by removing the hair from the neck to the lower rib line with a depilatory cream. On the day of the experiment, mice were anesthetized with 2-2.5% isoflurane such that no semiconscious response was elicited with toe pinching. Mice were laid in the dorsal decubitus position on a heating pad to maintain body temperature. The upper chest was elevated by placing a cotton swab under the mouse's mid-back. Compounds in DMSO were injected, in no more than 20μl total volume, through the pectoral muscle into the jugular vein. The syringe was then slowly removed and light pressure was applied to the chest for up to 1 minute to facilitate clotting at the injection site. Mice were

removed from anesthesia and allowed to wake on the warming pad before being placed back in their cages. Animals were observed for several minutes for signs of distress or injection site irritation. Animals that presented significant signs of distress were immediately euthanized by carbon dioxide asphyxiation. Euthanasia was not necessary for any of the animals in the described experiments as none showed significant signs of distress that would warrant termination. Animals were weighed before all injections.

For radiological tissue distribution experiments, a protocol approved by the Georgia Tech Office of Radiological Safety was followed. Mice were kept in static isolator cages with no bedding, water, or food, in order to minimize the spread of radioactive material. Slices of Napa Nectar (Lenderking), a gel-based water source were placed in the cage. All cages were retrieved before the experiment started and all cages remained in the experiment room for the duration of the timecourse. At the appropriate timepoints, animals were sacrificed by isoflurane inhalation overdose. The heart was quickly punctured and blood was removed and placed in serum isolator tubes. A general incision was then made to the abdomen of the animal. Liver, spleen, and adipose were removed and placed in microtubes on ice. The heart and lungs were then removed and skeletal muscle was collected from the flank and placed in microtubes. All samples were washed with PBS to remove blood and then quickly frozen in an acetone/dry ice mixture and stored.

Equal masses of samples from each tissue type and equal volumes of serum (55 mg of tissues, 55 μl of serum samples) were collected and solubilized using a commercially available aqueous tissue solubilizer (SOLVABLE, Perkin Elmer) in glass scintillation vials. Samples and solubilizer were heated to 60°C with shaking for at least 4 hours each. After the samples were

completely dissolved, a 30% hydrogen peroxide solution was added to all samples to bleach the pigments released by the tissues. This solution was further heated for 20 minutes before being allowed to cool on the bench top. After the solutions were cooled, scintillation fluid (Ultima Gold, Perkin Elmer) was added to the biological solutions, swirled, and allowed to sit at room temperature for 15 minutes. Vials were then counted using the Packard TriCarb 2900TR Scintillation Counter set to ^{14}C counts. Masses of drug within tissues were calculated based off a calibration curve generated for each compound.

4.6.5 Stable Transfection of LLC cells with luciferase gene plasmid.

LLC cells were obtained from ATCC and maintained in OPTI-MEM (Invitrogen) prior to transfection. The pGL4.50 vector was obtained from Promega. This vector contains a luciferase gene under control of a high expression promoter, with a hygromycin resistance gene for selection of stably transfected cells. Prior to transfection, a kill curve experiment was performed to determine the optimal concentration of hygromycin to use for selection. The Lipofectamine 2000 Transfection Reagent (Invitrogen) was used according to the manufacturer's directions and cells were maintained in hygromycin-containing media for 3 weeks with passaging as needed before testing for luciferase expression. The Luciferase Assay System (Promega) was used to test for luciferase activity.

4.6.6 On cell western blot of EGFR with NIR probe

LLC cells were seeded with a density of 1×10^5 cells/ml in complete Opti-Mem media in a 96-well tissue culture plate and allowed to grow for 24 hours. Media was then removed and serum-free Opti-Mem was added and incubated at 37°C for a duration of 4 hours. All

subsequent steps were performed at room temperature and shielded from light as much as possible. Dilutions of the probe were made in Opti-Mem with concentrations ranging from 1 to 500 ng/ml, and then added after serum-free media had been aspirated. After two minutes, the media was removed and the cells were fixed with 3.7% formaldehyde in PBS for 20 minutes. Cells were then washed 5 times for 5 minutes each with a Tween-based wash buffer (0.1% Tween-20 in PBS). After the last wash, the buffer was removed and the microplate was inverted and tapped gently on a paper towel to remove excess buffer. The plate was then scanned at both 700 and 800 nm channels on the Odyssey imaging system (LiCor).

4.7 References

1) Garber, K. HDAC inhibitors overcome first hurdle. Nature Biotech. 2007, 25, 18-19.

2) Shah, M. H.; Binkley, P.; Chan, K.; Xiao, J.; Arbogast, D.; Collamore, M.; Farra, Y.; Young, D.; Grever, M. Cardiotoxicity of histone deacetylase inhibitor depsipeptide in patients with metastatic neuroendocrine tumors. *Clin. Cancer Res.,* **2006**, *12*, 3997- 4003.

3) (a) Weichert, W. HDAC expression and clinical prognosis in human malignancies. *Cancer Lett*. **2009**, 280, 168-176. (b) Halkidou, K.; Gaughan, L.; Cook, S.; Leung, H.Y.; Neal, D.E.; Robson, C.N. Upregulation and nuclear recruitment of HDAC1 in hormone refractory prostate cancer. *Prostate*. **2004**, 59, 177-189. (c) Khabele, D.; Son, D.S.; Park, A.K.; Goldberg, G.L.; Augenlicht, L.H.; Mariadason, J.M.; Rice, V.M. Drug-induced inactivation or gene silencing of class I histone deacetylases suppresses ovarian cancer cell growth: implication for therapy. *Cancer Biol. Ther.* **2007**, 6, 795-801. (d) Bartling, B.; Hofmann, H.S.; Boettger, T.; Hansen, G.; Burdach, S.; Silber, R.E.; Simm,

A. Comparative application of antibody and gene array for expression profiling in human squamous cell lung carcinoma. *Lung Cancer*. **2005**, 49, 145-154.

4) Balasubramanian, S.; Verner, E.; Buggy, J.J. Isoform-specific histone deacetylase inhibitors: the next step? *Cancer Lett*. **2009**, 280, 211-221.

5) Jemal, A.; Siegel, R.; Xu, J.; Ward, E. Cancer statistics, 2010. *CA Cancer J. Clin*. **2010**, 60, 277-300.

6) Ramalingam, S.S.; Maitland, M.L.; Frankel, P.; Argiris, A.E.; Koczywas, M.; Gitlitz, B.; Thomas, S.; Espinoza-Delgado, I.; Vokes, E.E.; Gandara, D.R.; Belani, C.P. Carboplatin and paclitaxel in combination with either vorinostat or placebo for first-line therapy of advanced non-small-cell lung cancer. *J. Clin. Oncol*. **2010**, 28, 56-62.

7) Miller, T.A.; Witter, D.J.; Belvedere, S. Histone deacetylase inhibitors. *J. Med. Chem*. **2003**, 46, 5097-5116.

8) Grant, C.; Rahman, F.; Piekarz, R.; Peer, C; Frye, R.; Robey, R.W.; Gardner, E.R.; Figg, W.D.; Bates, S.E. Romidepsin; a new therapy for cutaneous T-cell lymphoma and a potential therapy for solid tumors. *Expert Rev. Anticancer Ther*. **2010**, 10, 997-1008.

9) Furumai, R.; Matsuyama, A.; Kobashi, N.; Lee, K.H.; Nishiyama, M.; Nakajima, H.; Tanaka, A.; Komatsu, Y.; Nishino, N.; Yoshida, M.; Horinouchi, S. FK228 (depsipeptide) as a natural prodrug that inhibits class I histone deacetylases. *Cancer Res*. **2002**, 62, 4916-4921.

10) (a) Furumai, R.; Komatsu, Y.; Nishino, N.; Khochbin, S.; Yoshida, M.; Horinouchi, S. Potent histone deacetylase inhibitors built from trichostatin A and cyclic tetrapeptide antibiotics including trapoxin. *Proc. Natl. Acad. Sci. U.S.A.* **2001**, 98, 87-92. (b) Yurek-George, A.; Cecil, A.R.L.; Mo, A.H.K.; Wen, S.; Rogers, H.; Habens, F.; Maeda, S.;

Yoshida, M.; Packham, G.; Ganesan, A. The first biologically active synthetic analogues of FK228, the depsipeptide histone deacetylase inhibitor. *J. Med. Chem*. **2007**, 50, 5720-5726. (c) Gomez-Paloma, L.; Bruno, I.; Cini, E.; Khochbin, S.; Rodriquez, M.; Taddei, M.; Terracciano, S.; Sadoul, K. Design and synthesis of cyclopeptide analogues of the potent histone deacetylase inhibitors FR235222. *ChemMedChem*. **2007**, 2, 1511-1519.

11) Tsai, W.C.; Standiford, T.J. Immunomodulatory effects of macrolides in the lung: lessons from in-vitro and in-vivo models. *Curr. Pharm. Des*. **2004**, 10, 3081-3093.

12) Shinkai, M.; Park, C.S.; Rubin, B.K. Immunomodulatory effects of macrolide antibiotics. Interstitial, inflammatory, and occupational lung disease. *Clin. Pulm. Med.* **2005**, 12, 341-348.

13) Gladue, R.P.; Bright, G.M.; Isaacson, R.E.; Newborg, M.F. In vitro and in vivo uptake of azithromycin (CP-62,993) by phagocytic cells: possible mechanism of delivery and release at sites of infection. *Antimicrob. Agents Chemother*. **1989**, 33, 277-282.

14) Vallée, É.; Azoulay-Dupuis, E.; Pocidalo, J.J.; Bergogne-Bérézin, E. Activity and local delivery of azithromycin in a mouse model of *Haemophilus influenza* lung infection. *Antimicrob. Agents Chemother*. **1992**, 36, 1412-1417.

15) Lucchi, M.; Damle, B.; Fang, A.; de Caprariis, P.J.; Mussi, A.; Sanchez, S.P.; Pasqualetti, G.; Del Tacca, M. Pharmacokinetics of azithromycin in serum, bronchial washings, alveolar macrophages and lung tissue following a single oral dose of extended or immediate release formulations of azithromycin. *J. Antimicrob. Chemother*. **2008**, 61, 884-891.

16) Azoulay-Dupuis, E.; Vallée, É.; Bedos, J.P.; Muffat-Joly, M.; Pocidalo, J.J. Prophylactic and therapeutic activities of azithromycin in a mouse model of pneumococcal pneumonia. *Antimicrob. Agents Chemother*. **1991**, 35, 1024-1028.

17) Randolph, J.T.; Waid, P.; Nichols, C.; Sauer, D.; Haviv, F.; Diaz, G.; Bammert, G.; Besecke, L.M.; Segreti, J.A.; Mohning, K.M.; Bush, E.N.; Wegner, C.D.; Greer, J. Nonpeptide luteinizing hormone-releasing hormone antagonists derived from erythromycin A: design, synthesis, and biological activity of cladinose replacement analogues. *J. Med. Chem*. **2004**, 47, 1085-1097.

18) (a) Freiberg, L.A. U.S. Patent 3725385, 1973. (b) Lartey, P.A.; Nellans, H.N.; Faghih, R.; Petersen, A.; Edwards, C.M.; Freiberg, L.; Quigley, S.; Marsh, K.; Klein, L.L.; Plattner, J.J. Synthesis of 4"-deoxy motilides: identification of a potent and orally active prokinetic drug candidate. *J. Med. Chem.* **1995**, 38, 1793-1798. (c) Stenmark, H.G.; Brazzale, A.; Ma, Z. Biomimetic synthesis of macrolide/ketolide metabolites through a selective N-demethylation reaction. *J. Org. Chem*. **2000**, 65, 3875-3876.

19) Awan, A.; Brennan, R.J.; Regan, A.C.; Barber, J. The conformations of the macrolide antibiotics erythromycin A, azithromycin and clarithromycin in aqueous solution: a ^{1}H NMR study. *J. Chem. Soc., Perkin Trans*. **2000**, 2, 1645-1652.

20) (a) Morris, G.M.; Goodsell, D.S.; Halliday, R.S.; Huey, R.; Hart, W.E.; Belew, R.K.; Olson, A.J. Automated docking using a Lamarckian genetic algorithm and empirical binding free energy function. *J. Comput. Chem*. **1998**, 19, 1639-1662; http://www.scripps.edu/pub/olson-web/doc/autodock/. (b) Wang, D.-F.; Wiest, O.; Helquist, P.; Lan-Hargest, H.-Y.; Wiech, N.L. On the function of the 14 Å long internal cavity of histone deacetylase-like protein: implications for the design of histone

deacetylase inhibitors. *J. Med. Chem*. **2004**, 47, 3409-3417. (c) Lu, Q.; Wang, D.-S.; Chen, C.-S.; Hu, Y.-D.; Chen, C.-S. Structure-based optimization of phenylbutyrate-derived histone deacetylase inhibitors. *J. Med. Chem*. **2005**, 48, 5530-5535.

21) Finnin, M.S.; Donigan, J.R.; Cohen, A.; Richon, V.M.; Rifkind, R.A.; Marks, P.A.; Breslow, R.; Pavletich, N.P. Structures of a histone deacetylase homologue bound to the TSA and SAHA inhibitors. *Nature* **1999**, 401, 188-193.

22) Chen, P.C.; Patil, V.; Guerrant, W.; Green, P.; Oyelere, A.K. Synthesis and structure-activity relationship of histone deacetylase (HDAC) inhibitors with triazole-linked cap group. *Bioorg. Med. Chem*. **2008**, 16, 4839-4853.

23) (a) Somoza, J.R.; Skene, R.J.; Katz, B.A.; Mol, C.; Ho, J.D.; Jennings, A.J.; Luong, C.; Arvai, A.; Buggy, J.J.; Chi, E.; Tang, J.; Sang, B.-C.; Verner, E.; Wynands, R.; Leahy, E.M.; Dougan, D.R.; Snell, G.; Navre, M.; Knuth, M.W.; Swanson, R.V.; McRee, D.E.; Tari, L.W. Structural snapshots of human HDAC8 provide insights into the class I histone deacetylases. *Structure* **2004**, 12, 1325-1334. (b) Vannini, A.; Volpari, C.; Filocamo, G.; Casavola, E.C.; Brunetti, M.; Renzoni, D.; Chakravarty, P.; Paolini, C.; De Francesco, R.; Gallinari, P.; Steinkuhler, C.; Di Marco, S. Crystal structure of a eukaryotic zinc-dependent histone deacetylase, human HDAC8, complexed with a hydroxamic acid inhibitor. *Proc. Natl. Acad. Sci. U.S.A*. **2004**, 101, 15064-15069.

24) KrennHrubec, K.; Marshall, B. L.; Hedglin, M.; Verdin, E.; Ulrich, S.M. Design and evaluation of "Linkerless" hydroxamic acids as selective HDAC8 inhibitors. *Bioorg. Med. Chem. Lett*. **2007**, 17, 2874-2878.

25) Gurard-Levin, Z.A.; Mrksich, M. The activity of HDAC8 depends on the local and distal sequences of its peptide substrates. *Biochemistry* **2008**, 47, 6242-6250.

26) *HDAC Fluorimetric Assay/Drug Discovery Kit. AK-500 Manual. Fluorescent Assay System;* BIOMOL International, L.P.; Plymouth Meeting, PA, 2005.

27) Haggarty, S.J.; Koeller, K.M.; Wong, J.C.; Grozinger, C.M.; Schreiber, S.L. Domain-selective small-molecule inhibitor of histone deacetylase 6 (HDAC6)-mediated tubulin deacetylation. *Proc. Natl. Acad. Sci. U.S.A.* **2003**, 100, 4389-4394.

28) Freshney, R. *Culture of Animal Cells: A Manual of Basic Technique*; Alan R. Liss, Inc.; New York, 1987; p117.

29) Suzuki, T.; Nagano, Y.; Kouketsu, A.; Matsuura, A.; Maruyama, S.; Kurotaki, M.; Nakagawa, H.; Miyata, N. Novel inhibitors of human histone deacetylases: design, synthesis, enzyme inhibition, and cancer cell growth inhibition of SAHA-based non-hydroxamates. *J. Med. Chem.* **2005**, 48, 1019-1032.

30) Butler, L.M.; Agus, D.B.; Scher, H.I.; Higgins, B.; Rose, A.; Cordon-Cardo, C.; Thaler, H.T.; Rifkind, R.A.; Marks, P.A.; Richon, V.M. Suberoylanilide hydroxamic acid, an inhibitor of histone deacetylase, suppresses the growth of prostate cancer cells in vitro and in vivo. *Cancer Res.* **2000**, 60, 5165-5170.

31) Rundlett, S.E.; Carmen, A.A.; Kobayashi, R.; Bavykin, S.; Turner, B.M.; Grunstein, M. HDA1 and RPD3 are members of functionally distinct yeast histone deacetylase complexes. *Proc. Natl. Acad. Sci. U.S.A.* **1996**, 93, 14503-14508.

32) Marks, P.; Rifkind, R.A.; Richon, V. M.; Breslow, R.; Miller, T.; Kelly, W.K. Histone deacetylases and cancer: causes and therapies. *Nat. Rev. Cancer* **2001**, 1, 194-202.

33) Olsen, K.M.; San Pedro, G.S.; Gann, L.P.; Gubbins, P.O.; Halinski, D.M.; Campbell, Jr., G.D. Intrapulmonary pharmacokinetics of azithromycin in healthy volunteers given five oral doses. *Antimicrob. Agents Chemother.* **1996**, 40, 2582-2585.

34) Girard, A.E.; Girard, D.; English, A.R.; Gootz, T.D.; Cimochowski, C.R.; Faiella, J.A.; Haskell, S.L.; Retsema, J.A. Pharmacokinetic and in vivo studies with azithromycin (CP-62,993), a new macrolide with an extended half-life and excellent tissue distribution. *Antimicrob. Agents Chemother*. **1987**, 31, 1948-1954.

35) Sugie, M.; Asakura, E.; Zhao, Y.L.; Torita, S.; Nadai, M.; Baba, K.; Kitaichi, K.; Takagi, K.; Takagi, K.; Hasegawa, T. Possible involvement of the drug transporters P glycoprotein and multidrug resistance-associated protein Mrp2 in disposition of azithromycin. *Antimicrob. Agents Chemother*. **2004**, 48, 809-814.

36) Laskin, B.L.; Weinberger, B.; Laskin, J.D. Functional heterogeneity in liver and lung macrophages. *J. Leukoc. Biol*. **2001**, 70, 163-170.

37) Vallée, E.; Azoulay-Dupuis, E.; Pocidalo, J.-J.; Bergogne-Bérézin, E. Activity and local delivery of azithromycin in a mouse model of *Haemophilus influenza* lung infection. *Antimicrob. Agents Chemother*. **1992**, 36, 1412-1417.

38) Azoulay-Dupuis, E.; Vallée, E.; Bedos, J.-P.; Muffat-Joly, M.; Pocidalo, J.-J. Prophylactic and therapeutic activities of azithromycin in a mouse model of pneumococcal pneumonia. Antimicrob. Agents *Chemother*. **1991**, 35, 1024-1028.

39) Wijburg, O.L.; Heemskerk, M.H.; Boog, C.J.; Van Rooijen, N. Role of spleen macrophages in innate and acquired immune responses against mouse hepatitis virus strain A59. *Immunology*. **1997**, 92, 252-258.

40) Kim, M.S.; Kwon, H.J.; Lee, Y.M.; Baek, J.H.; Jang, J.-E.; Lee, S.-W.; Moon, E.-J.; Kim, H.-S.; Lee, S.-K.; Chung, H.Y.; Kim, C.W.; Kim, K.-W. Histone deacetylases induce angiogenesis by negative regulation of tumor suppressor genes. *Nat. Med*. **2001**, 7, 437-443.

41) Montgomery, J.A.; Mayo, J.G. Quantitative structure-activity relationships in anticancer agents. Activity of selected nitrosoureas against a solid tumor, the Lewis lung carcinoma. *J. Med. Chem.* **1974**, 17, 477-480.

42) Colombo, T.; Delaini, F.; Ferrari, R.; Donati, M.B.; Donelli, M.G.; Poggi, A. Interaction between heparin and adriamycin in mice bearing the Lewis lung carcinoma. *Biomedicine*. **1981**, 43, 124-128.

43) Giermasz, A.; Makowski, M.; Kozlowska, E.; Nowis, D.; Maj, M.; Jalili, A.; Feleszko, W.; Wójcik, C.; Dabrowska, A.; Jakóbisiak, M.; Golab, J. Potentiating antitumor effects of a combination therapy with lovastatin and butyrate in the Lewis lung carcinoma model in mice. Int. J. Cancer 2002, 97, 746-750.

APPENDIX

Examples of Inhibition Graphs and Logit Analysis for Determining HDAC or anticancer IC_{50}'s.

Concentration (nM)	Fluorescence	Control	% Inhibition	log(conc.)	logit(fluor)	**4b**
0	410.15	410.15	100.00	1.40	0.55	
25	319.17		77.82	1.70	0.26	
50	264.43		64.47	2.00	0.02	
100	210.31		51.28	2.40	-0.28	
250	140.95		34.37	2.70	-0.54	
500	91.67		22.35	3.00	-0.76	
1000	60.99		14.87			

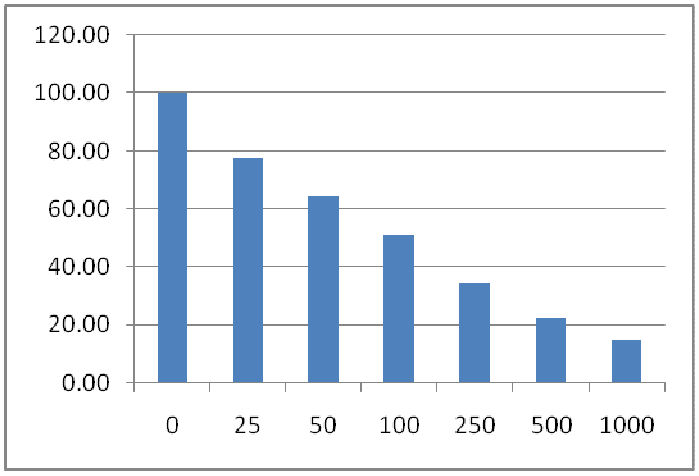

Control		25	50	100	250	500	1000
	423.258	275.265	268.347	218.325	145.53	90.56	57.163
	410.258	340.007	307.063	199.304	146.568	94.552	66.854
	396.94	342.229	217.885	213.293	130.76	89.904	58.965

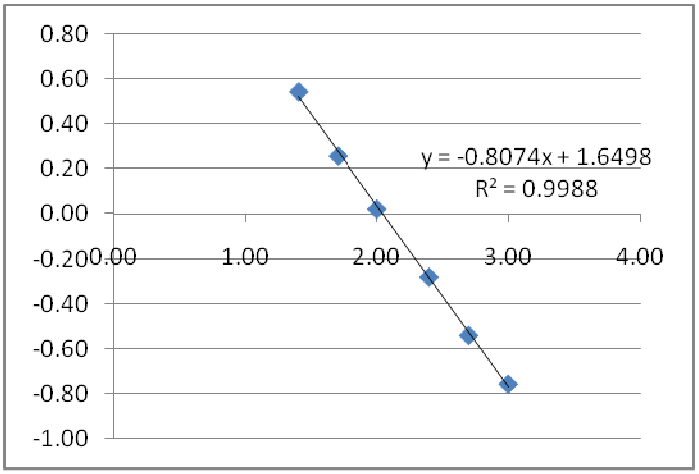

IC_{50} (nM)
110.50

Concentration (nM)	Fluroescence	Control	% Inhibition	log(conc)	logit(fluor)	**7y**
0	366.47	366.47	100.00	1.40	1.23	
25	345.91		94.39	1.70	0.78	
50	314.48		85.81	2.00	0.54	
100	283.87		77.46	2.40	0.53	
250	283.49		77.36	2.70	0.34	
500	251.21		68.55	3.00	0.52	
1000	281.40		76.79			

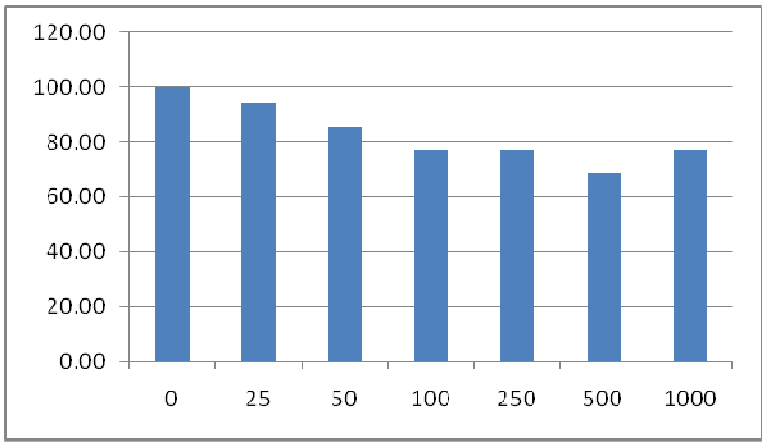

Control		25	50	100	250	500	1000
	375.029	315.258	328.158	285.111	337.056	248.212	279.264
	344.155	378.216	301.162	304.745	268.956	214.763	284.642
	380.215	344.256	314.108	261.746	244.452	290.666	280.303

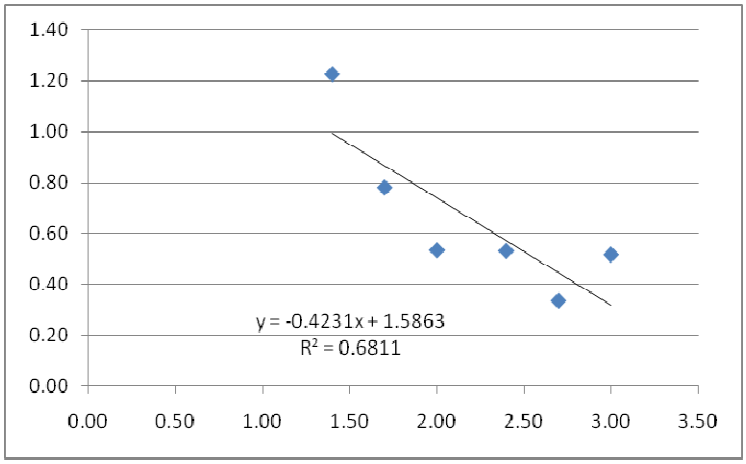

IC_{50} (nM)
N.D.

Calibration Curve for Radiolabeled compound **17a.**

Concentration (mg/ml)	DPM
0.25	15507
0.1	6152
0.05	3264
0.025	1477
0.01	593
0.001	244

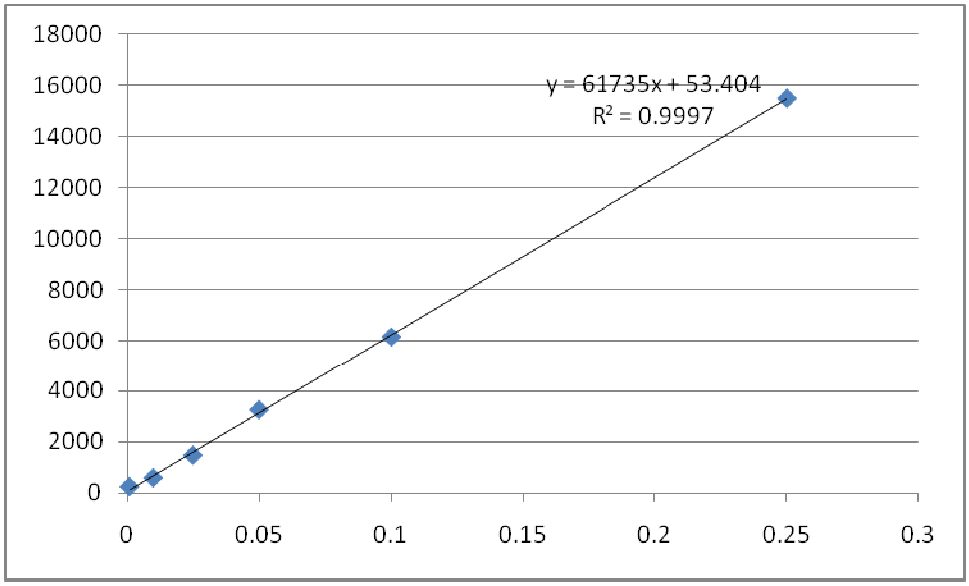

Calibration curve for radiolabeled compound **17c.**

Concentration (mg/ml)	DPM
0.25	16024
0.1	6233
0.05	3109
0.025	1542
0.01	609
0.001	275

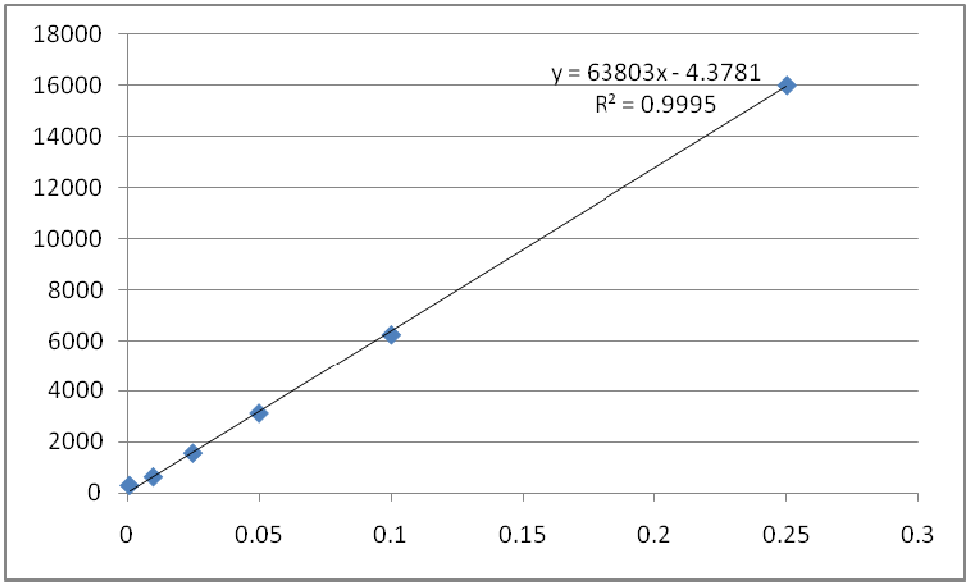

Vita

William Guerrant was born in Thomson, Georgia. He attended public schools in Thomson, Georgia and received a B.S. in Biochemistry and Molecular Biology from the University of Georgia, Athens, GA in 2005 before coming to Georgia Tech to pursue a doctorate in Chemistry. When he is not working on his research, William enjoys spending time with his friends, playing soccer, and exercising.